MSc Thesis - Silvy Rijsdijk

Exploring Electrochemical Advanced Oxidation Processes as Novel Method for Arsenic Removal from Dune Water

dunea
DUIN & WATER

TUDelft

Exploring Electrochemical Advanced Oxidation Processes
as Novel Method for Arsenic Removal
from Dune Water

by

Silvy Rijsdijk

to obtain the degree of Master of Science

at the Delft University of Technology,

to be defended publicly on Monday July 4, 2022 at 15:00.

Student Number:	4445244		
Project Duration:	November 8, 2021 – July 4, 2022		
Thesis Committee:	Dr. Ir. D. van Halem,	Chair,	TU Delft
	Ir. E. Kraaijeveld,	First Supervisor,	TU Delft
	Dr. B. van Breukelen,	Second Supervisor,	TU Delft
	Dr. Ir. R. Lindeboom,	External Supervisor,	TU Delft

TUDelft Delft University of Technology

Preface and Acknowledgements

This work on "Exploring Electrochemical Advanced Oxidation Processes as Novel Method for Arsenic Removal from Dune Water" presents the final thesis of the Master programme (MSc.) Civil Engineering, with a specialization in Water Management (section of Sanitary Engineering), at the Delft University of Technology (TU Delft) in cooperation with Dunea.

After finalising my BSc Civil Engineering, I started in September 2020 with my MSc Water Management. Although, the last month was sometimes stressful, I really enjoyed the 9 last months while working on this thesis. This would not have been possible without the love and support of many people.

I would like to start with thanking all my supervisors. Erik Kraaijeveld, I could not have had a better daily supervisor. Thank you so much for helping me in the lab, answering my many questions and giving me lots of feedback but also for the less serious talks we had. I really enjoyed the days in the dunes, especially the sunny ones! Doris van Halem, I am grateful for your guidance and support and for helping me to continue in the right direction and of course the opportunity to work on this thesis. I am really looking forward to the coming years. Boris van Breukelen, thank you for sharing your hydrogeochemical expertise and helping me understanding all the complicated processes in the ground when I no longer understood. Ralph Lindeboom, thank you for giving me feedback and being in my thesis committee. I learned a lot from all of you. Furthermore, thank you Suzanne van der Poel for helping us during the (cold) days in the dunes, even though it was raining and freezing I enjoyed the beautiful dune area in Monster and the good company. Korneel Rabaey, thank you for letting me work with your eAOP cell and for explaining eAOPs and answering my questions.

Besides my supervisors, I am thankful to the TU Delft Waterlab technicians. Armand Middeldorp, thank you for helping me with general questions and with the IC analyses. Patricia van den Bos, Jane Erkemeij and Judith Jahn, thank you for the many ICP-MS analyses. Additionally, I would like to thank the drinking water team of Doris for providing feedback on my work and also for the nice chats.

My student time in Delft would not have been so great without my friends. Soesja, the 5 years of living together was amazing. Thank you for all the wonderful moments we shared and for the many long coffee breaks at the TU. Sanna, even though I missed you during my master, since you exchanged Civil Engineering for Mechanical Engineering, I would like to thank you for the amazing time we had during our bachelor thesis in Bandung. This tremendous experience made me choose this master in Water Management. My friends and housemates Ilva, Fé, Eva, Josien and Floor, you have made the last year so much fun. Thank you for all the good times we had and the nice dinners outside sitting on the grass beside the water. You all made my last 7 years fantastic!

I would like to thank my family for their endless support during this thesis and throughout my studies. Amy, I am always so happy to see you. Even though you are my younger sister, you always have the best advice. Mama and Papa, thank you for always supporting me. During the past 7 years, I could always call you or come by when I needed advice. When I had struggles with my last bachelor course, which I rather forget than mention here, you encouraged me not to give up and you came immediately to Delft to celebrate my bachelor graduation. Furthermore, I would like to thank my grandparents for their endless love. Finally, Bas thank you for supporting me and listening to my stories about my thesis. You know how to put everything into perspective when I am stressed. Thank you all for being in my life.

Highlights

- Each well section in Solleveld showed elevated arsenic concentrations > 1 µg/L, while below WHO, European and Dutch guidelines of 10 µg/L.

- Water was being extracted from an arsenic-bearing layer, present between -2.5 and -8.5 m NAP.

- The combination of strongly fluctuating groundwater tables, infiltration of oxygenated water, the observed pH decrease and synchronous mobilisation of several TEs, indicated that As was most probably mobilised by pyrite oxidation.

- Complete As(III) oxidation by electrochemical advanced oxidation processes was observed at a current density of 7.5 A/m^2, with a corresponding charge dosage and hydraulic retention time of 30 C/L and 1.4 min, respectively.

- The energy consumption at 7.5 A/m^2 was 0.066 kWh/m^3 with operational costs of 0.04 €/m^3.

- Free chlorine was minimized by reducing the charge dosage, hydraulic retention time and current density.

- The estimated cathodic OH$^-$ production was proved to be sufficient to replace the dosed chemicals for pellet softening, however it was not sufficient to buffer for the anodic pH decrease.

Abstract

Dunea's drinking water treatment plants (DWTPs) want to reach the new arsenic (As) company target of < 1 µg/L, due to uncertainties on toxicity at the current WHO, European and Dutch guideline of 10 µg/L. The aim of this research was to lower the As concentration in Dunea's effluent to < 1 µg/L by improving our system understanding and exploring novel techniques for As(III) oxidation. Fieldwork was performed to assess whether each well section contributed to the elevated As concentrations. In order to enhance As(III) oxidation at Dunea's DWTP, the use of electrochemical advanced oxidation processes (eAOPs) with a RuO_2/IrO_2-coated anode was examined during laboratory experiments. Fieldwork results showed that in each monitoring point the measured As concentration was > 1 µg/L, indicating that each well section contributed to the elevated As concentrations. The combination of strongly fluctuating groundwater tables, infiltration of oxygenated water, the observed pH decrease and synchronous mobilisation of several TEs, indicated that As was most probably mobilised by pyrite oxidation. It was observed that the As-bearing layer was present between -2.5 and -8.5 m NAP. With an average filter depth from -1.6 to -7.4 m, water was being extracted from the As-bearing layer. Laboratory results showed complete As(III) oxidation by eAOPs at a current density (i) of 7.5 A/m^2, with a corresponding charge dosage (q) and hydraulic retention time (HRT) of 30 C/L and 1.4 min, respectively. At the aforementioned condition, the energy consumption of the eAOP cell was 0.066 kWh/m^3 with operational costs of 0.04 €/m^3. Free chlorine formation was minimized by reducing q, HRT and i. During the optimal anodic configuration of 7.5 A/m^2, the estimated cathodic OH$^-$ production was sufficient to replace the dosed chemicals for pellet softening (PS). However, it was not sufficient to buffer for the anodic pH decrease. It was proposed to implement the eAOP cell at Dunea's DWTP after PS and before aeration and rapid sand filtration.

Contents

List of Figures

List of Tables

1 Introduction

In this chapter, background information on arsenic in water will be provided, followed by followed by an explanation why arsenic is relevant to the drinking water production at Dunea. Then, the technology of electrochemical advanced oxidation processes will be explained. Finally, the research questions of this report will be presented.

1.1 Background Information

Arsenic (As) exposure has adverse effects on human health due to its toxicity (WHO, 2011a). The adverse health effects depend on the As dose, exposure duration and nutrition status of the affected people (Rahman et al., 2009). Drinking water is a major source of As exposure (WHO, 2011a). The medical complications that arise after long-term As exposure are termed as arsenicosis and are related to skins lesions, developmental effects, cardiovascular disease, diabetes, neurotoxicity and several types of cancer (Howard, 2003; McCarty et al., 2011; WHO, 2011b; Gomez-Caminero et al., 2001). Symptoms of acute exposure include skin lesions, abdominal pain, vomiting, diarrhoea, muscular pain and gastrointestinal symptoms such as burning lips, thirst, nausea and painful swallowing (WHO, 2011a; Goebel et al., 1990).

Due to these serious health problems caused by As poisoning, the World Health Organization (WHO) set the guideline for As in drinking water to 10 μg/L in 1993 (WHO, 2017). However, some countries such as India and Bangladesh, apply the older limit of 50 μg/L (Masuda, 2018; Unicef Bangladesh, 2010). In addition, it is estimated that approximately 94-220 million people worldwide are exposed to As levels > 10 μg/L in domestic water supply (Podgorski & Berg, 2020). In the Netherlands, As concentrations are below the WHO, European and Dutch drinking water guidelines of 10 μg/L (WHO, 2017; European Union, 2020; Overheid, 2021). However, rather recently Dutch drinking water companies have adopted a new, challenging target of < 1 μg/L, making them leading worldwide. Uncertainties in health effects resulting from low As exposure are the reason for this lower target. Moreover, study of Saint-Jacques et al. (2018), provided evidence for the presence of cancer effects at As concentrations < 10 μg/L.

In natural waters, As occurs in the oxidation states +3, arsenite (As(III)) and +5, arsenate (As(V)), with As(III) being a more toxic form than As(V) (Smedley & Kinniburgh, 2002; WHO, 2011a; Bissen & Frimmel, 2003; Cullen & Reimer, 1989). The As speciation is mostly controlled by pH and redox potential (Smedley & Kinniburgh, 2002). As is most likely to be present as As(V) in aerated waters under oxidising conditions, whereas in anaerobic waters under reducing conditions, As(III) is most likely to be the predominant As form (Gomez-Caminero et al., 2001; WHO, 2017). Methods that are currently used for As removal from drinking water are adsorption, membrane techniques, ion exchange, electrocoagulation, electrolysis and chemical methods such as coagulation, precipitation and dosing of chemical oxidants (Pal, 2015; Alka et al., 2021; Sharma et al., 2007).

1.2 Arsenic at Drinking Water Treatment Plant Dunea

Dunea's drinking water treatment plants (DWTPs) supply drinking water to consumers in the western part of South-Holland and are located in Monster, Scheveningen and Katwijk. Pre-treated river water from the Dammed Meuse is transported to the dunes between Monster and Katwijk. Here, the water is pumped into infiltration lakes, from which the water infiltrates into the dunes. During this dune infiltration, bacteria and viruses present in the water are inactivated. After a residence time of two months, the water is recovered by wells and transported to the DWTP for post-

treatment (Figure 48, Supplementary Information 6.1) (Dunea, n.d.). A system in which drinking water is produced from surface water by dune infiltration is indicated by managed aquifer recharge (MAR) (Stuyfzand & van der Schans, 2018). This research exclusively considers the Dunea's DWTP in Monster of which the well field is referred to as Solleveld (Figure 49, Supplementary Information 6.2).

Dunea wants to reach the new As company target of < 1 μg/L, due to uncertainties on toxicity at the current WHO, European and Dutch guideline of 10 μg/L. As enters the water during dune infiltration, resulting in an average concentration of 4.9 μg/L (Table 5, Supplementary Information 6.3). However, it is still unknown whether each well section at Solleveld contributes equally to the elevated As concentration. Furthermore, the processes that cause As mobilisation during dune infiltration are not yet known. The contribution of each well section and the As mobilisation processes will be examined in this research.

In Dunea's DWTP, the As concentration is lowered from 4.9 to 3.4 μg/L via adsorption onto ferric hydroxides ($Fe(OH)_3$) during rapid sand filtration (RSF) (Gude et al., 2018). The coagulant ferric chloride ($FeCl_3$) is dosed which, together with naturally present iron, hydrolyzes to form $Fe(OH)_3$ during aeration (Sancha, 2006). At neutral pH, As(III) species are electrically neutral, whereas As(V) species are negatively charged and will therefore be able to adsorb to positively charged hydroxylated surface of $Fe(OH)_3$ (Jain et al., 1999; Sancha, 2006). As a result, adsorption of As(V) is more effective compared to As(III), showing the importance of oxidising As(III) to As(V) prior to RSF for efficient adsorption to $Fe(OH)_3$ (Bissen & Frimmel, 2003; S. I. Siddiqui & Chaudhry, 2017). Study of Gude et al. (2018) observed that As largely remained present as As(III) during aeration, indicating little As(III) oxidation by oxygen. This explains the As concentration of 3.4 μg/L in Dunea's effluent, since not all As(III) was oxidised by aeration. As concentrations after dune passage and in the drinking water effluent have proven to be rather constant over the years. Hence, constant As removal is obtained, indicating constant As(III) influent concentrations and As(III) oxidation efficiencies. The aim of this research is the oxidation of all present As(III) to As(V) to enhance As removal by adsorption during RSF. In order to oxidise all present As(III) prior to RSF, a novel oxidation technique will be examined in this research.

1.3 Electrochemical Advanced Oxidation Processes

An effective method for oxidising As(III) to As(V) are advanced oxidation processes (AOPs) (Babu et al., 2019). AOPs are based on the production of ˙OH radicals, which are powerful oxidants (Oturan & Aaron, 2014; Sirés et al., 2014). Several AOPs methods exist, which differ in their ˙OH radicals production (Andreozzi et al., 1999; Babu et al., 2019). Electrochemical advanced oxidation processes (eAOPs) are AOPs based on electrochemistry and without addition of expensive reactants, such as hydrogen peroxide (H_2O_2) and ozone (O_3) for ˙OH production (Oturan & Aaron, 2014; Andreozzi et al., 1999; Brillas et al., 2009). Advantages of eAOPs include the clean reagent (electron) causing no pollution, the high energy efficiency and the easy handling of the system (Sirés et al., 2014).

In this research, anodic oxidation (AO) is considered, which is a well known eAOP. Other eAOPs such as electro-Fenton and photoelectro-Fenton are less suitable for this study because Fe^{2+} is needed as catalyst, as well as chemical dosing of H_2O_2 (Sirés et al., 2014). The anode used in this research is a mixed RuO_2/IrO_2-coated anode, which is classified as active electrode. Hence, only active electrodes and their processes are considered in this research. In AO, As oxidation can be obtained by three processes; direct oxidation, oxidation via intermediates of the oxygen evolution reaction (OER) and indirect oxidation (Figure 1) (Wang & Xu, 2012; Panizza & Cerisola, 2009; Martínez-Huitle & Panizza, 2018).
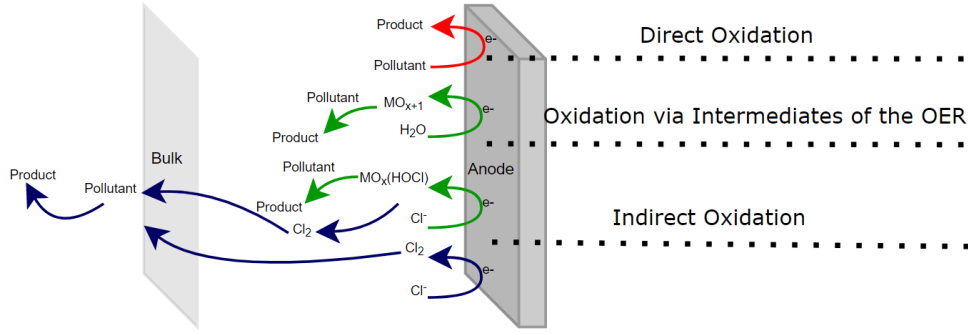
Figure 1: The 3 Anodic Oxidation Processes. Direct oxidation (red), oxidation via intermediates of the OER (green) and indirect oxidation (blue). Direct oxidation and oxidation via intermediates of the OER take place on the anode surface. The latter oxidises pollutants by chemisorbed active oxygen or adsorbed HOCl. Indirect oxidation is driven by electrogenerated Cl_2 which oxidises pollutants in the bulk solution, adapted from (Sirés et al., 2014).

In direct oxidation, pollutants are oxidised after adsorption on the anode surface where electrons are exchanged directly without participation of any substances. This process is possible before the OER (Panizza & Cerisola, 2005; Comninellis & Chen, 2010; Brillas & Martínez-Huitle, 2015).

Oxidation via intermediates of the OER is presented in Figure 2. $\cdot$OH radicals can be formed on the anode oxide surface, indicated by MO_x, via the oxidation of water (Equation 1) (Comninellis, 1994). On the anode surface, two active oxygen states can be present; physisorbed and chemisorbed active oxygen. The first one, physisorbed active oxygen, is the adsorbed OH$\cdot$ radicals (Equation 1). The latter, chemisorbed active oxygen which is the chemically bonded MO_{x+1} (Equation 2), can be formed when the adsorbed OH$\cdot$ radicals interact with the anode and form a higher oxide (MO_{x+1}). This higher oxide can act as intermediary in the oxidation of pollutants (R) (Equation 3) (Comninellis, 1994; Brillas & Martínez-Huitle, 2015).

$$MO_x + H_2O \rightarrow MO_x(\cdot OH) + H^+ + e^- \tag{1}$$

$$MO_x(\cdot OH) \rightarrow MO_{x+1} + H^+ + e^- \tag{2}$$

$$MO_{x+1} + R \rightarrow MO_x + RO \tag{3}$$
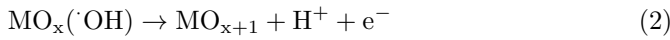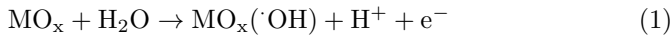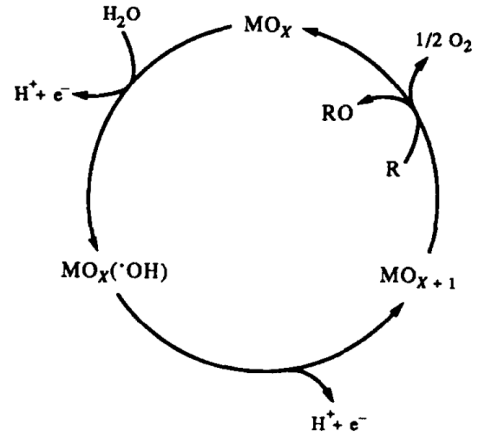
Figure 2: Oxidation via Intermediates of the OER. Schematic overview of formation of physisorbed active oxygen followed by chemisorbed active oxygen on the anode, from (Comninellis, 1994).

Indirect oxidation is the AO process in which oxidation is mediated by electrogenerated oxidants, which are generated at the anode (Wang & Xu, 2012; Panizza & Cerisola, 2009). These oxidants can oxidise pollutants in the bulk solution (Martinez-Huitle & Ferro, 2006; Panizza & Cerisola, 2009). The free chlorine species chlorine (Cl_2), hypochlorous acid (HOCl) and hypochlorite (OCl^-) are common oxidants, which can be formed in the presence of Cl^- ions (Luna-Trujillo et al., 2020; da Cruz Nizer et al., 2020). The presence of the free chlorine species is strongly dependent on the solution pH (Ghurye & Clifford, 2001). At acidic conditions, Cl_2 predominates, whereas HOCl

can be found at pH values in the range from 2.5-7.5, followed by the dominant OCl^- at alkaline conditions (Luna-Trujillo et al., 2020). Equations 4 and 5 show the oxidation reaction of As(III) by HOCl and OCl^-, respectively (Vasudevan et al., 2006; Sorlini & Gialdini, 2010).

$$H_3AsO_3 + HOCl \rightarrow H_2AsO_4^- + Cl^- + 2H^+ \tag{4}$$

$$H_3AsO_3 + OCl^- \rightarrow H_2AsO_4^- + Cl^- + H^+ \tag{5}$$
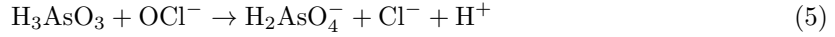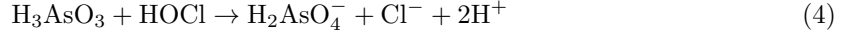
De Battisti's group (Bonfatti et al., 1999; Bonfatti, Ferro, et al., 2000; Bonfatti, De Battisti, et al., 2000) proposed the theory that besides free chlorine in the bulk solution, adsorbed oxychloro species $(HOCl_{ads})$ on the anode surface can play a role in oxidation of pollutants. Chloride ions inhibit the OER so that oxygen transfer is performed by adsorbed HOCl instead of by chemisorbed active oxygen (Luna-Trujillo et al., 2020; Panizza & Cerisola, 2009). Figure 3 shows the oxidation of pollutants by $HOCl_{ads}$ together with the formation of Cl_2.

The relevance of considering free chlorine is the possible reaction with natural organic matter (NOM) forming disinfection by-products (DPBs) (Hua & Reckhow, 2007). The most prevalent DPBs are the trihalomethanes (THMs) and haloacetic acids (HAAs) (Singer, 1994; Srivastav et al., 2020). Production of these DPBs in drinking water is undesired due to their adverse human health effects which include carcinogenicity and genotoxicity (Richardson et al., 2007). Furthermore, eAOPs can lead to the direct production of inorganic DPBs, such as chlo-

Figure 3: Indirect Oxidation via Adsorbed HOCl. Schematic overview of chloride ions inhibition in the OER with subsequent formation of $HOCl_{ads}$ on the anode, from (Bonfatti, Ferro, et al., 2000).

rite (ClO_2^-), chlorate (ClO_3^-), perchlorate (ClO_4^-) (D. Wang et al., 2015; Chaplin, 2014; Bergmann et al., 2014). These inorganic DPBs have potentially human health effects such as change in red blood cells and in thyroid hormones (WHO, 2017).

On the cathode, hydrogen gas (H_2) and hydroxyl (OH^-) ions are produced by splitting water (Equation 6) (Comninellis & Chen, 2010). Study of Clauwaert et al. (2020) demonstrated the possibility of water softening with eAOPs by cathodic base (OH^-) production. This process, referred to as e-softening, could be used at Dunea's DWTP, where the water is currently softened by pellet softening (PS) with addition of the chemical caustic soda (NaOH).

$$2H_2O + 2e^- \rightarrow 2OH^- + H_2 \tag{6}$$

The oxidation of As(III) by AO was reported in literature (Zhao et al., 2010; Zhang et al., 2014; Lacasa et al., 2011). Zhao et al. (2010) demonstrated almost complete oxidation of As(III) within 30 minutes with a current density of 2.4 A/m^2. Study of Zhang et al. (2014) investigated the performance and mechanisms of As(III) oxidation by an $TiO_2NTs/Sb–SnO_2$ anode. Complete As(III) oxidation was observed within 60 minutes by a current of 50 mA. Furthermore, the relative contributions of direct and indirect oxidation were quantified. However, this anode was classified as non-active electrode which differed from the active electrode used in this research. Lacasa et al.

(2011) showed complete As(III) oxidation by eAOPs using an anode made of mixed ruthenium oxide, which was close to the used anode in this research. However, the As(III) oxidation was not obtained for a wide range of current densities. Moreover, minimizing the free chlorine formation while optimising As oxidation was not considered in this study. Furthermore, no quantification of the cathodic OH^- production was made, showing the need for our research.

1.4 Research Questions

The aim of this research is to lower the As concentration in Dunea's effluent to < 1 µg/L by improving our system understanding and exploring novel techniques for As(III) oxidation. This research consists of two parts. The first part examines the As distribution and hydrological origin in Solleveld and the second part investigates the application of eAOPs for As(III) oxidation to 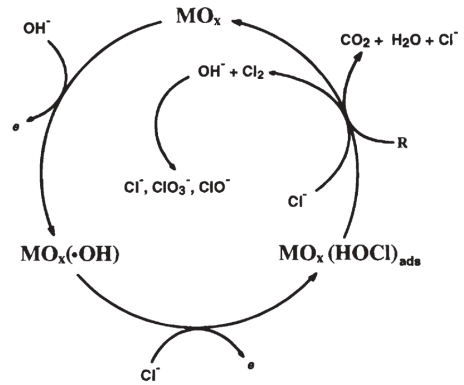facilitate a more efficient As removal. In order to obtain this lowered As concentration in the effluent, four research questions will be answered.

It is unknown whether each well section in Solleveld contributes to the elevated As concentration or whether this applies to specific well sections. This knowledge is important in deciding to apply As(III) oxidation at specific well sections (decentralised) or to apply centralised As(III) oxidation in the DWTP. This leads to the first research question, *What is the contribution of each well section to the elevated As concentrations and where does this As originate from?* This question will be answered by measuring As concentrations in monitoring points located in the Solleveld area, resulting in a spatial distribution of As concentrations. Additionally, the As-bearing layers will be localised in order to identify the As origin.

To start with the research on As(III) oxidation by eAOPs, the second research question, *What is the eAOP system performance in terms of As oxidation and energy consumption for a RuO_2/IrO_2-coated anode?*, will be answered. The performance of eAOPs with a RuO_2/IrO_2-coated anode on As(III) oxidation will be tested in laboratory experiments. System performance will include the applied current density, charge dosage and hydraulic retention time.

This research focuses on the implementation of eAOPs for drinking water, making the formation of chlorine undesired. Formation of free chlorine affects the taste and odor and, more importantly, can lead to the formation of DBPs, which have adverse effects on human health. This results in the third research question, *How do anodic operating conditions affect formation of free chlorine?*

The main drawback of implementing eAOPs at Dunea is the high energy consumption of the system and the costs related to this electrical supply (Sirés et al., 2014). In order to make this treatment system more attractive for implementation, the cathodic formation of OH^- is examined. Addition of OH^- to the pellet softening reactor could replace the currently dosed caustic sode (NaOH). This leads to the fourth research question, *What is the optimal cathodic configuration to produce OH^- during the optimal anodic configuration for As(III) oxidation and to what extent can this reduce the chemical use for pellet softening?*

The report is set out as follows. Chapter 2 will give a description of the fieldwork and laboratory experiments and the materials that are used in this research. Chapter 3 will present the results of experiments. Then, Chapter 4 will explain the results by literature. At last, Chapter 5 will present the conclusions and recommendations.

2 Methodology

In this chapter, the materials and methods that were used to answer the research questions will be explained. To examine the As origin in Solleveld, a description of the site where the fieldwork was performed will be presented. After that, the spatial analysis will be explained, followed by the experimental procedure for creating a hydrochemical profile. To examine the As(III) oxidation by eAOPs, a characterization of the eAOP cell will be given. Then the experimental procedure of As(III) oxidation will be described followed by the procedure to determine the free chlorine formation. Lastly, the quantification of cathodic base formation will be presented. In the last paragraph, the sampling method and chemical analysis will be explained.

2.1 Arsenic at Solleveld

As explained, it is still unknown to what extend each well section in Solleveld contributes to the elevated As concentrations. In addition, there is no current knowledge on the hydrological origin. Fieldwork was performed to answer the first research question.

2.1.1 Site Description and Previous Observations

The MAR system of Solleveld consisted of infiltration lakes for recharge, an aquifer to flush and store water and a remote recovery system composed of wells. Recharge and recovery were simultaneous and the system had a continuous infiltration water supply and water delivery demand (Stuyfzand & van der Schans, 2018). This type of MAR belongs to 'dune filtration' that ensures water quality improvement as well as buffer between supply and demand (Dillon, 2005). Figure 4 presents a schematic overview of the MAR system in Solleveld. Pre-treated river water in the infiltration lakes is indicated as 'infiltration water'. Infiltration water flowed through the dune soil where it was mixed with infiltrated rainfall. The infiltration water together with rainfall was the total recharge. Approximately 300 vertical abstraction wells were present in Solleveld which extracted water from the phreatic aquifer (Huizer et al., 2016). This extracted water is referred to as 'dune filtrate'.
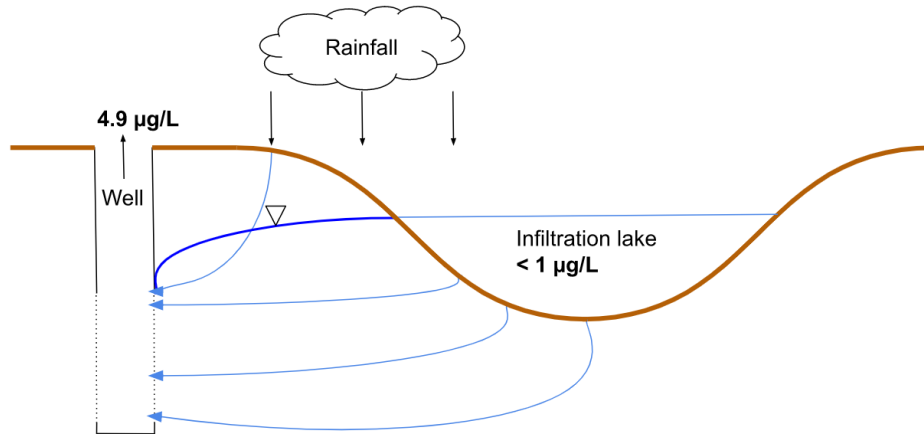
Figure 4: Schematic Overview of the MAR System in Solleveld. The infiltration water contains < 1 µg/L As and is infiltrated in the dune soil where it mixes with rainfall. Dune filtrate is extracted in a vertical well and contains 4.9 µg/L As.

According to the geological profile of Solleveld (Figure 50, Supplementary Information 6.2), the upper 10-30 m of the subsoil was composed of sand, clay and peat from the Holocene. In the higher situated dunes, mainly sand was present, while in the lower section, between -15 and -20 m mean sea level (MSL), mainly clay and peat were present. The boundaries for fresh, brackish and saline groundwater were based on chloride measurements that indicated that the fresh and brackish boundary was between -20 and -40 m MSL, whereas the brackish and saline boundary was between -40 and -60 m MSL (Huizer et al., 2016).

Study of Stuijfzand (2014), presented a hydrochemical depth profile of trace elements (TEs) in the Amsterdam coastal dune area (Figure 5). This hydrochemical depth profile shows an As-bearing layer from -1 until -12 m NAP. In addition, synchronous iron (Fe) mobilisation was observed in this profile. Nitrate (NO_3^-) reduction was completed near the boundary between layers 1A2 and 1A3 and As mobilisation occured at depths free from NO_3^-. There were several similarities between the study of Stuijfzand (2014) and this research. Firstly, both studies focused on a MAR system located in the west of the Netherlands along the North Sea. Secondly, in both MAR systems, pre-treated river water was infiltrated in a coastal dune aquifers. Thirdly, the upper subsoil of the study area of Stuijfzand (2014) consisted of Holocene sand, as observed at Solleveld. Hence, this study was used as reference.
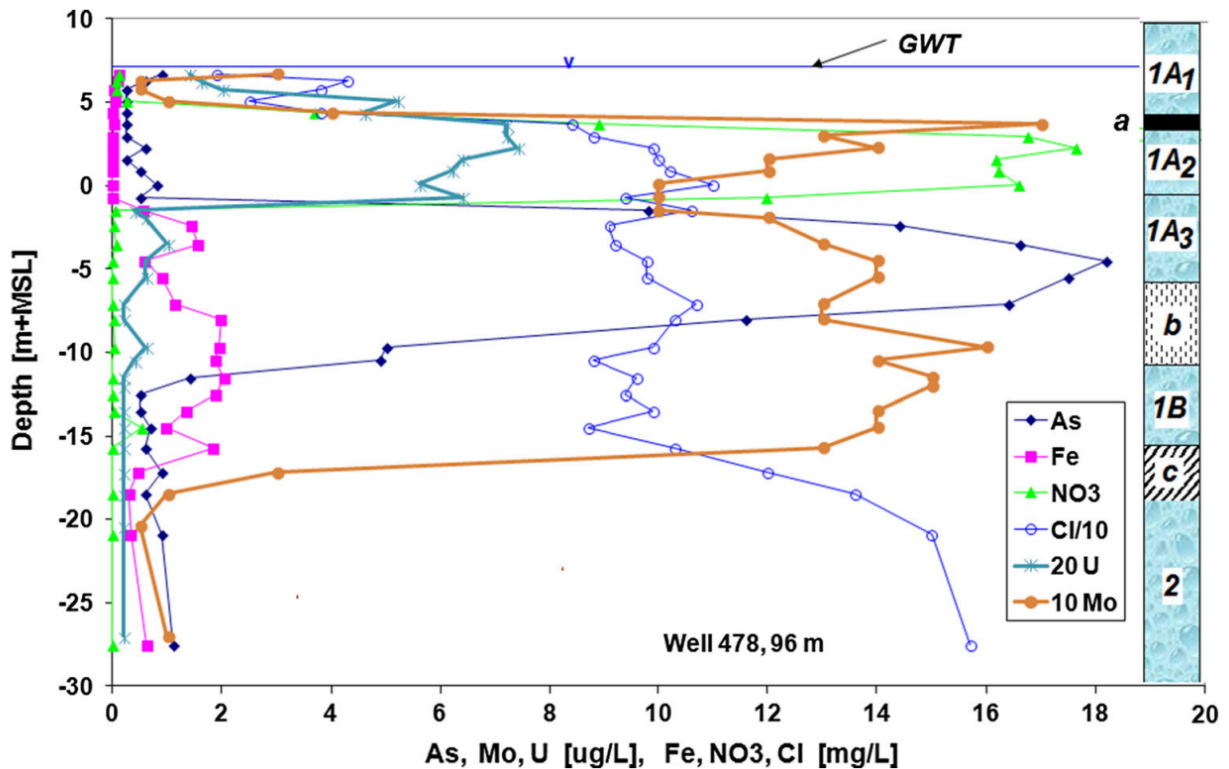
Figure 5: **Hydrochemical Depth Profile in Dutch Coastal Dune Area.** This profile shows As mobilisation between -1 until -12 m NAP with synchronous Fe mobilisation, from (Stuijfzand, 2014).

Three redox categories could be distinguished for groundwater; oxic, suboxic and anoxic (McMahon & Chapelle, 2008). Relevance of this classification is obtaining insight into processes that will probably occur in the groundwater. Additionally, it will help to understand As mobilisation processes. Table 1 was used to classify the redox categories of the groundwater present at Solleveld. Concentrations of O_2, $NO_3^- - N$, Mn^{2+}, Fe^{2+} and SO_4^{2-} were used to determine the redox processes.

Table 1: Threshold Concentrations [mg/L] for Identifying Redox Category in Groundwater. O_2, $NO_3^- - N$, Mn^{2+}, Fe^{2+} and SO_4^{2-} concentrations are used to identify the redox category and redox processes in water, adapted from (McMahon & Chapelle, 2008).

Redox Category	Redox Processes	O_2	$NO_3^- - N$	Mn^{2+}	Fe^{2+}	SO_4^{2-}
Oxic						
	O_2 reduction	≥ 0.5	-	< 0.05	< 0.1	-
Suboxic						
	-	< 0.5	< 0.5	< 0.05	< 0.1	-
Anoxic						
	NO_3^- reduction	< 0.5	≥ 0.5	< 0.05	< 0.1	-
	Mn^{4+} reduction	< 0.5	< 0.5	≥ 0.05	< 0.1	-
	Fe^{3+} reduction	< 0.5	< 0.5	-	≥ 0.1	≥ 0.5
	SO_4^{2-} reduction	< 0.5	< 0.5	-	≥ 0.1	≥ 0.5

2.1.2 Spatial Analysis

Each abstraction well in Solleveld was connected to a pipe by which the dune filtrate was transported to the DWTP. At 12 locations monitoring points (MPs) were present, where it was possible to abstract water so that the quality of the connected wells could be monitored. Figure 6 illustrates Solleveld with MPs 1A, 1B and 1-10 which are indicated by circles with their numbers. The colour of the circle corresponds to the colour of the pipe that is connected to that MP. This shows which wells were connected to which MPs. Some pipes were joined together, which can be seen by a change of colour. Two main transport pipes entered the DWTP, located at the bottom middle; Duinwinning and Randwinning. Later, these pipes were merged and the product was called VOW. Three sampling locations were present in the DWTP indicated as Duin, Rand and VOW. The MPs in Solleveld and their connected transport pipe are described in Table 4 (Supplementary Information 6.2). The last column describes whether a MP was connected to other MPs.

Due to a high amount of air bubbles in the tube, no measurements were performed at MP 1B. This point was therefore disregarded in this report. No wells were present between MP 1 and 1A. MP 1 was omitted in the results for clarity. The reason for omitting MP 1 instead of 1A was that MP 1A was next to the wells, making this MP more representative. Together with Duinwinning, Randwinning and VOW, a total of 13 sampling locations were analysed. The lowered groundwater table during the sampling period probably led to oxygen intrusion. This lowered groundwater table was caused by an intake stop of the pre-treated river water. In addition, measurements were performed at Dunea's DWTP to see how the As concentrations changed after treatment steps. Samples were taken after PS before and after aeration followed by RSF and after slow sand filtration (SSF).
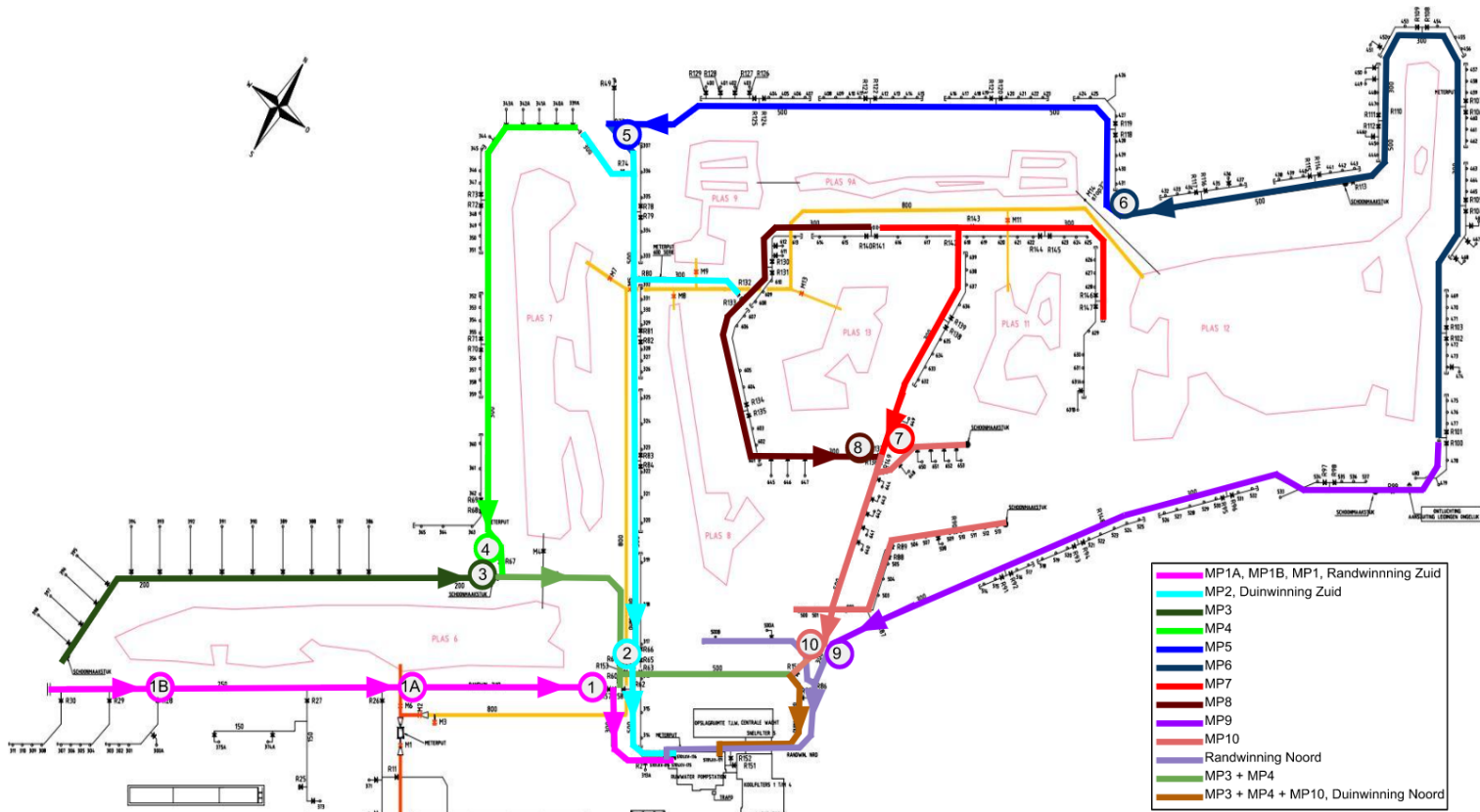
Figure 6: Monitoring Points in Solleveld. The MPs are circled and the colours of the circles and pipes indicate to which wells the MPs are connected. The arrows indicate the direction of the water flow.

2.1.3   Hydrochemical Depth Profile

The depth of the As-bearing layer was clearly visible in the hydrochemical depth profile (Figure 5), showing the relevance of creating such a profile in this research. In order to create a hydrochemical depth profile, the concentrations of several main constituents and dissolved TEs were measured in monitoring wells (MWs). The main constituents were NO_3^-, sulfate (SO_4^{2-}) and chloride (Cl^-) and the TEs were As, Fe, manganese (Mn), cobalt (Co), nickel (Ni) and zinc (Zn). Figure 7 shows the five MWs X1-X5, that were used for the measurements. The MWs had the same location but a different depth so that water from different layers was extracted. All presented depths in this research are in [m NAP].
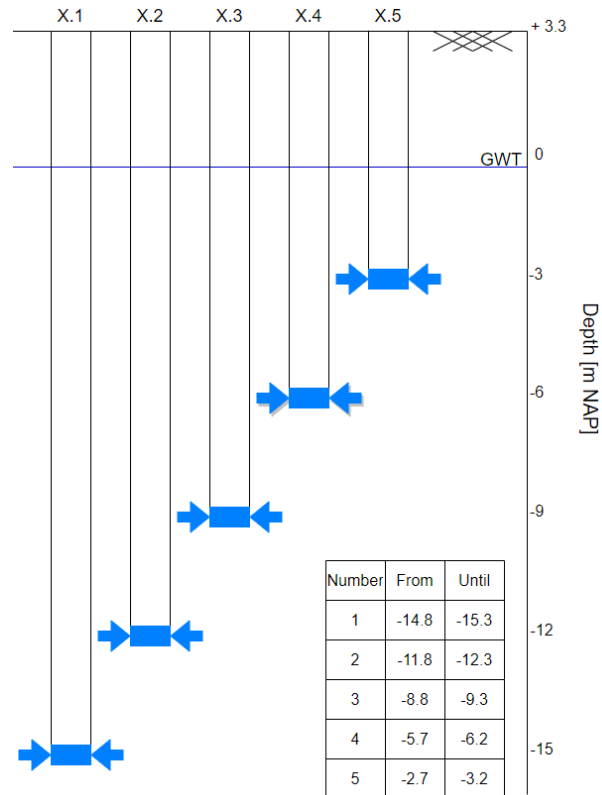
Figure 7: Depths of Monitoring Wells X [m]. Monitoring wells X1-X5 with a description of their depths. The ground level was at +3.3 m and the groundwater table was at -0.2 m, from (Dunea, 2021).

Figure 8 shows the wells 386 until 398. MWs X, indicated with the red cros, were located next to well 392. Infiltration water from infiltration lake 'Plas 6', shown in pink, flowed to the wells and became dune filtrate. Hence, the dune filtrate in MP 3 was a mixture of water from wells 386-398.
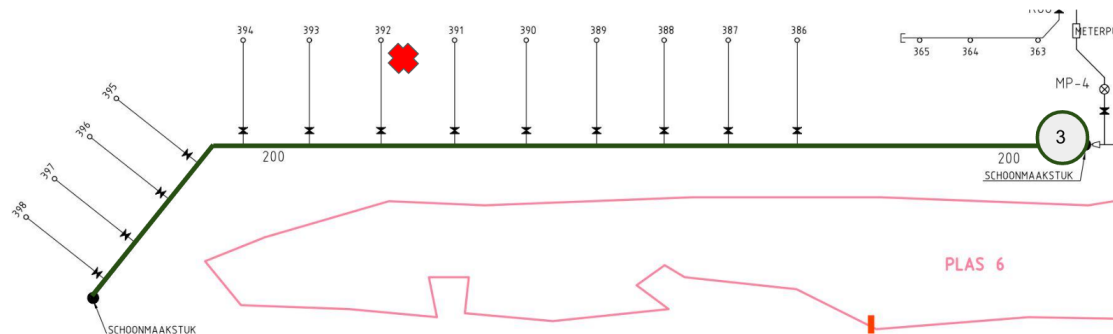
Figure 8: Wells 386-398 Connected to MP 3. MWs X are indicated with the red cross and MP 3 is indicated by the green circle.

Filters of wells 386-398 were located at different depths, as depicted in Figure 9. However, the total filter height was 5.8 m at every well. The average depth of the filter is indicated as 'Average Filter' and went from -1.6 to -7.4 m. The three measurement depths of MWs X that were relevant for the water inflow in the filter are indicated with red crosses. The ground level (brown line) fluctuated and the average groundwater table (blue line) was at -0.2 m.
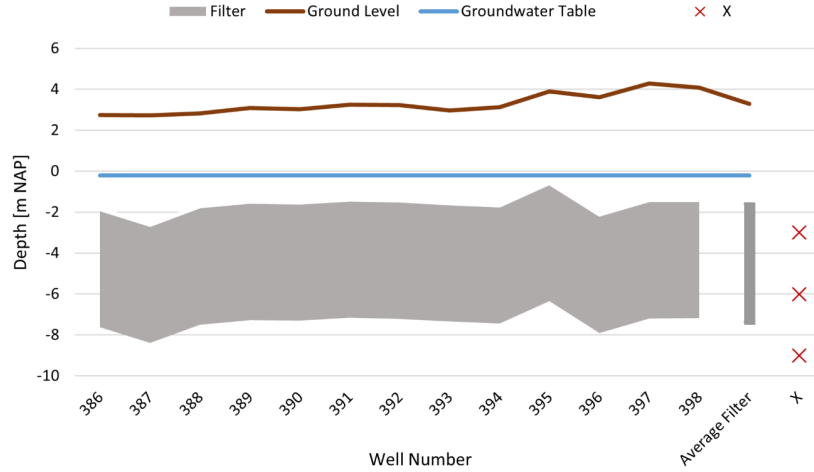
Figure 9: Filter Depths of Wells 386-398. The filters are indicated in the grey area and have a total height of 5.8 m. The average filter was from -1.6 to -7.4 m. Relevant depths of MWs X are shown as red crosses.

In order to validate the results from MWs X, measurements were performed at MWs Y (Y1-Y5) (Figure 51, Supplementary Information 6.4). These MWs had a similar depth in relation to NAP, however the ground level was at +2.8 m, resulting in a different depth in relation to ground level (Dunea, 2022). In addition, measurements were performed at MW Z (Figure 52, Supplementary Information 6.4). MW Z was situated at a lower depth at -2 m, making this MW relevant for measurements. Figure 53 (Supplementary Information 6.4), gives an overview of the MWs in Solleveld that were used for measurements.

2.2 Operation eAOPs

After finding out more about the spatial As distribution as well as the origin in Solleveld, the As(III) oxidation by eAOPs can be examined. This is done by answering the remaining three research questions during laboratory experiments.

2.2.1 eAOP Cell

The eAOP cell, borrowed from Ghent University, was equipped with two electrodes; anode and cathode. They were covered in 2 Perspex frames with internal dimensions of 20 x 5 x 2 cm (200 cm^3). A RuO_2/IrO_2-coated anode (100 cm^2) was used and a stainless steel mesh (100 cm^2) was used as cathode (Figures 54 and 55, Supplementary Information 6.5). A similar eAOP cell was used in the study of Radjenovic et al. (2011). In between the electrodes, a cation exchange membrane (CEM) was present. The CEM allowed monovalent cations to pass the membrane. A DC power supply of TENMA® 72-10500 (0-30 V, 0-3 A) was used to apply a fixed current and to read the operational voltage of the cell.

The experimental setup consisted of two feed water tanks of 25 L each, used to store the feed water (Figure 10). One feed water tank was connected to the anode, whereas the other to the cathode. Both feed water tanks were connected to two buffer tanks (one for anode and one for cathode) to which the feed water was pumped by peristaltic pumps. The buffer tanks were used to maintain a constant water level. Water flowed back to the feed water tanks under gravity when the water level was too high. From the buffer tanks, the feed water was pumped by two peristaltic pumps to the eAOP cell. After the water had passed the electrodes, it flowed to two disposal tanks where the effluent of both anode and cathode was collected separately. Formed O_2 and H_2 gas left the system after electrode passage.
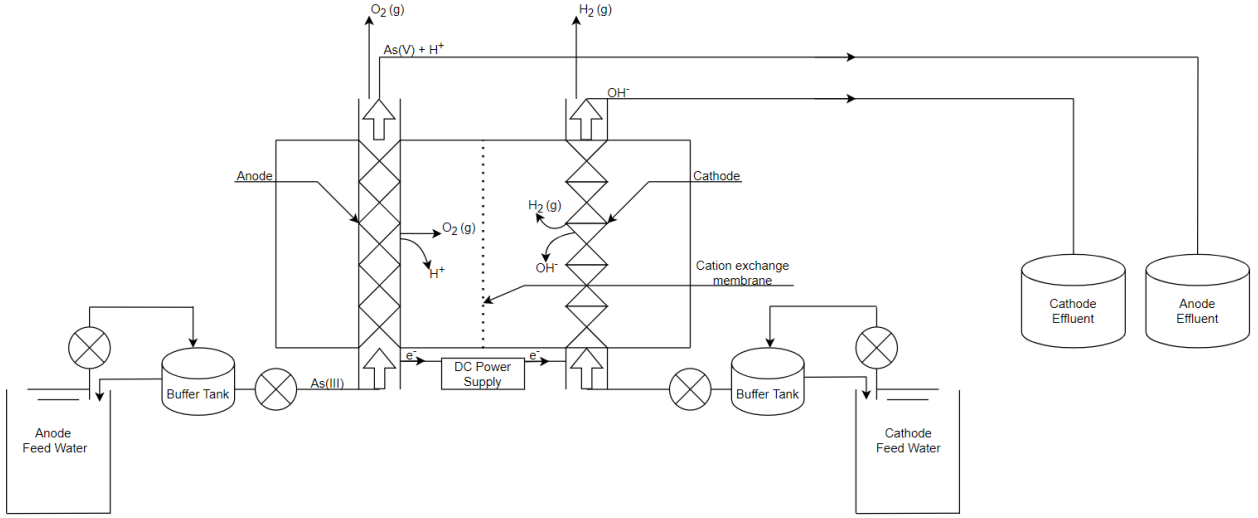
Figure 10: Schematic Overview of the Experimental Setup. Feed water enters the eAOP cell via the buffer tanks. At the anode, H^+ and O_2 are produced and As(III) is oxidised to As(V). At the cathode, OH^- and H_2 are produced.

The anodic performance depends on various parameters such as the supplied current density (i) [A/m²] and electrode potential (E) [V], known to show dependence, and flow rate [L/h], temperature [°C] and pH (Moreira et al., 2017). The supplied i was calculated by dividing the supplied current (I) [A] by the eAOP cell area of 100 cm², which equals 0.01 [m²] (Equation 7), whereas the E was provided to the anode by a potentiostat (Moreira et al., 2017). The standard electrode potentials (E^0) under standard conditions (25 °C, pH 0, 1 Pa and 1 M), for reactions of interest have been reported in literature and can be calculated by Equation 8 (Comninellis & Chen, 2010; Moreira et al., 2017; Renner, 2007; Armstrong et al., 2013).

$$i = \frac{I}{0.01} \tag{7}$$

$$E^0 = \frac{-\Delta G^0}{n * F} \tag{8}$$

$-\Delta G^0$ is the standard free energy [J/mol], n is the number of electrons [-] and F is the Faraday's constant of 96485 [C/mol] (Comninellis & Chen, 2010; Arnau, 2004).

Figure 11 gives an overview of the E^0 values for anodic oxidation reactions of interests with corresponding reaction. The presented potentials were measured with a standard hydrogen electrode and therefore had the unit V vs SHE (standard hydrogen electrode). However, in this research the E was measured with a Nanoelectra NEV3 potentiostat (0-1000 mA, 0-2.45 V) with an Ag/AgCl (3.5M KCl) electrode. The E results in V vs Ag/AgCl were converted to V vs SHE by +205 mV. All presented E values are in V vs SHE unless stated otherwise. In addition, the E^0 was dependent on the anode material and the values for the RuO_2/IrO_2-coated anode will therefore vary from the values presented in Figure 11.

Figure 11: Anodic Oxidation Reactions with E^0 [V]. E^0 is under standard conditions. 1) Direct oxidation of As(III) to As(V) at E^0= 0.56 V (Lacasa et al., 2011; Gupta & Chatterjee, 2017). 2). Direct oxidation of Cl^- to ClO^- at E^0= 0.89 V. HOCl is in equilibrium with ClO^- and under pH values < 7.5, HClO is the predominant form which can oxidise As(III) (Luna-Trujillo et al., 2020). 3) Oxygen evolution at E^0= 1.23 V. The higher oxide (MO_{x+1}) can oxidise As(III). In addition, ClO^- can inhibit the reaction leading to Cl_2 formation (Brillas & Martínez-Huitle, 2015; Panizza & Cerisola, 2009; Luna-Trujillo et al., 2020). 4) Direct oxidation of Cl^- to Cl_2 at E^0= 1.36 V, which hydrolyses to HClO which can oxidise As(III) (Luna-Trujillo et al., 2020; Hansen et al., 2010; Sirés et al., 2014). 5) Direct oxidation of Cl^- and formation of HClO at E^0= 1.49 V, which can oxidise As(III) (Berger, 1987; Luna-Trujillo et al., 2020).

In this research, the focus was on i because it was more straightforward to measure than E. However, the exact i per reaction was beyond the scope of this research, since this research focused on the anodic performance of the RuO_2/IrO_2-coated anode. In addition, the applied charge dosage (q) [C/L], was a parameter of interest, since it included the hydraulic retention time (HRT), indicated by the flow rate, and the supplied I. q was calculated by dividing the supplied I [A] by the flow rate [L/s] (Equation 9).

$$q = \frac{I}{\text{flow rate}} \qquad (9)$$

2.2.2 Anodic Oxidation of Arsenic

Demineralized water was used as feed water to exclude the influence of other naturally occurring constituents. Chemicals that were added to the demineralized water were NaCl and $NaHCO_3$, with concentrations representative for water at Dunea (Table 6, Supplementary Information 6.6) (Dunea, 2021). NaCl was used as electrolyte to provide the desired conductivity. In addition, $NaHCO_3$ was

added to the feed water to increase the alkalinity and acted as pH buffering agent. The feed water of the anode was spiked with 3.47 mg sodium (meta)arsenite ($AsNaO_2$), resulting in an As(III) concentration of 80 μg/L. Relatively high As concentrations were used in the oxidation experiments to be able to distinguish oxidation patterns. The pH of the anodic feed water varied between 8.0 and 8.2 and the temperature was approximately 8 °C.

During the anodic oxidation experiments, the As(III) oxidation was measured for i between 0 and 7.5 A/m^2 and a constant hydraulic retention time (HRT) of 2.3 min. After that, the As(III) oxidation was measured for a constant q of 20 and 30 C/L for a i in the range of 1.5-9 A/m^2 and 4.5-15 A/m^2, respectively. No experiments were performed for a q of 20 C/L, with a i of 1.5 and 3 A/m^2, since no significant As(III) oxidation was assumed to be obtained based on observed results with a q of 30 C/L. The As(III) oxidation was expressed in percentage oxidised [%] and calculated by Equation 10.

$$\text{As(III) oxidation} = 1 - \frac{\text{Measured As(III)}}{\text{Influent As(III)}} * 100 \tag{10}$$

The energy consumption of the eAOP cell [kWh/m^3] was determined by reading the cell operational voltage (V) [V] of the cell. Experiments were performed with a i in the range of 0.5-7.5 A/m^2 and a constant flow rate of 5.2 L/h and experiments with a i in the range of 1.5-9 A/m^2 with a constant q of 30 C/L. The operational V together with I (Equation 7) were used to calculate the energy consumption (Equation 11). The flow rate was converted from [L/h] to [m^3/h] by dividing 5.2 L/h by 1000. Additionally, the energy consumption could be calculated by multiplying V and q and dividing by 3.6 to obtain [kWh/m^3] (Equation 12).

$$\text{Energy consumption} = \frac{V * I}{\text{flow rate}/1000} \tag{11}$$

$$\text{Energy consumption} = \frac{V * q}{3.6} \tag{12}$$

The potentiostat was used to measure the corresponding E and i. This gave insight in the theoretical i that was needed for reactions (Figure 11). In addition, the potentiostat was used to set the E to 0.89 V vs SHE (E^0 for ClO$^-$ formation). The free chlorine concentration was measured after eAOP cell passage to see whether the theoretical ClO$^-$ formation matched the observations. The purpose of these measurements was to measure the E instead of observing the As(III) oxidation. Therefore, As(III) was excluded during the anodic feed water matrix (Table 6).

2.2.3 Free Chlorine Formation

Free chlorine was expected to contribute to As(III) oxidation in previous experiments by indirect oxidation. As a result, measured free chlorine concentration were expected to be lower than the actual produced free chlorine concentrations. In order to quantify the possible free chlorine formation, experiments were performed with exclusion of As(III) in the anodic feed water matrix (Table 6). The other constituents remained unchanged. The free chlorine concentrations were measured in [mg/L] for a i between 4 and 26 A/m^2 and a q of 20 C/L and for a i between 4 and 40 A/m^2 and a q of 40 C/L. Due to disturbances by NaCl, the spectrometer results showed elevated free chlorine concentrations. To correct for these errors, the free chlorine concentration of the feed water was subtracted from the measured free chlorine concentration.

2.2.4 Quantification of Cathodic Base Formation

As explained, anodic oxidation resulted in the formation of H^+, whereas cathodic reduction resulted in OH^- production. The cathodic performance depends on the OH^- production calculated by PHREEQC models (PHREEQC 3, with 'PHREEQC.DAT' database). Anodic and cathodic effluent pH measurements with a i between 1.5 and 12 A/m^2 were used as input data, together with the feed water concentrations (Table 6). The feed water pH and temperature were set to 8.04 and 8 °C, respectively. The PHREEQC models were created by Kraaijeveld (2022) (Supplementary Information 6.7). Model 1 was used to determine the amount of OH^- formation that was needed to increase the feed water pH to the measured cathodic effluent pH. Model 2 was used to calculate the amount of produced H^+ at the anode, based on feed water and anodic effluent pH. The produced H^+ was translated to the amount of OH^- needed to buffer the pH decrease (Equation 13).

$$H^+ + OH^- \rightarrow H_2O \tag{13}$$

The theoretical H^+ and OH^- production were calculated according to Faraday's law (Equation 14) (Sundén, 2019). m is the produced H^+ or OH^- [g] (in general, the amount of species produced or consumed at the electrode), Q_c is the total electric charge transferred to or from the electrode [C], MW is the molecular weight [g/mol] and n and F are similar as in Equation 8 (Comninellis & Chen, 2010; Arnau, 2004). Q_c is calculated by multiplying I [A] ([C/s]) by the time (t) [s] (Equation 15) (Sundén, 2019). In this research, the amount of electrochemical produced species (M) was presented in [mmol/L] (Equation 16).

$$m = \frac{Q_c * MW}{n * F} \tag{14}$$

$$Q_c = I * t \tag{15}$$

$$\text{M} = \frac{q * 1000}{n * F} \tag{16}$$

To allow for a fair comparison of experimental results, the produced H^+ and OH^- in [mmol/L] were converted to [mmol/h] by multiplying the results by the flow rate [L/h] (Equation 17) (Kraaijeveld, 2022).

$$\text{M [mmol/h]} = \text{M [mmol/L] * flow rate [L/h]} \tag{17}$$

It was assumed that the anodic effluent pH had to be returned to the orginal value of the feed water (8.04). This lowered pH affects the Saturation Index (SI) (Equation 18) (Delft, n.d.). The SI could decrease to < 0 by a lowered pH, indicating that the water is corrosive. Corrosive water may cause release of pipeline materials, including (toxic) metals, and could result in water leakages (Davil et al., 2009; Shams et al., 2012). To sustain for a desired SI (around 0), the low anodic effluent pH could be buffered by produced cathodic effluent (Figure 56, Supplementary Information 6.8). The required amount of OH^- that should be dosed to the anodic effluent was considered as a loss, since this OH^- could not be used for PS.

$$\text{SI} = \text{pH} - \text{pH}_s \tag{18}$$

2.3 Sampling and Chemical Analysis

During the fieldwork, dune filtrate was extracted from the MPs and MWs by a pump and was evacuated for at least 15 minutes prior to measuring and sampling. Water samples from sampling points in the DWTP were collected from taps. Dissolved oxygen (DO), electrical conductivity (EC), oxidation reduction potential (ORP), pH and temperature were measured in the field by a flow cell. Four devices were used for DO (FDO® 925), EC (TentraCon® 925), ORP (SenTix® ORP-T 900) and pH and temperature (SenTix® 940) measurements. The other quality parameters were measured in the laboratory by ICP-MS (Analytikal Jena model PlasmaQuant MS ICP-MS) and IC (Metrohm 881 Compact IC pro and 883 Basic IC plus). Four sample categories were prepared; filtered, filtered + acidified, unfiltered + acidified and resin-filtered + acidified. 0.2 μm membrane filters were used for filtration. In the acidified samples, 0.1 mL of 69 % HNO_3 was added to approximately 9.9 mL sample to get a 1% v/v acidification. Acidification caused dissolution of all solids and ending of all chemical reactions.

Filtered (non acidified) samples were prepared for IC analysis to measure Cl^-, NO_3^- and SO_4^{2-}. Some samples used the cuvette test (HACH®, 1-60 mg/L NO_3^- and Spectroquant® NOVA 60) to measure the NO_3^- concentration, as this was easier and faster compared to the IC analysis. After the samples were taken, they were stored in ice to ensure reactions would not take place. Acidified filtered and unfiltered samples were used to measure the dissolved and total TEs concentrations, respectively, by ICP-MS analysis. The resin-filtered samples were used for As(III) speciation according to the Clifford method (Karori et al., 2006). In this method, the filtered sample went through a syringe with the strong-base anion resin (Amberlite® IRA-402 Cl), which retained dissolved As(V). As a result, only As(III) passed the resin and ended in the filtrate, consequently being measured by ICP-MS analysis. The detection limit of the ICP-MS was 1 μg/L.

During eAOPs experiments, 10 mL samples were collected after 5 times the HRT to ensure representative samples. The collected samples were filtered and passed the strong-base anion resin for As(III) speciation (Clifford method) and were analysed by ICP-MS (Karori et al., 2006). Furthermore, the pH of the anode and cathode were measured (SenTix® 940). The pH was measured to ensure it was in the range of 6-9 and As(V) could effectively be removed by the resin. In addition, pH measurements were used to quantify cathodic OH^- production. The free chlorine concentrations were measured by the free chlorine test kit (Spectroquant®, 0.010-6.00 mg/L Cl_2 and the Spectroquant® NOVA 60).

3 Results

In this chapter, the results of the fieldwork and laboratory experiments will be presented. In the first section, the spatial analysis of groundwater constituents will be shown. Then a hydrochemical depth profile of TEs will be created to identify the As-bearing layer, followed by the fate of As during existing treatment. Thereafter, the results of the eAOPs experiments will be presented in the second section, which consists of the anodic As(III) oxidation, followed by the energy consumption of the eAOP cell. Then the formation of free chlorine will be shown and finally the cathodic base production will be presented.

3.1 Arsenic Origin at Solleveld

Fieldwork results are presented in order to answer the first research question.

3.1.1 Spatial Analysis of Groundwater Constituents

In this paragraph, the measured DO, ORP and groundwater constituents including As, Fe, NO_3^-, SO_4^{2-} are shown. To indicate in the graphs to which pipe (Duinwinning or Randwinning) and wells a MP is connected, the Duinwinning points are filled and the Randwinning points are open. VOW concentrations, which was the raw water, are indicated with dotted lines.

DO and ORP
Figure 12 shows the DO and ORP measurements in the sampling locations. Note that no flow cell measurements were carried out at MP 3 due to a high amount of air bubbles in the tube. Results showed DO and ORP values between 0.2 and 2.0 mg/L and -151.9 and 44.4 mV, respectively. It was observed that the MPs from Randwinning had DO values > 1 mg/L, identified as oxic water (Table 1). In addition, the Randwinning MPs showed positive ORP values, indicating oxidising conditions. The MPs from Duinwinning had DO values $\leq$ 0.65 mg/L and only MPs 4 and 5 showed DO values that were > 0.5 mg/L. Therefore, MPs from Duinwinning were identified as anoxic, except for MPs 4 and 5, which were identified as oxic. The ORP values were negative, except at MP 4 where the ORP was slightly positive, 13 mV. In general, the MPs of Duinwinning showed reducing conditions.

The strong positive correlation between DO and ORP, with a Pearson coefficient of 0.76, is shown in Figure 13. Results showed that the DO and ORP were higher for Randwinning than for Duinwinning, with average DO values of 1.8 and 0.4 mg/L and average ORP values of 32.4 and -45.0 mV, respectively. This higher DO and ORP were assumed to be caused by varying groundwater tables in relation to the ground level. The ground levels were lower at Randwinning than at Duinwinning, leading to a smaller distance between ground level and groundwater table at Randwinning wells. This resulted in more oxygen intrusion (higher DO) and a higher ORP at Randwinning.
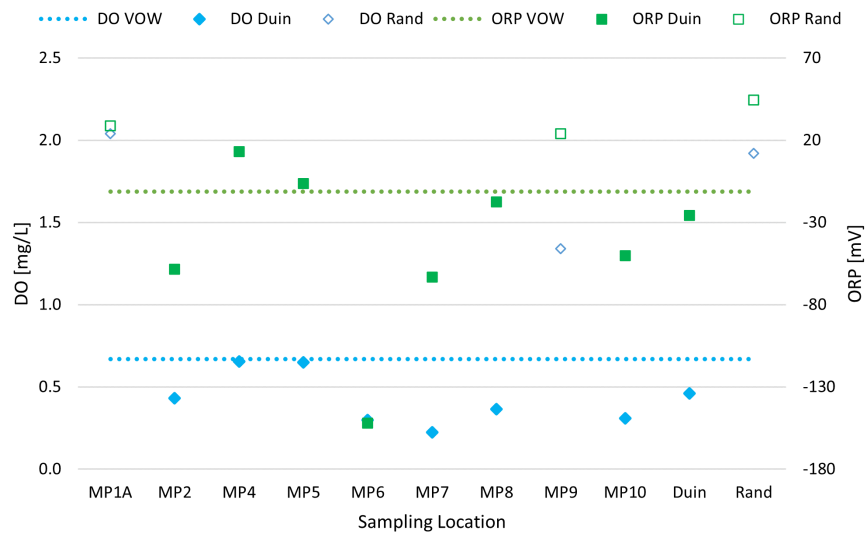
Figure 12: Concentrations DO [mg/L] and ORP [mV] in Sampling Locations.
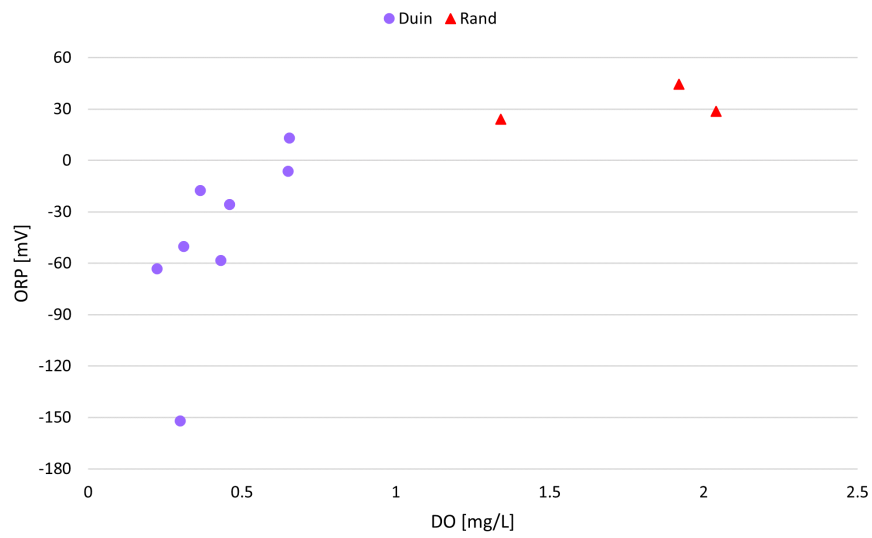
Figure 13: DO [mg/L] versus ORP [mV].

Arsenic

Figure 14 shows the measured total As and dissolved As concentrations in the sampling points. Results showed that the total As and total dissolved As concentrations ranged from 3.1 to 13.0 µg/L and from 2.4 to 8.2 µg/L, respectively. The measured dissolved As(III) and As(V) concentrations in the sampling points are depicted in Figure 15. Concentrations ranged from < 1 to 3.4 µg/L and from 2.4 to 8.2 µg/L for As(III) and As(V), respectively. Results of MP 1A (0.90 µg/L) and MP 8 (0.62 µg/L) were below the detection limit of ICP-MS and were therefore indicated as < 1 µg/L. Remarkable was the high total As concentration of 13.0 µg/L in MP 3. Furthermore, the observed As(III) concentration was relatively high at that point, however not as outstanding as total As. Second measurements were carried out in MP 3 for verification and these results are indicated with crosses.

During the second measurements, the observed concentrations total As and As(III) decreased by 3.6 µg/L (to 9.4 µg/L) and 0.5 µg/L (to 2.9 µg/L), respectively, whereas the concentration As(V) increased by 1.5 µg/L (to 6.4 µg/L). Although MP 3 showed a lower total As concentration during the second measurements, all observed As concentrations were still high compared to the other MPs. However, the difference was not as significant as observed in the first results.

Duinwinning MPs showed a slightly higher total As concentration than Randwinning MPs with measured concentrations of 5.6 and 3.8 µg/L, respectively. The total dissolved As concentration was approximately similar for Duinwinning and Randwinning MPs with measured concentrations of 5.4 and 4.8 µg/L, respectively. The dissolved As(III) was slightly higher for Duinwinning than for Randwinning MPs, with measured concentrations of 2.0 and 1.1 µg/L, respectively. The dissolved As(V) was higher for Randwinning than for Duinwinning MPs with measured concentrations of 3.7 and 3.3 µg/L, respectively.
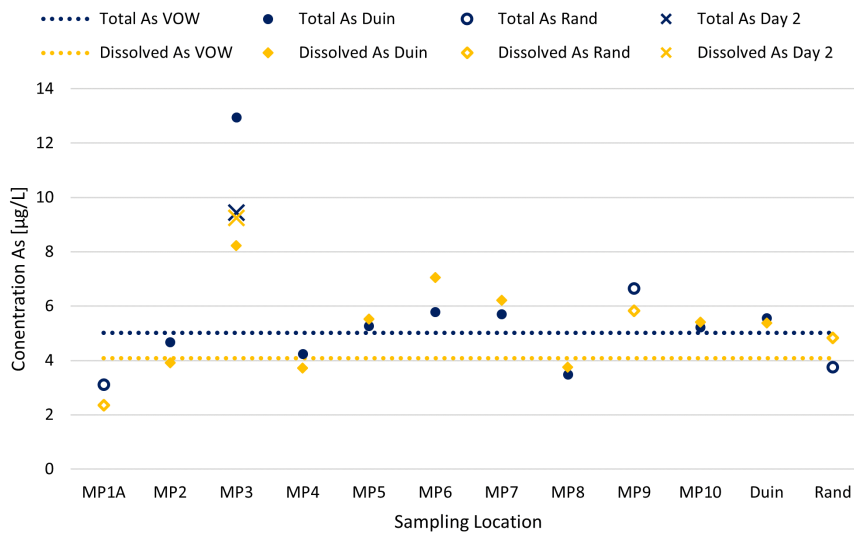
Figure 14: Concentrations of Total As and Dissolved As [µg/L] in Sampling Locations.
Second measurement results in MP 3 are indicated with crosses.
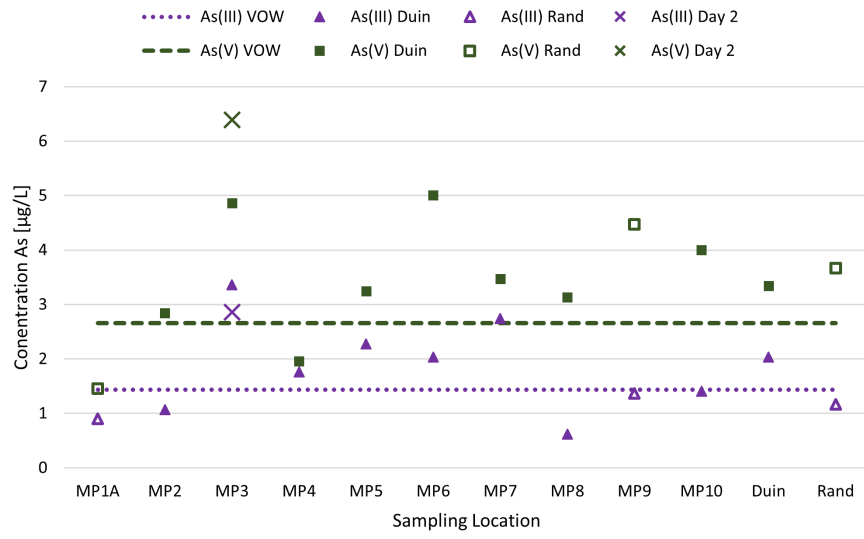
Figure 15: Concentrations of Dissolved As(III) and As(V) [µg/L] in Sampling Locations.
Second measurement results in MP 3 are indicated with crosses.

Iron

Figure 16 depicts the measured total and dissolved Fe concentrations in the sampling points. Results showed that the total Fe and dissolved Fe concentrations ranged from 0.1 to 1.2 mg/L and from 0.03 to 0.2 mg/L, respectively. Second measurement results at MP 3 are indicated by crosses. Observed total Fe concentrations during second measurements showed a significant decrease from 1.2 to 0.16 mg/L. Dissolved Fe results showed approximately similar concentrations of 0.16 and 0.13 mg/L during first and second measurements, respectively. Moreover, results showed approximately similar total and dissolved Fe concentrations during the second measurements, indicating that almost all Fe was present as Fe^{2+}. This was in contrast to the first measurements, during which almost all Fe was present as particulate Fe (Total Fe - dissolved Fe).
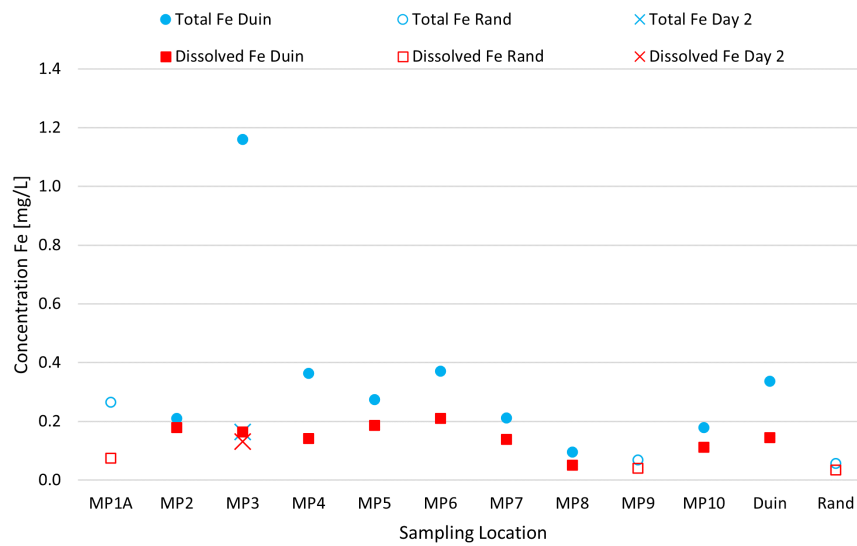
Figure 16: Concentrations of Total Fe and Dissolved Fe [mg/L] in Sampling Locations.
Second measurement results in MP 3 are indicated with crosses.

Nitrate and Sulfate

Figure 17 depicts the measured NO_3^-, SO_4^{2-} and total As concentrations in the sampling locations. Observed NO_3^- and SO_4^{2-} concentrations ranged from 1.7 to 4.2 mg/L and from 34 to 44 mg/L, respectively. Randwinning MPs showed higher NO_3^- concentrations than Duinwinning MPs with measured concentrations of 3.8 and 2.2 mg/L, respectively. Furthermore, higher SO_4^{2-} concentrations were observed at Randwinning MPs with measured concentrations of 42.6 mg/L at Randwinning and 39.8 mg/L at Duinwinning.
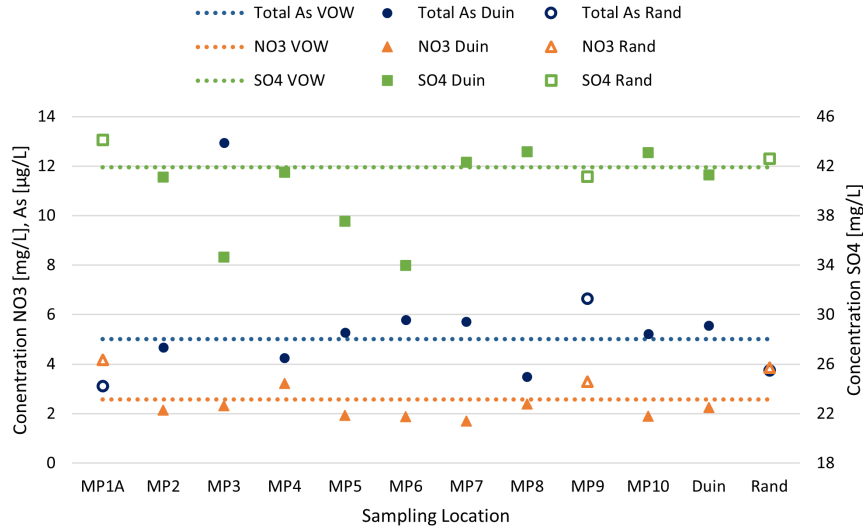
Figure 17: Concentrations of Total As [µg/L], NO_3^- and SO_4^{2-} [mg/L] in Sampling Locations.

Figure 18 shows the concentration DO versus NO_3^-. A very strong positive correlation between DO and NO_3^- concentration was observed with a Pearson coefficient of 0.94. Measured DO values were in the range of 1.3-2.0 mg/L and 0.2-0.7 mg/L for Randwinning and Duinwinning MPs, respectively. Measured NO_3^- concentrations were in the range of 3.3-4.2 mg/L and 1.7-3.2 mg/L for Randwinning and Duinwinning MPs, respectively, showing that higher DO and NO_3^- concentrations were found at Randwinning than at Duinwinning MPs.
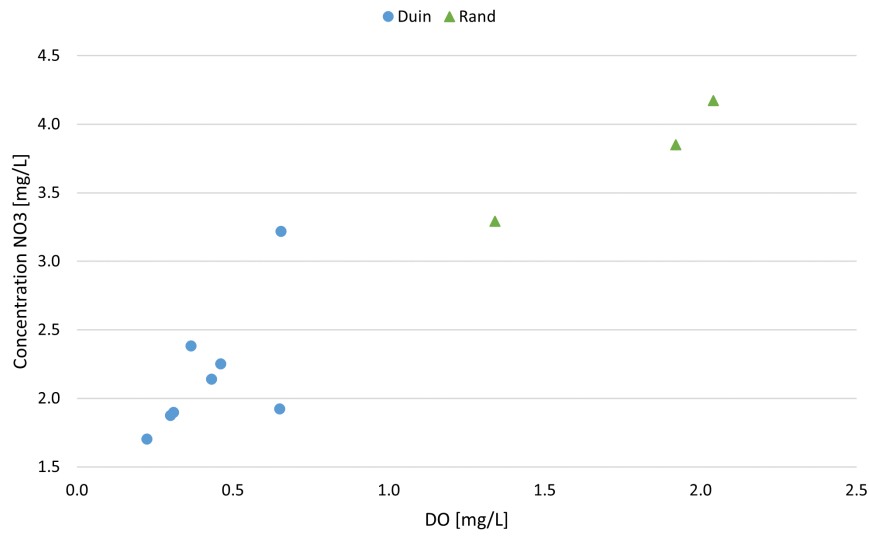
Figure 18: DO [mg/L] versus NO$_3^-$ [mg/L].

Figure 19 shows the moderate negative correlation between total As and NO$_3^-$ with a Pearson coefficient of -0.49. Measured total As values were in the range of 3.1-6.7 μg/L and 3.5-9.4 μg/L for Randwinning and Duinwinning MPs, respectively. The outlier was caused by the high measured total As concentration at MP 3. Except for this outlier, there was only a minor difference in total As concentrations between Randwinning and Duinwinning. This was in contrast to the observed differences in DO and NO$_3^-$ concentrations between Randwinning and Duinwinning.
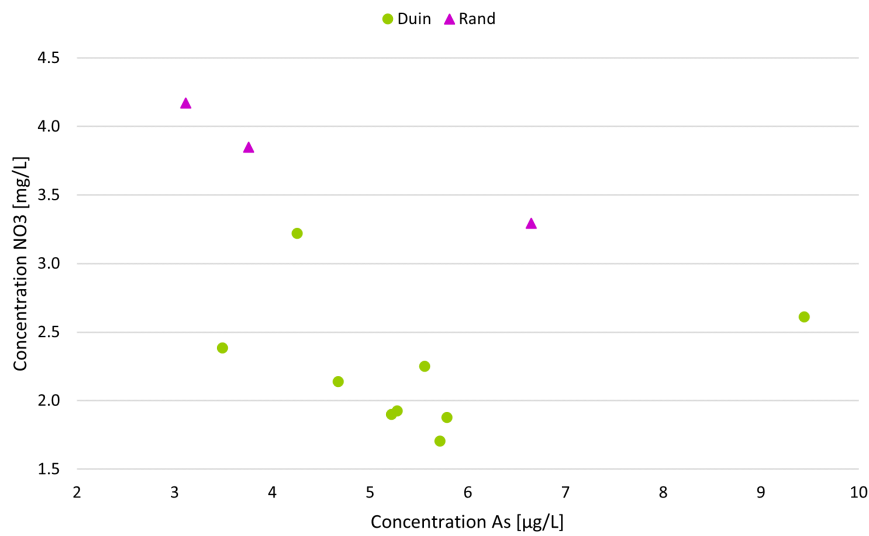
Figure 19: Total As [μg/L] versus NO$_3^-$ [mg/L].

Figure 20 shows the strong negative correlation between As and SO_4^{2-} with a Pearson coefficient of -0.72. Measured SO_4^{2-} concentrations were in the range of 41.2-44.1 mg/L and 34.0-43.1 mg/L for Randwinning and Duinwinning MPs, respectively, showing that SO_4^{2-} concentrations were found at Randwinning than at Duinwinning MPs.
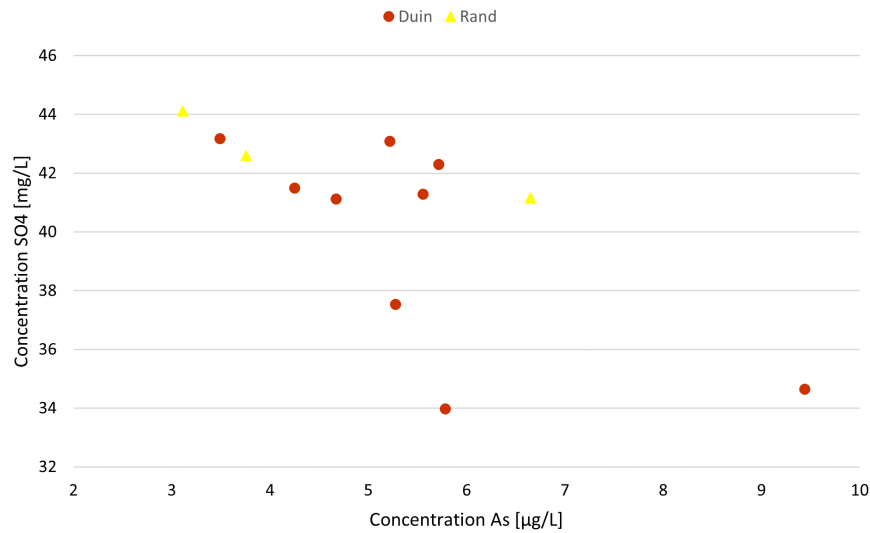
Figure 20: Total As [μg/L] versus SO_4^{2-} [mg/L].

3.1.2 Identification Arsenic-Bearing Layer

To identify the As-bearing layer, a hydrochemical depth profile was created from the measurements at MWs X (Figure 7). Figure 21 depicts the results of the dissolved TEs concentrations. The groundwater table was at -0.2 m and the ground level at +3.3 m. Although both Figures (5 and 21) showed a hydrochemical profile, it was hard to compare the two profiles due to absence of NO_3^-, Cl, U and MO in Figure 21. Cl and U concentrations were not measured by ICP-MS or IC and MO was not depicted because this TE was not relevant for As mobilisation. The NO_3^- concentrations were not depicted because they were below the detection limit of 1 mg/L NO_3^-. Results showed As mobilisation between -3 and -6 m and a decrease in concentration with depth. The observed As concentration was 14.9 µg/L at -3 m and decreased to 2.2 µg/L at -6 m. A slight increase in concentration was shown at depths > -9 m from 0.20 to 0.96 µg/L. However, 0.20 µg/L was below the detection limit of ICP-MS, which made this data inaccurate. Although the results showed that As originated from the layer between -3 and -6 m, the exact As-bearing layer could not determined. This was due to the lack of measurements at depths < -3 m.

Results showed an Fe concentration of 0.5 mg/L at -3 m and a decrease to 0.3 mg/L at -9 m. From -9 m, Fe slightly increased to 0.7 mg/L at -15 m. Mn concentrations were 3.7 mg/L (multiplied by 10) at -3 m and increased to 17.4 mg/L at -12 m. At -15 m, the concentration decreased to 15.0 mg/L. Co results showed 0.4 µg/L at -3 m and no Co was observed at depths > -3 m. It was observed that Ni concentrations decreased from 4.0 µg/L at -3 m to 1.6 µg/L at -15 m. At -3 m, the observed Zn concentration was 6.0 µg/L. It decreased to 2.4 µg/L at -12 m and slightly increased to 3.1 µg/L at -15 m.
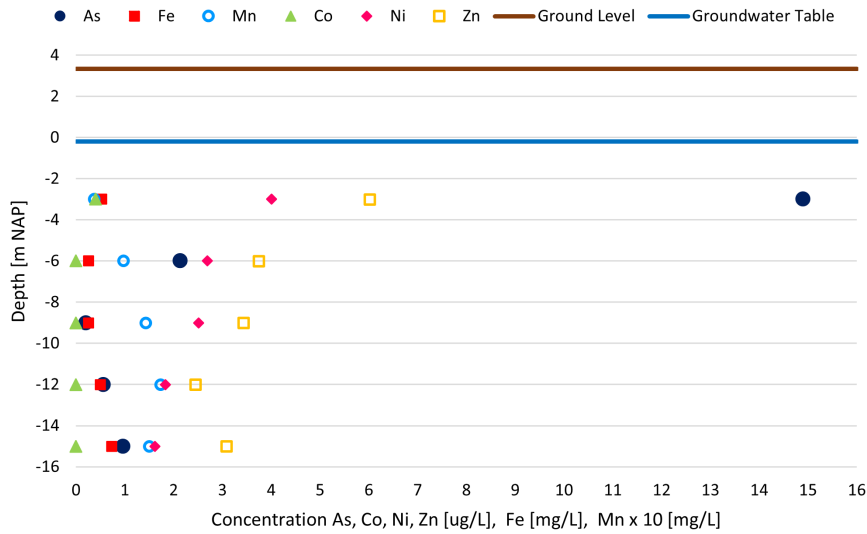
Figure 21: Concentrations Trace Elements in MWs X. Dissolved As, Co, Ni, Zn [µg/L] and Fe [mg/L] and Mn x 10 [mg/L]. Concentrations are depicted at -3, -6, -9, -12 and -15 m. The ground level was at +3.3 m and the groundwater table was at -0.2 m.

Figure 22 shows DO results in MWs X. Results showed approximately constant DO concentrations of 0.16 mg/L, except at -6 m where the DO was 0.34 mg/L. The O_2 concentrations were < 0.5 mg/L at each depth, meaning that no MW contained water from the oxic zone (Table 1). Hence, the oxic zone was assumed to be higher than -3 m (highest MW). In addition, the suboxic zone was not identified because the Fe concentrations exceeded 0.1 mg/L (Figure 21). It followed that each MW contained anoxic water. However, the redox processes that occurred varied per MW. Observed Mn^{2+} concentrations were higher than 0.05 mg/L in MWs 1-4 (Figure 21), indicating that Mn^{4+} reduction occurred from -6 m. Fe^{3+} reduction occurred simultaneously, since all measured Fe^{2+} concentrations were exceeding 0.1 mg/L. Unfortunately, SO_4^{2-} concentrations were not measured and therefore the SO_4^{2-} reduction zone was not identified. Observed ORP results showed reducing conditions at each depth, varying between -36.3 and -148.6 mV at -6 and -12 m, respectively.
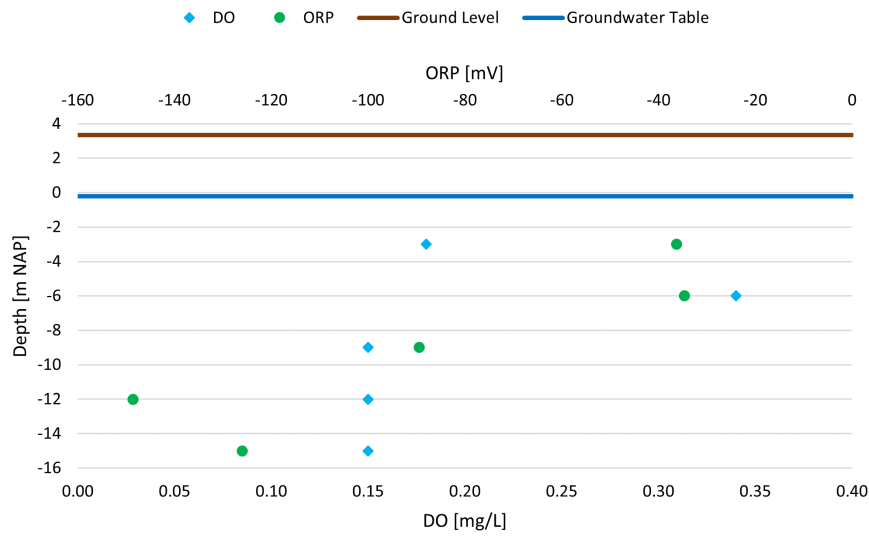
Figure 22: DO [mg/L] and ORP [mV] in MWs X.

Figure 23 depicts the pH results at the MWs X. Results showed a pH of 7.4 at -3 m and an increase in pH over depth. At -12 m, the highest pH of 7.8 was observed. Results showed an input pH of 7.9 in the infiltration water, which was higher than the pH measured at the MWs (Table 5). Therefore, it was assumed that the pH in the MWs was decreased due to acidifying processes.
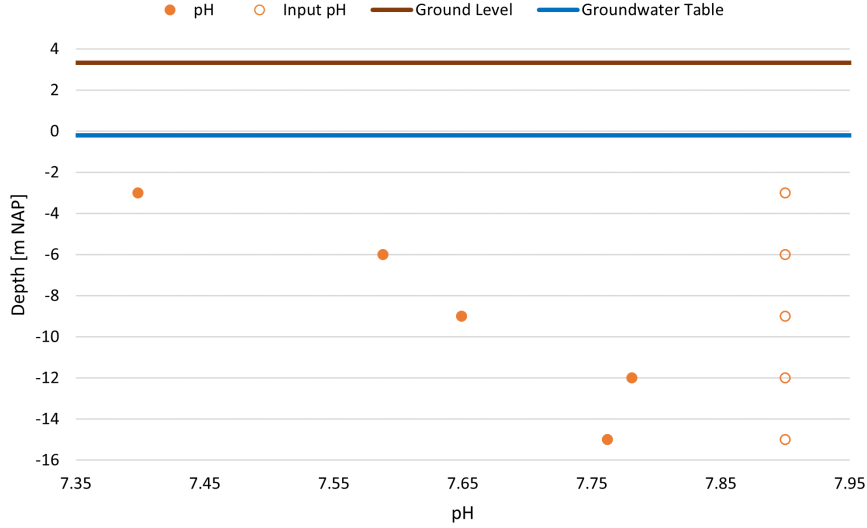
Figure 23: pH in MWs X. Input pH is indicated by open circles.

No similar hydrochemical depth profile was created from measurement results of MWs Y (Figure 51), since no As-bearing layer was observed. Results showed As concentrations of 1.6 and 1.0 μg/L at -3 and -15 m, respectively and concentrations below the detection limit of ICP-MS (1 μg/L) at the other depths. In addition, the NO_3^- concentrations were below the detection limit (1 mg/L). The observed As concentration in MW Z (Figure 52) was 1.6 μg/L at -2 m, indicating little As mobilisation. However, a NO_3^- concentration of 5.1 mg/L was measured, showing the presence of a NO_3^- layer at -2 m.

Infiltration water was mixed with rainfall of which the contribution was estimated at 6 % (Table 7, Supplementary Information 6.9). This allowed for determination of the NO_3^-, SO_4^{2-} and Cl^- concentrations in the mixed infiltration and rainwater, referred to as 'Input' (Table 2). Results showed a decrease in NO_3^- concentration of 2 mg/L, an increase in SO_4^{2-} concentration of 3.8 mg/L (+/- 3.9) and an increase in Cl^- concentration of 4.2 mg/L.

Table 2: Concentrations NO_3^-, SO_4^{2-} and Cl^- [mg/L]. Infiltration water and VOW concentrations are from (Dunea, 2022) and rainwater concentrations are from (Paulissen, 2007).

	Infiltration Water	Rainwater	Input	VOW
NO_3^-	2.9	2.4	2.9	0.9
SO_4^{2-}	46.9 (+/- 4.4)	2.6	44.3 (+/- 4.2)	48.1 (+/- 3.5)
Cl^-	48.0 (+/- 8.4)	3.4	45.3 (+/- 7.9)	49.5 (+/- 4.0)

Measured concentrations in MWs Y were used to create a SO_4^{2-} and Cl^- depth profile (Figure 24). At -3 m, similar measured and input SO_4^{2-} concentrations were observed of 44.3 mg/L. The SO_4^{2-} concentration at -6 m of 48.9 mg/L exceeded the input concentration. For depths > -6 m, the measured SO_4^{2-} concentrations were lower than the input SO_4^{2-} concentration with an observed decrease to 8.4 mg/L at -15 m. Measured Cl^- concentrations were higher than the input Cl^- concentration at each depth. The Cl^- concentrations increased between -3 and -15 m from 45.4 to 68.6 mg/L.
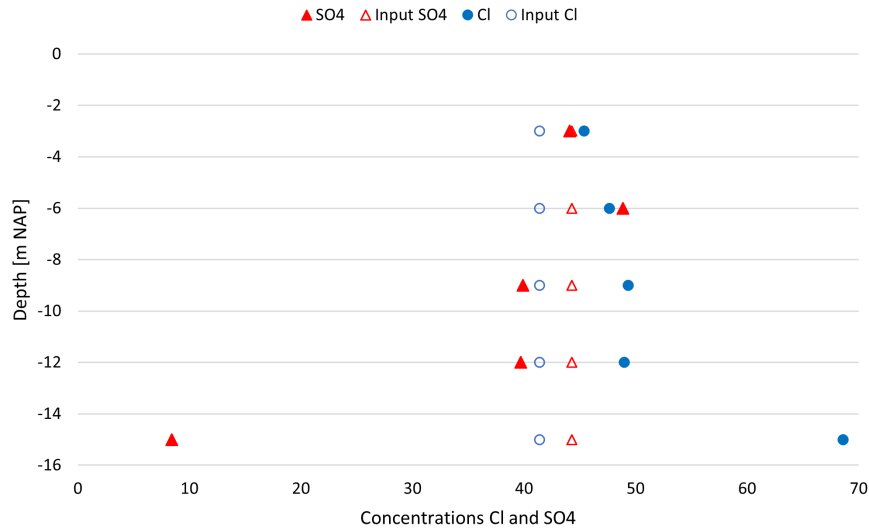
Figure 24: Concentrations SO_4^{2-} [mg/L] and Cl^- [mg/L] in MWs Y. Input concentrations are indicated by open symbols.

3.1.3 Fate of Arsenic during Existing Treatment

Figure 25 shows the dissolved As(III), As(V) and the bound As concentrations, which add up to the total As concentrations. Concentrations were measured at VOW, in the PS effluent and in the RSF influent and effluent. Important to take into account is that the PS effluent did not contain the bypass flow, while the bypass flow was included in the RSF influent. It was observed that the As(III) remained constant at 1.4 µg/L until the RSF, where all As(III) was oxidised by adsorption. Results showed that the As(V) concentration was higher in the RSF influent than in the PS effluent, which was assumed to be caused by the addition of the bypass flow. Moreover, measurement errors during analysis or during speciation according the Clifford method could have caused the higher As(V) concentration in the RSF influent (Karori et al., 2006). A decrease in As(V) concentration was observed from VOW to the RSF effluent from 4.3 to 3.1 µg/L, respectively. Bound As was observed at VOW with a concentration of 1.2 µg/L. After PS, all As was present as dissolved As(III) and As(V). It was observed that after RSF, all measured As was present as As(V) at a concentration of 3.1 µg/L, which was slightly lower than Dunea's measured concentration of 3.4 µg/L. These results showed that not all As(III) was oxidised to As(V) prior to RSF, leading to an elevated As(V) concentration in the drinking water. This shows the importance of complete As(III) oxidation by eAOPs prior to RSF to reach the company target of < 1 µg/L As.
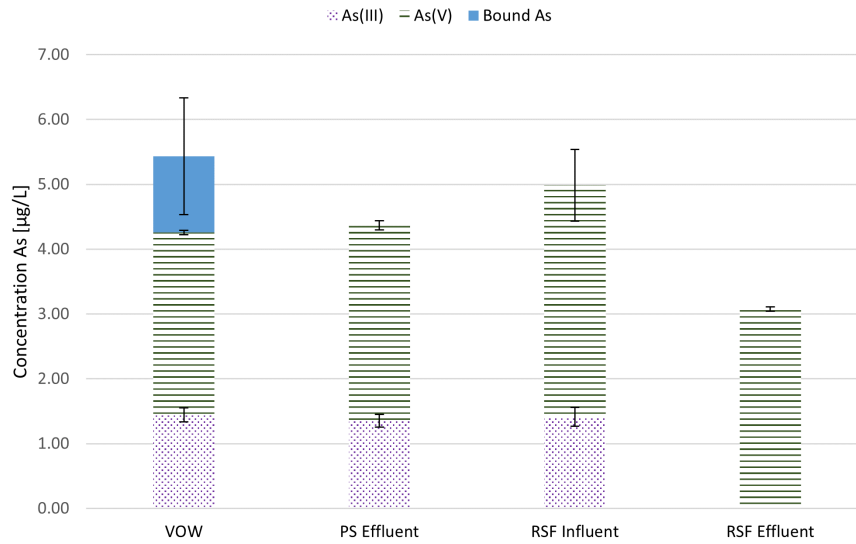
Figure 25: As(III) and As(V) Bound As Concentrations [µg/L] in the DWTP. As(III) (purple dotted bars), As(V) (green striped bars) and bound As (blue filled bars) are presented with standard deviation.

29

3.2 Outcomes of the eAOPs

The outcomes of the laboratory experiments are presented in order to answer the remaining three research questions.

3.2.1 Anodic As(III) Oxidation

The As(III) oxidation for increasing i [A/m^2] with a constant HRT of 2.3 min is presented in Figure 26. Results showed an increase in As(III) oxidation for an increase in i. Until 3.5 A/m^2, no As(III) oxidation was observed. It was assumed that the observed 20 % oxidation until 3.5 A/m^2 was caused by measurement errors caused by As(III) speciation according the Clifford method (Karori et al., 2006). For a i between 3.5 to 5.5 A/m^2, an increase in As(III) oxidation was observed, from approximately 25 to 84 %. At $i \geq 6$ A/m^2, a lower HRT could be selected as all As(III) had been oxidised for a HRT of 2.3 min. The observed relation between i (and q) and As(III) oxidation was non-linear. A very strong positive correlation between i (and q) and As(III) oxidation was obtained with a Pearson coefficient of 0.93. Besides the i, the q increased which could potentially caused the increase in As(III) oxidation. To quantify the effect of i on As(III) oxidation, while excluding q, experiments with a constant q were performed.
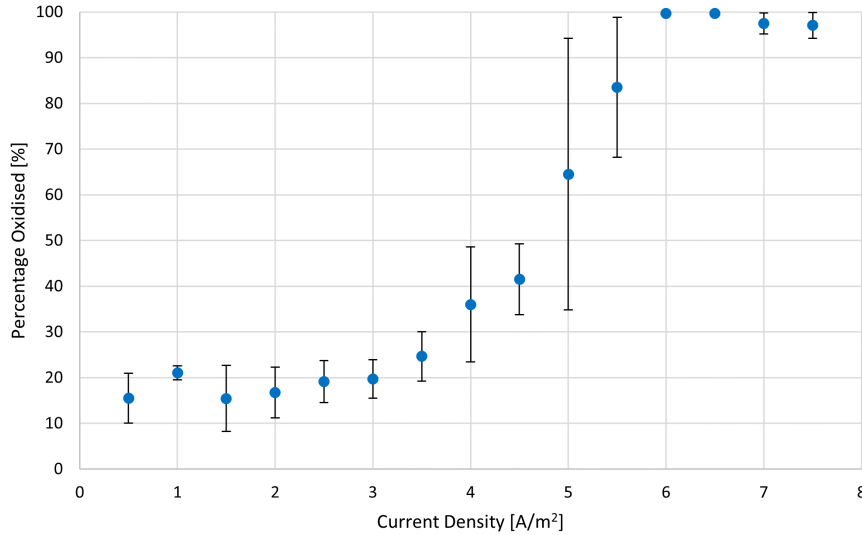
Figure 26: As(III) Oxidation [%] with a Constant HRT [min]. The oxidation As(III) is presented for a HRT of 2.3 min for increasing i [A/m^2] with the standard deviation.

In order to examine the effect of i on As(III) oxidation without a varying q, Figure 27 shows the As(III) oxidation with a constant q of 20 and 30 C/L for increasing i. Results showed that an increase in i for a constant q resulted in an increase in As(III) oxidation. Lower As oxidation was observed for a lower q. For a q of 20 C/L, the As(III) oxidation increased from approximately 34 to 96 % for a i between 4.5-9 A/m^2. At 12 A/m^2, 100 % As(III) oxidation was observed. The results showed a non-linear relation between i and As(III) oxidation with a strong positive correlation with a Pearson coefficient of 0.78. For a q of 30 C/L, the As(III) oxidation increased from approximately 30 to 98 % for a i between 1.5-7.5 A/m^2 and 100 % oxidation was observed at 9 A/m^2. A non-linear relation between i and As(III) oxidation was observed and a very strong positive correlation with a Pearson coefficient of 0.97.
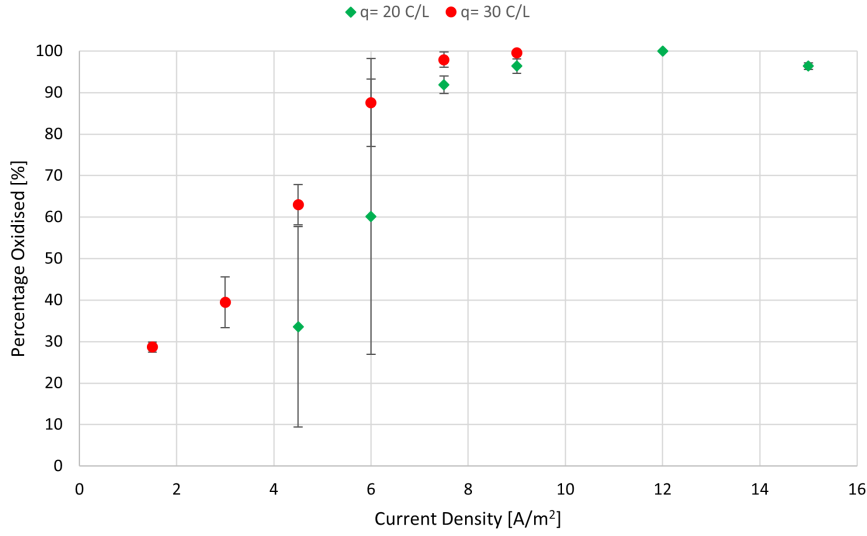
Figure 27: As(III) Oxidation [%] with a Constant q [C/L]. The oxidation is presented for a q of 20 and 30 C/L for increasing i [A/m^2] with the standard deviation.

Figure 28 shows the pH in the anode effluent for a constant HRT and increase in i and hence an increase in q. It was observed that the pH decreased from approximately 8.2 to 7.1 due to an increase in i (and q). A very strong negative correlation was found between i and pH with a Pearson coefficient of -0.99. Figure 29, on the other hand, shows the pH in the anode effluent for a constant q. During these experiments, the i increased, which implied that the flow rate increased correspondingly. Results showed a rather constant pH with values in the range from 7.27 to 7.33 for experiments with a constant q and increasing i (and flow rate).
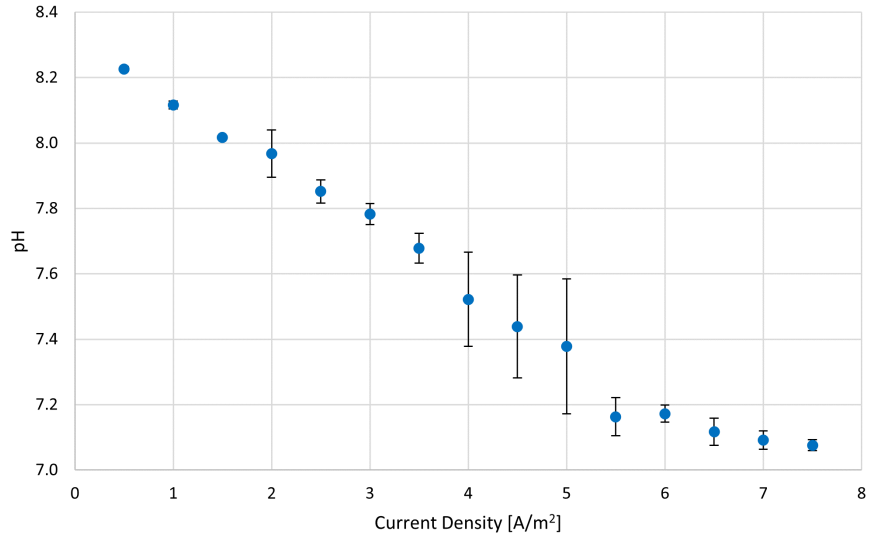
Figure 28: Anodic pH with a Constant HRT [min]. The pH is presented for a HRT of 2.3 min per i [A/m^2] with the standard deviation.
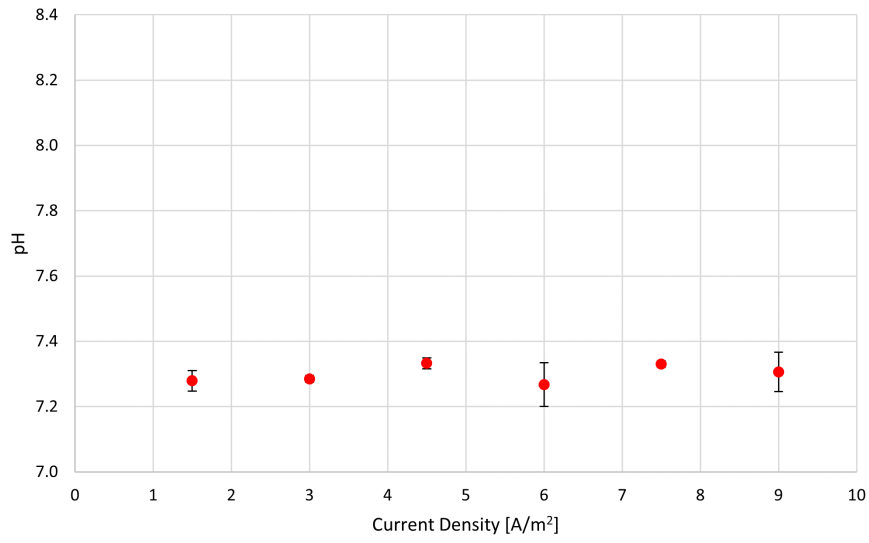
Figure 29: Anodic pH with a Constant q [C/L]. The pH is presented for a q of 30 C/L per i [A/m^2] with the standard deviation.

3.2.2 Energy Consumption eAOP Cell

Figure 30 shows the energy consumption of the eAOP cell [kWh/m^3] for increasing i in the range of 0.5-7.5 A/m^2 with a constant flow rate of 5.2 L/h. The energy consumption increased from approximately 0.002 to 0.13 kWh/m^3. Results showed that the energy consumption and i had a very strong positive correlation with a Pearson coefficient of 0.98 and the relation was observed to be non-linear. A doubled i (and q) gave an energy consumption that was approximately 3 times higher. Observed results of the operational V for increasing i (and q), showed that a doubled i resulted in a V multiplied by a factor of approximately 1.5 (Figure 57, Supplementary Information 6.10). Hence, the energy consumption was tripled by a doubled i.
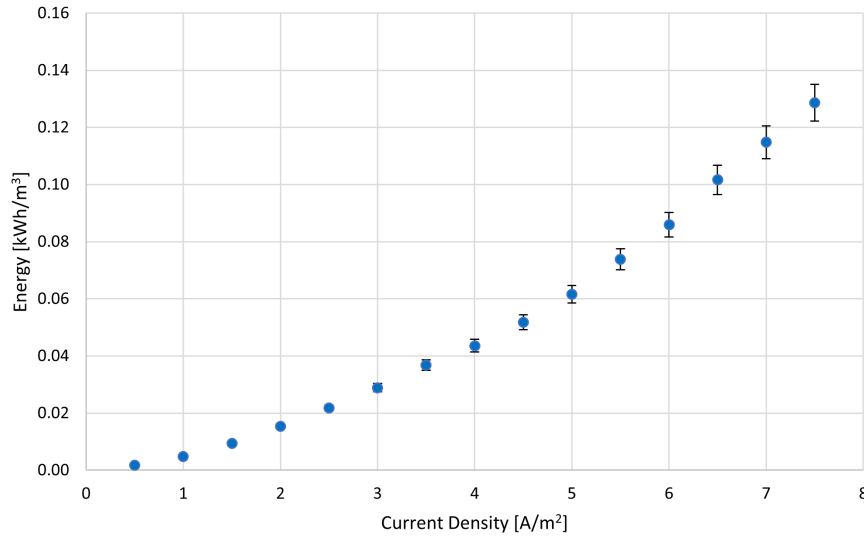
Figure 30: Energy Consumption Cell [kWh/m^3] with a constant HRT [min]. The energy consumption is presented for a constant HRT of 2.3 min per i [A/m^2] and standard deviation.

Figure 31 shows the energy consumption for increasing i in the range of 1.5-9 A/m^2 with a constant q of 30 C/L. The flow rate varied per measurement due to the constant q. Results showed that the energy consumption increased from approximately 0.035 to 0.075 kWh/m^3. A very strong positive correlation was observed between energy consumption and i with a Pearson coefficient of 1. A doubled i resulted in an energy consumption as well as operational V that were approximately 1.4 times higher (Figure 58, Supplementary Information 6.10).
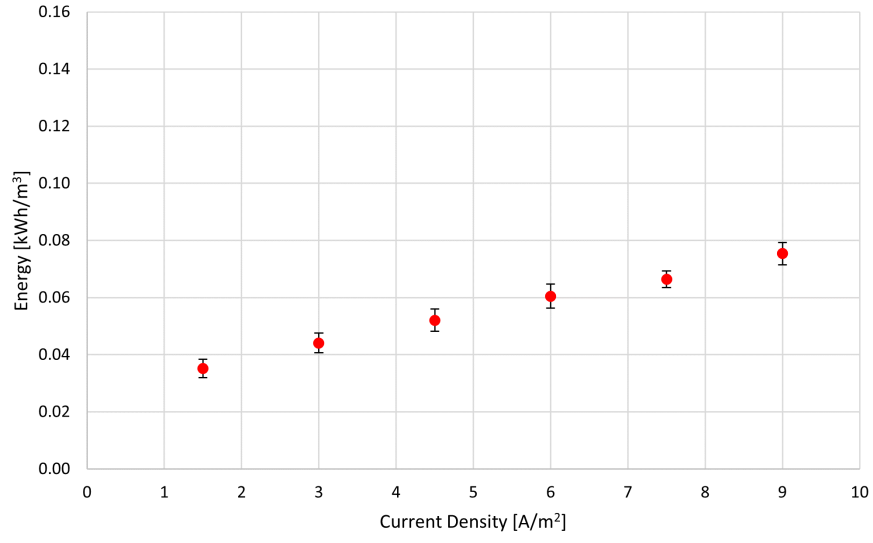
Figure 31: Energy Consumption Cell [kWh/m³] with Constant q [C/L]. The energy consumption is presented for a constant q of 30 C/L per i [A/m²] and standard deviation.

3.2.3 Anodic Free Chlorine Formation

Figure 32 shows the free chlorine formation [mg/L] for a q of 20 and 40 C/L. Results showed an increase in free chlorine formation with increasing i for both q values. The maximum measured free chlorine concentration for a q of 20 C/L was 0.33 mg/L at a i of 26 A/m^2. The q reached its maximum of 1.29 mg/L at a i of 40 A/m^2. The increasing trend in free chlorine concentration was observed to be non-linear. Furthermore, the q was doubled by halving the flow and consequently doubling the HRT. Results showed that a doubled q (and HRT) led to more than a doubled free chlorine formation. The free chlorine increased by an average factor of 3.2 by doubling the HRT (and q). Stabilisation in free chlorine formation was observed for a q of 20 and 40 C/L from approximately 16 and 22 A/m^2, respectively. Results showed average stable concentrations of 0.29 (+/- 0.02) and 0.94 mg/L (+/- 0.14) for a q of 20 and 40 C/L, respectively. Very strong positive correlations were observed between i and free chlorine formation for both q values, with Pearson coefficients of 0.95 and 0.92 for a q of 20 and 40 C/L, respectively.
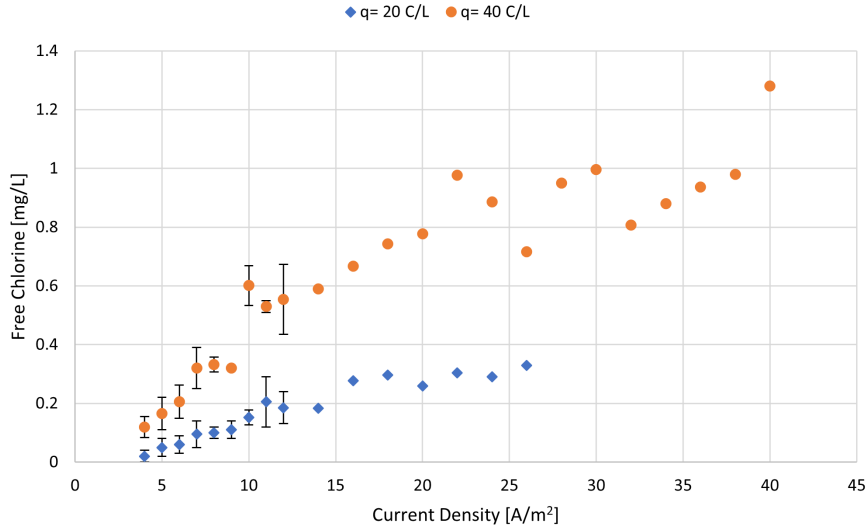
Figure 32: Free Chlorine Formation [mg/L] per i [A/m^2]. Results are presented for q 20 and 40 C/L with the standard deviation.

3.2.4 Cathodic e-softening

All results concerning cathodic OH^- production were performed with a constant flow rate of 2.2 L/h and a constant HRT of 5.5 min. Figure 33 shows the observed pH of the cathodic effluent for an increase in q [C/L] and therefore an increase in i [A/m^2]. The observed cathodic pH increased from 8.1 to 10.6.
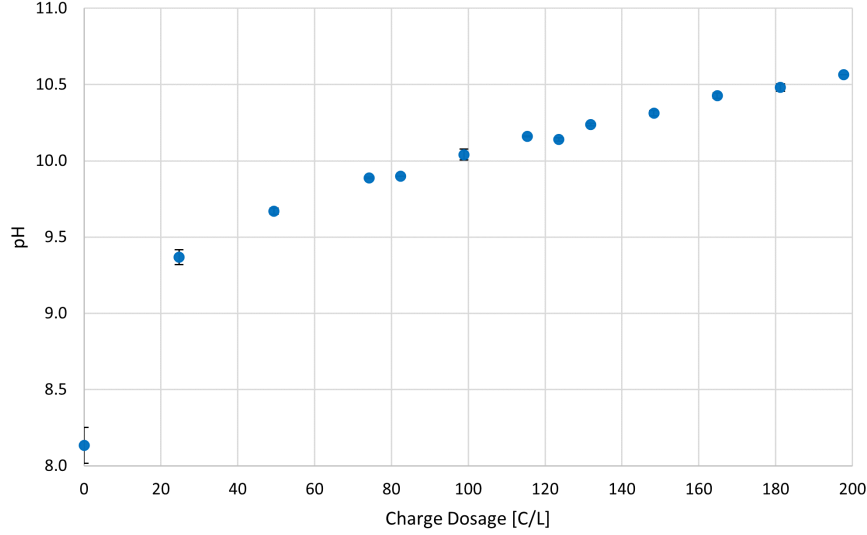
Figure 33: Cathodic pH for increasing q [C/L]. pH results are shown with the standard deviation.

The PHREEQC model was used to quantify the cathodic OH^- production. For each measured effluent pH value, the produced OH^- was estimated based on the feed water pH. The modelled results are shown in Figure 34, where the relation between OH^- dosing [mmol/L] and measured pH during the performed experiments is shown. Dosing additional OH^- resulted in a pH increase. The observed relation between dosing OH^- and pH was non-linear due to the presence of the pH buffer HCO_3^-, showing the relevance of using the PHREEQC model.

In addition, the PHREEQC model was used to determine the required OH^- dosage to compensate for the lowered anodic pH. The modelled results of dosed acid (H^+) and pH are shown in Figure 35. Results showed that dosage of H^+ resulted in a pH decrease. As with the OH^- dosing (Figure 34), a non-linear relation between dosed H^+ and pH was observed, showing the need of the PHREEQC model.
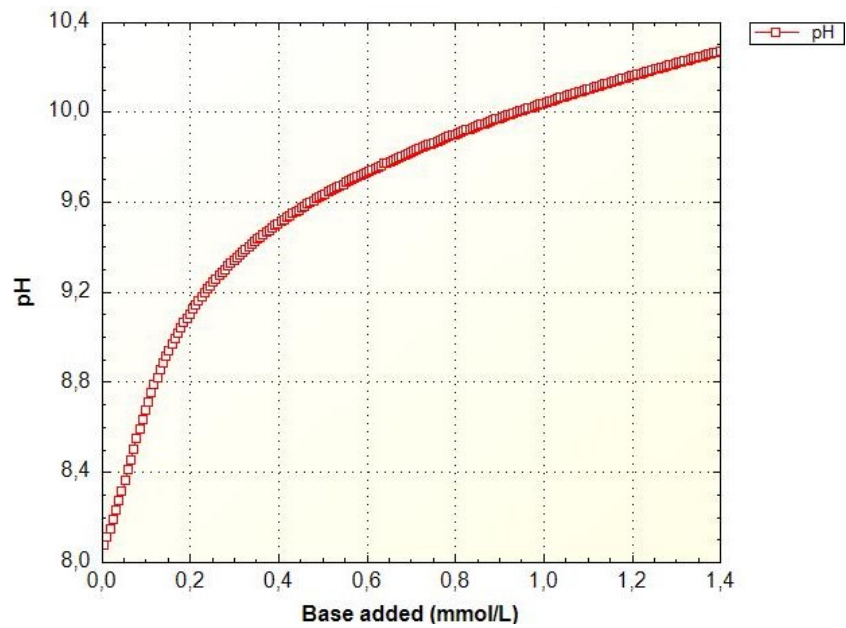
Figure 34: Modelled Effect of OH⁻ Dosing [mmol/L] on pH. PHREEQC output, from (Kraaijeveld, 2022).
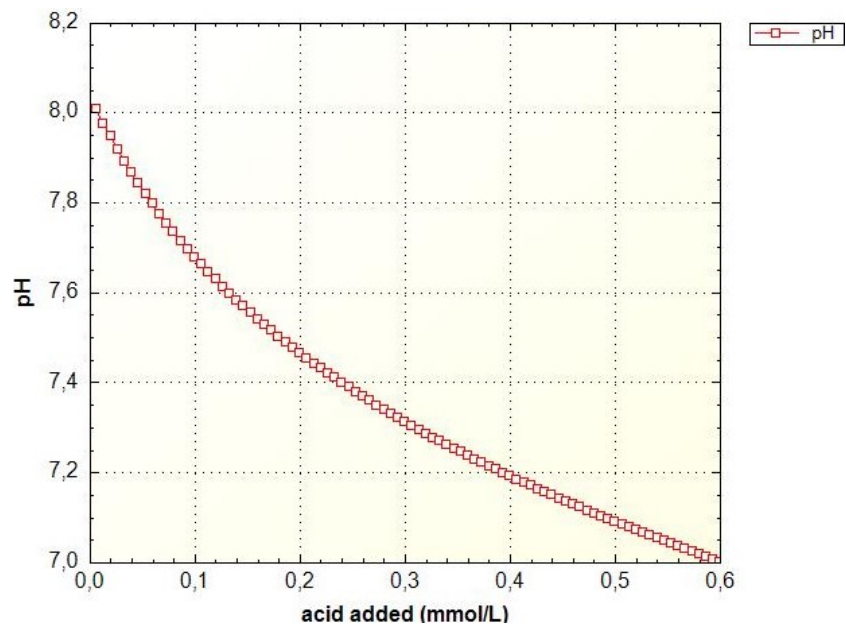
Figure 35: Modelled Effect of H⁺ Dosing [mmol/L] on pH. PHREEQC output, from (Kraaijeveld, 2022).

Figure 36 shows the modelled results of cathodic produced (blue) and anodic required (yellow) OH^- for increasing i. Cathodic produced OH^- results showed a linear increase between produced OH^- [mmol/h] and applied i (and q). A very strong positive correlation was found with a Pearson coefficient of 1. Anodic required OH^- results showed that more OH^- was required for increasing i (and q). This corresponded to the observed anodic pH results that showed a decrease in pH for increasing i (Figure 28). A non-linear relation was observed between i and required OH^- with a very strong positive correlation with a Pearson coefficient of 0.98. For low i, between 1.5 and 4.5 A/m^2, results showed higher produced OH^- than required OH^- for anodic pH buffering. At higher i between 5 and 7.5 A/m^2, however, the opposite was found, as more Na OH^- required than was produced. In general, the difference between produced and required OH^- was strongly dependent on supplied i.
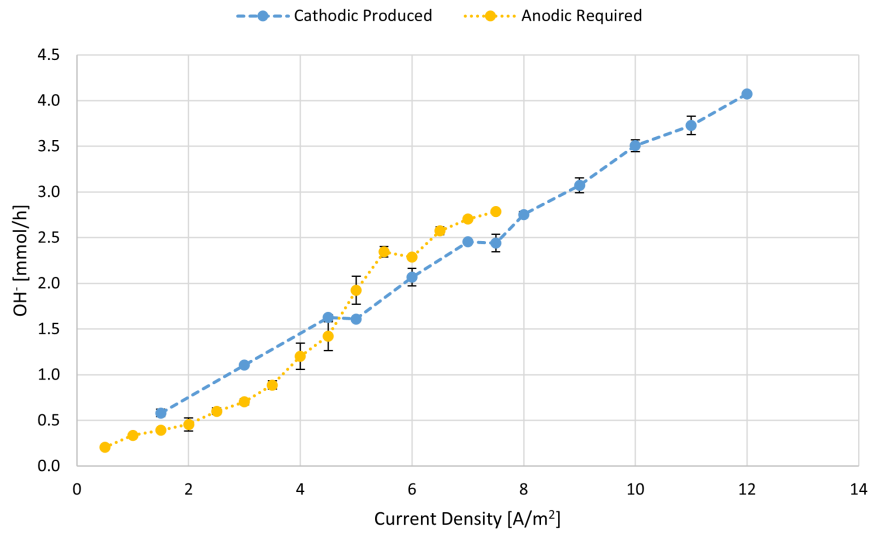
Figure 36: Produced Cathodic and Required Anodic OH^- [mmol/L]. Estimated by PHREEQC Model with standard deviation, from (Kraaijeveld, 2022).

3.2.5 Measured Potentials

The potentiostat was used to measure the E [V] at varying i [A/m^2] to obtain the relation between i and E. This was used to determine which theoretical reactions could possibly occur for a certain supplied i (Figure 11). Figure 37 shows the measured E for increasing i. It was observed that the i was 1 A/m^2 for a E between approximately 0.9 and 1.15 V and increased to 1.5 A/m^2 for a E of 1.2 V. At a E of 1.3 V, the observed i was 3 A/m^2 and a strong increase in i was found at $E > 1.3$ V.
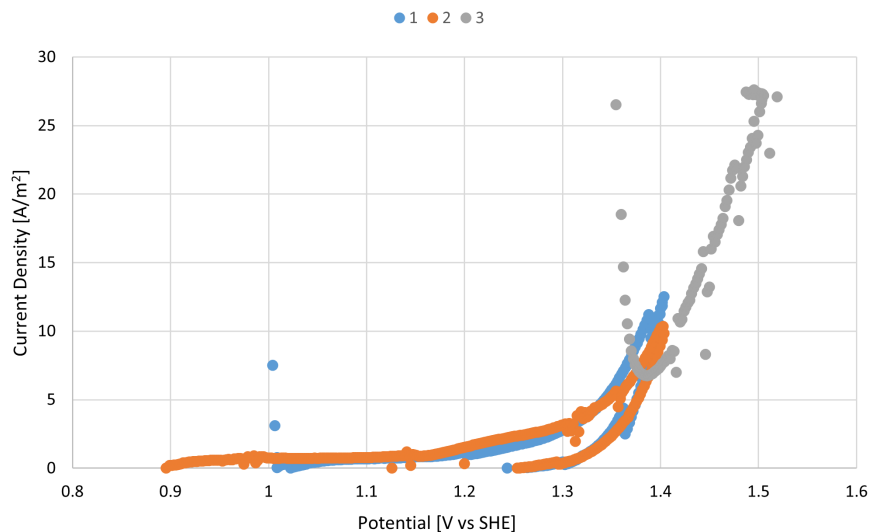
Figure 37: Measured E [V] for increasing i [A/m^2]. Results of three measurements are presented.

4 Discussion

In this chapter, the results of the fieldwork and laboratory experiments will be explained. In the first section, the presence of observed groundwater constituents will be analysed and explained. This is followed by analysing the possible As mobilisation processes. Then an As depth profile will be created. Finally, the occurrence of nitrate-dependent iron oxidation will be examined. Results of the eAOPs experiments will be further analysed and explained in the second section. Thereafter, the implementation of eAOPs at Dunea's DWTP will be presented. Lastly, an analysis will be performed on the effects of Dunea's water matrix on the As(III) oxidation performance.

4.1 Arsenic Occurrence and Related Processes

In this section, the first research question will be answered by explaining the fieldwork results.

4.1.1 Observed Groundwater Constituents

The presented MPs results were measurements from one day of fieldwork (except for MP 3). To improve the spatial groundwater constituents analysis, future research should repeat the performed measurements to verify the results. The same applies to the MWs measurements, as these resulted from one day of fieldwork.

It was hypothesised that the high As concentration in MP 3 of 13.0 μg/L during first measurements was caused by adsorption of As to $Fe(OH)_3$ flocs (Figure 16). Particulate Fe could have precipitated and formed $Fe(OH)_3$ flocs to which As could have adsorbed (Stuyfzand, 1998). It was observed that most Fe was present as particulate Fe when the high total As concentration was measured, which confirmed the hypothesis of adsorption to $Fe(OH)_3$ flocs. Results showed an average measured dissolved Fe concentration at the sampling locations of 0.12 mg/L (Figure 16). This concentration was expected to be higher based on the results of approximately 2 mg/L Fe during As mobilisation (Figure 5). It was assumed that this lower dissolved Fe concentration was caused by water extraction from multiple layers. This would mean that the wells extracted water from Fe-bearing and non-Fe-bearing layers.

NO_3^- results in the sampling points were used to determine whether the water was anoxic. The criterion for anoxic water of $NO_3^- - N \geq 0.5$ mg/L, which was equal to $NO_3^- \geq 2.2$ mg/L (Table 1). The observed NO_3^- concentrations in MPs 5, 6, 7 and 10 did not meet this criterion, indicating oxic water. This contradicted the DO measurements in which anoxic conditions at MPs 6, 7 and 10 were observed (Figure 12). In addition, MP 4 was identified as oxic, while the NO_3^- concentration indicated anoxic water. Furthermore, As concentrations < 1 μg/L were expected due to the presence of NO_3^-, based on Figure 5, which was not obtained in any of the MPs. These observations supported the assumption that wells extracted water from multiple layers.

Several MPs were interconnected, making it interesting to compare their results (Table 8, Supplementary Information 6.11). Water flowed from MP 1 to 1A without any wells in between. Therefore, no significant differences in As, NO_3^- and DO measurements were expected. This corresponded to the results that showed approximately similar results for MPs 1 and 1A (Figure 59, Supplementary Information 6.11). Water flowed from MP 6 to 5 and then further to 2. However, many wells were present between MP 6 and 5 and between MP 5 and 2. Because the contribution of flows by the MPs was not quantified, no assumptions could be made on the wells feeding additional water to MP 5 and 2. In addition, MP 10 contained water from MPs 7 and 8 and several other wells. Hence, no assumption could be made here as the flows were not quantified.

Figure 38 provides a graphical overview of the total As concentrations at the MPs, where the size of the circle represents the magnitude of the total As concentration. The contribution of each well section was presented in this Figure. The highest As concentration of 9 µg/L was observed at MP 3, whereas the lowest As concentrations were observed at MP 1A and 8 of 3 µg/L. Results showed that the well section connected to MP 3 had the highest contribution to the elevated As concentration. MP 3 was connected to 13 out of the 300 wells and was estimated to supply 4.3 % of the total flow. Closing MP 3 would therefore not lower the elevated As concentration of > 1 µg/L. Moreover, all MPs showed arsenic concentration > 1 µg/L, indicating that each well section contributed to the elevated As concentrations. These findings answered part of the first research question, *What is the contribution of each well section to the elevated As concentrations and where does this As originate from?*
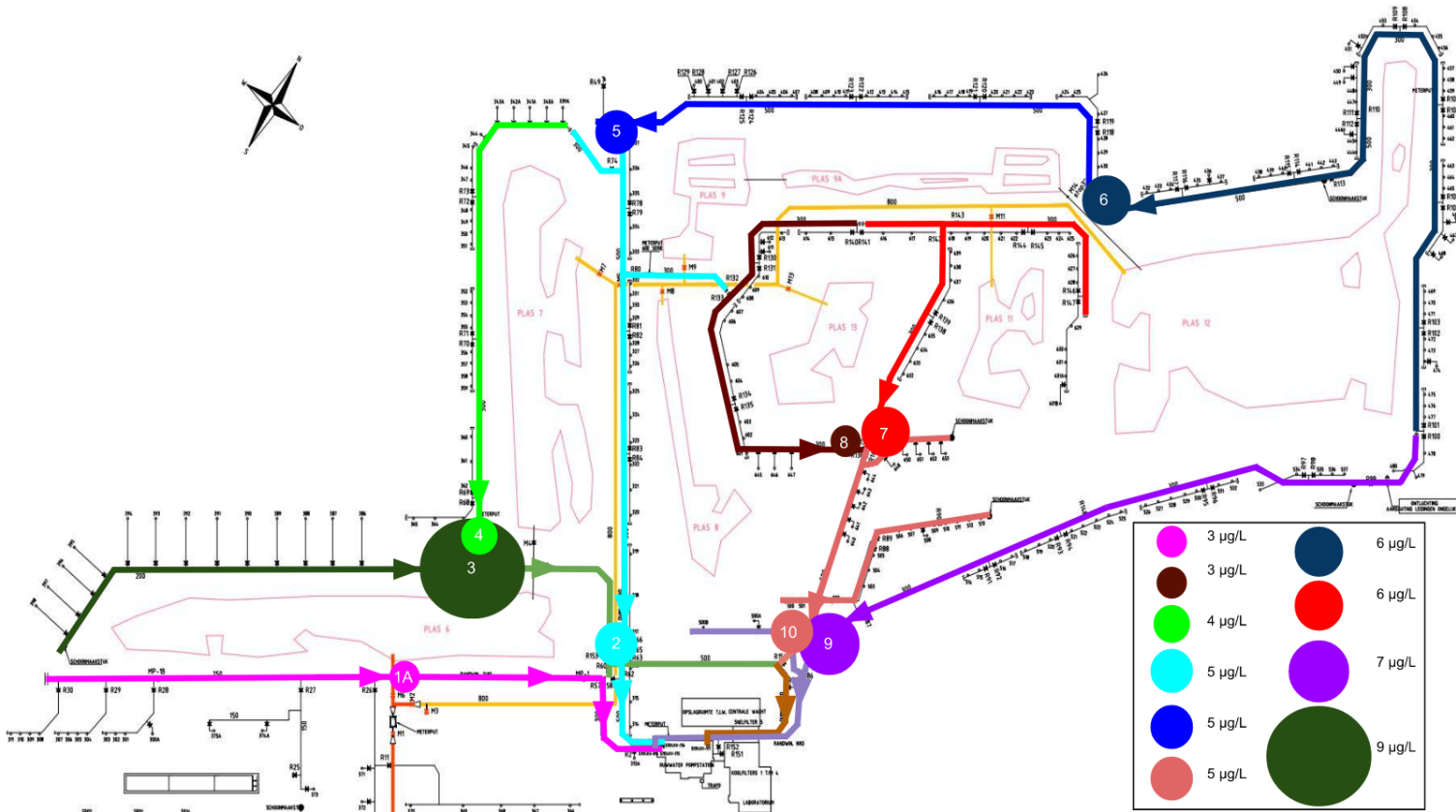
Figure 38: Overview Total As concentrations [µg/L] at MPs. The size of the circles indicate the magnitude of the As concentration.

It was hypothesised that the construction year of the wells could have played a role in the As concentration, as the As source could have been depleted over the years. MWs X and Y were constructed in 1984 and 1978, respectively. Several wells connected to MWs Y (near MP 7) were build in 1987, while several wells connected to MWs X, near MP 3, were build 17 years later, in 2004 (Dunea, 2022). The more recently constructed wells near MP 3 could have caused the elevated As concentration of 9.4 µg/L.

4.1.2 Mobilisation of Arsenic

In order to reduce the presence of As in the dune filtrate, it is of importance to understand the possible As mobilisation processes at Solleveld. Mobilisation of As may occur under both reducing and oxidising conditions (Smedley & Kinniburgh, 2002). Study of Stuijfzand (2014) demonstrated synchronous mobilisation of As and Fe and denitrification in anoxic layers 1A2, 1A3 and b (Figure 5). This supported the theory that As mobilisation could derive from reductive dissolution of As-bearing Fe oxyhydroxide ($Fe(OH)_3$) and release of adsorbed As (Nickson et al., 2000; McArthur et al., 2001; Stuijfzand et al., 2008). The reductive dissolution of As-bearing $Fe(OH)_3$ is caused by microbial degradation of sedimentary organic matter (Nickson et al., 2000).

The observed As peak in MWs X (Figure 21) did not show a synchronous Fe peak as seen in the hydrochemical depth profile of Stuijfzand (2014) (Figure 5). However, at depths > -9 m, slight mobilisation of As and Fe was shown, since concentrations increased from 0.20 to 0.96 µg/L and from 0.26 to 0.73 mg/L, respectively. This could indicate As mobilisation by reductive dissolution of $Fe(OH)_3$. Moreover, reducing conditions were observed in the MWs, as the ORP values were all < -34 mV (Figure 22). However, these measured As concentrations were below the detection limit, making the results inaccurate. In addition to $Fe(OH)_3$, Mn oxides could lead to As mobilisation by reductive dissolution and desorption (Smedley & Kinniburgh, 2002). However, the Mn mobilisation showed an opposite trend to that of As (Figure 21). Hence, it was assumed that the As mobilisation was not derived from reductive dissolution and desorption from Mn oxides.

As mobilisation under oxidising conditions may occur by oxidation of As-bearing sulphide minerals and As ore minerals, of which the most abundant are As-bearing (or arsenian) pyrite (FeS_2) and arsenopyrite (FeAsS), respectively (Smedley & Kinniburgh, 2002; Stuijfzand et al., 2008). Although both minerals are As sources, As-bearing pyrite is much more abundant than arsenopyrite (Nordstrom, 2000). Therefore, pyrite oxidation was considered in this research.

Pyrite oxidation (Equation 19), may take place when water levels are lowered or during infiltration of oxygenated water (Smedley & Kinniburgh, 2002; Das et al., 1996; Schippers & Jørgensen, 2002). The groundwater table at Solleveld was lowered 1.3 m three weeks before the measurements. In addition, the infiltration water contained 10.4 mg/L oxygen (Dunea, 2021). During pyrite oxidation, acidity is generated and TEs such as As, Co, Ni and Zn could be released (Antoniou et al., 2012; Stuyfzand, 1998). Results showed that the highest observed concentrations of Co, Ni and Zn, were at -3 m, where the highest As concentration was observed (Figure 21). Studies of Antoniou et al. (2012) and Stuyfzand (1998) observed As, Co, Ni and Zn mobilisation due to pyrite oxidation. The pH of the infiltration water was 7.9, whereas pH values between 7.4 and 7.8 were observed at MWs X (Figure 23). In addition, the observed pH measurements showed an increase in pH over depth, presenting the lowest pH of 7.4 at -3 m. This lowered pH could be the result of acidity generation by pyrite oxidation.

$$FeS_2 + 4.25O_2 + 2.5H_2O \rightarrow Fe(OH)_3 + 2SO_4^{2-} + 2H^+ \tag{19}$$
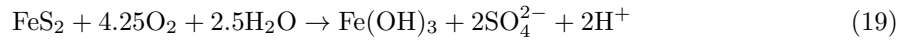
Study of Broers (2004) proved that denitrification, which is the NO_3^- reduction process, was coupled to pyrite oxidation in part of the aquifer where the dissolved oxygen levels were ≤ 0.7 mg/L. Additionally, Broers (2004) observed that the pyrite oxidation caused the release of Fe, SO_4^{2-} and the TEs As, Co, Ni and Zn. Equation 20 shows the oxidation of pyrite by NO_3^- (Schippers & Jørgensen, 2002).

$$2FeS_2 + 6NO_3^- + 4H_2O+ \rightarrow 2Fe(OH)_3 + 4SO_4^{2-} + 3N_2 + 2H^+ \tag{20}$$
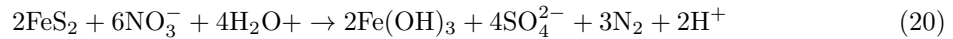
Pyrite oxidation could be determined by Equation 21, with $SO4_M$ and Cl_M the measured concentrations SO_4^{2-} and Cl^- [mg/L], respectively. $(SO4/Cl)_{INF,YEAR}$ is the mean ratio of SO_4^{2-} and Cl^- input concentrations during one year of recharge. A positive $\Delta SO4_{PYRITE}$ value indicated pyrite oxidation, whereas a negative value indicated pyrite formation (Stuijfzand, 2014). SO_4^{2-} and Cl^- measurements from MWs Y (Figure 24) were used to determine whether there was pyrite oxidation (Stuijfzand, 2014).

$$\Delta SO4_{PYRITE} = SO4_M - Cl_M * (SO4/Cl)_{INF,YEAR} \tag{21}$$

Results of MWs Y showed positive $\Delta SO4_{PYRITE}$ values, except at -15 m, while the ratio $(SO_4/Cl)_{INF,YEAR}$ was 0.4 (Table 9, Supplementary Information 6.12). This would indicate pyrite oxidation at depths between -3 and -12 m and pyrite reduction at -15 m. However, these findings were rejected by Figure 39, which shows the measured SO_4^{2-} concentrations in MWs Y and the input SO_4^{2-} concentration of 44.3 mg/L (+/- 4.2) (Table 2). It was observed that the measured SO_4^{2-} concentration exceeded the input SO_4^{2-} concentration at -6 m. This would mean that exclusively at -6 m, SO_4^{2-} was increased and hence pyrite was oxidised. However, the observed As concentration at -6 m was below the detection limit and no significant As mobilisation was observed in MWs Y. Hence, the SO_4^{2-} and Cl^- results in MWs Y could not be coupled to pyrite oxidation. Overall, an increase in SO_4^{2-} concentration was observed between input and VOW concentration of 3.8 (+/- 3.9) mg/L (Table 2). This increase in SO_4^{2-} concentration could be coupled to pyrite oxidation.
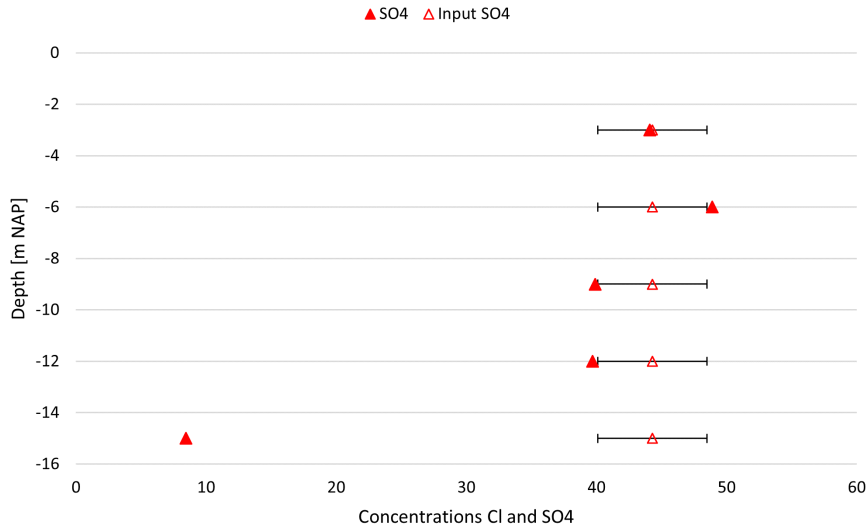
Figure 39: Concentrations SO_4^{2-} [mg/L] in MWs Y. Input concentrations are indicated by open symbols with standard deviation.

Although the decreased pH (Figure 23) and mobilisation of Co, Ni and Zn (Figure 21) were pyrite oxidation indicators, the expectations of As mobilisation caused by pyrite oxidation were contradicted by the results of a negative correlation between As and SO_4^{2-} (Figure 20). Pyrite oxidation would result in SO_4^{2-} release (Equation 19), leading to a positive As and SO_4^{2-} correlation. This could be explained by water extraction from multiple layers, including As-bearing layers with pyrite oxidation and SO_4^{2-} release, as well as layers without As and SO_4^{2-} release.

4.1.3 Arsenic Depth Profile

It was observed that As was mobilised between -3 and -6 m (Figure 21). With an average filter depth from -1.6 to -7.4 m, it was assumed that water was extracted from the As-bearing layer. However, it was unknown what the As concentrations were between -1.6 and -2.7 m (MW 5 was from -2.7 to -3.2 m) and between -6.2 and -7.4 m (MW 4 was from -5.7 to -6.2 m) (Figure 7). Extracting water from the As-bearing layer should be prevented, showing the relevance of knowing the exact As profile between -1.6 and -7.4 m. To create this complete As depth profile, estimations of the As concentrations were performed by making a mass balance and making use of characteristics from the previously discussed hydrochemical As profile of Stuijfzand Stuijfzand (Figure 5), indicated as 'reference profile'. For consistent comparisons, the estimated As profile represents the total dissolved As concentrations as observed in the reference profile.

Figure 40 shows the result of the estimated As profile. The circles indicate the measured dissolved As concentrations in MWs X (Figure 21) and the blue line is the estimated As profile. Besides the As profile, Figure 40 depicts the Fe^{2+} and NO_3^- concentrations in the average well which determinations will be explained in Chapter 4.1.4. The blue arrows indicate the dune filtrate entering the filter. The concentrations dissolved As, Fe^{2+} and NO_3^- measured at MP 3 were depicted as concentrations in the dune filtrate. Important to consider is that the concentrations at MP 3 deviated from the values showed in Chapter 3.1.1 because the results were from different days.

In the dune filtrate of MP 3, the measured concentration As and NO_3^- were 9.3 µg/L and 2.6 mg/L, respectively. It was observed that NO_3^- was present in all sampling locations (Figure 17). However, NO_3^- concentrations measured at MWs X were under the detection limit of 1 mg/L NO_3^-. This indicated that NO_3^- should be present above the highest MW (> -2.7 m). Based on the reference profile, it was assumed that As concentrations were low when NO_3^- was present. Moreover, it was assumed that the As profile had a similar shape as the reference profile. Therefore, the As profile should have a peak around 18.2 µg/L at a certain depth. When assuming a linear trend between -3 m and -6 m, the total calculated As concentration was lower than the measured dune filtrate concentration of 9.3 µg/L. Due to the NO_3^- layer which should be present > -2.7 m, it was assumed that the As peak of 18.2 µg/L was lower than -3 m. The As measurement at -3 m of 14.9 µg/L corresponded to the reference profile at approximately -2 m.

At -6 m, the measured As concentration was 2.1 µg/L, which corresponded to the reference profile at approximately -11 m. Hence, the As-bearing layer from 14.9 until 2.1 µg/L was 9 meters in the reference profile, whereas the layer was only 3 meters in MWs X. As a result, it was assumed that the As-bearing layer had a similar shape but was 3 times smaller than the reference profile. The peak of 18.2 µg/L was at -5 m in the reference profile, which was 3 meters below 14.9 µg/L. Hence, 18.2 µg/L was assumed to be 1 m below 14.9 µg/L, which was at -4 m. The reference profile showed that the concentration was 14.9 µg/L again at -8 m, which was 3 meters below the peak. Hence, at -5 m the concentration was 14.9 µg/L again. At -6 m, the As concentration was measured again and resulted in 2.1 µg/L. Between -6 and -9 m, the concentrations were assumed to be linear, due to the low concentration of 0.2 µg/L at -9 m. This concentration was lower than the concentrations observed in the reference profile, so no clear comparison could be made. The As concentration rapidly decreased to approximately 0.5 µg/L in the reference profile. Therefore, the As concentration at -2 m was assumed to be 0.5 µg/L.
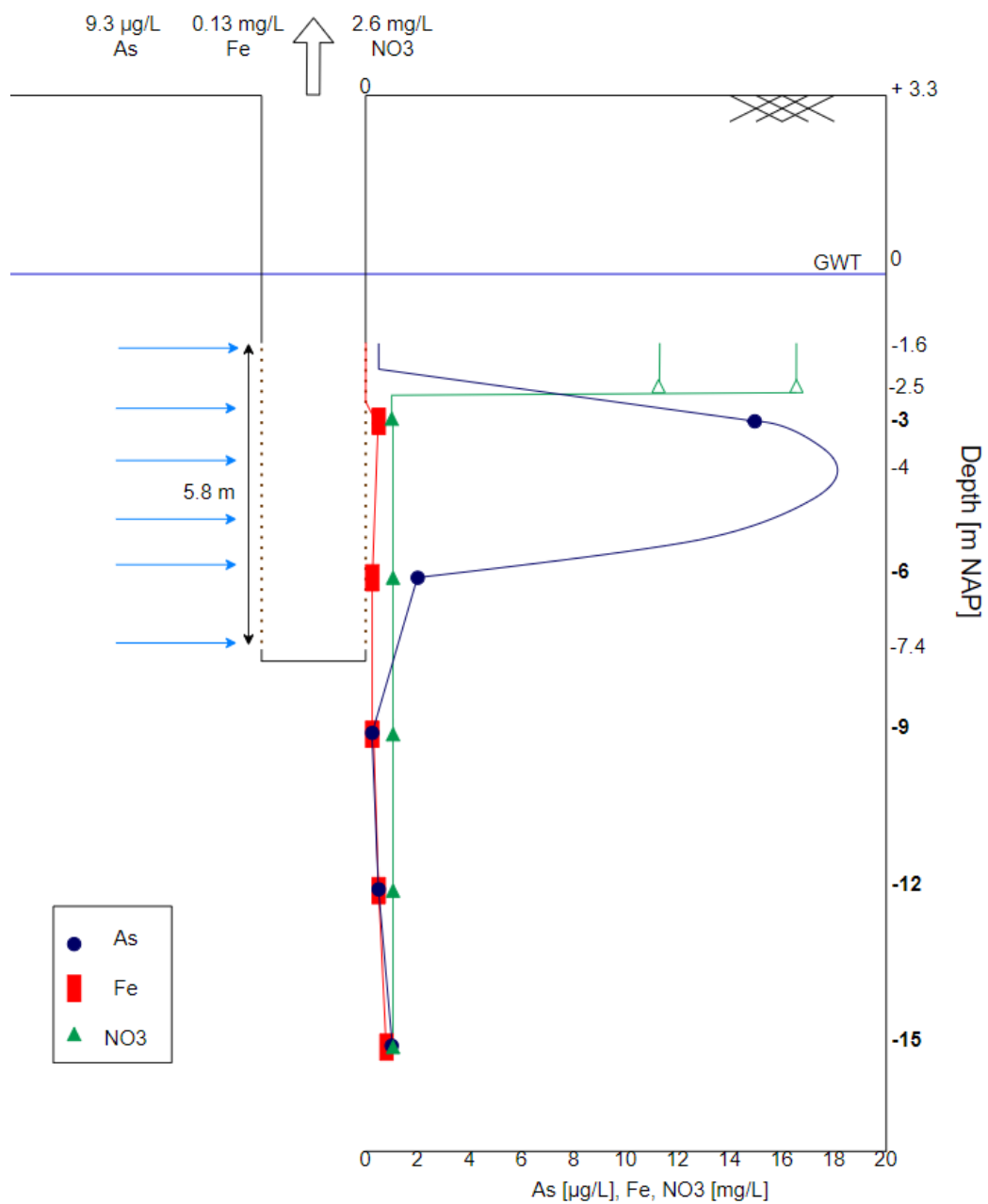
Figure 40: As [µg/L], Fe^{2+} [mg/L] and NO$_3^-$ [mg/L] Profiles in the Average Well. Profiles are depicted in the average well (brown dotted line), from -1.6 until -7.4 m. The ground level was at +3.3 m (brown line) and the groundwater table was at -0.2 m (blue line). Measured As (blue circles), Fe^{2+}(red rectangles) and NO$_3^-$ (green triangle) concentrations in MWs X are presented as filled symbols, while the estimated NO$_3^-$ concentrations are presented by open symbols.

The measured and estimated As concentrations are shown in Table 10 (Supplementary Information 6.13). The estimated As concentration in the average well was 9.0 μg/L, which was close to the measured concentration of 9.3 μg/L in MP 3. This indicated an accurate estimation of the As profile. Results showed that the As-bearing layer was present between -2.5 and -8.5 m (Figure 40). With an average filter depth from -1.6 to -7.4 m, water was being extracted from the As-bearing layer. However, the results in MWs Y that were showing no As-bearing layer, indicated that this profile may vary across the Solleveld area.

4.1.4 Nitrate-Dependent Iron Oxidation

In literature it was demonstrated that microbial oxidation of Fe^{2+} in absence of oxygen is possible with NO_3^- as electron acceptor (Straub et al., 1996; Oshiki et al., 2013). This process is referred to as Nitrate-Dependent Iron Oxidation (NDFO). Furthermore, studies have shown that As(III) oxidation can be mediated by microbial NO_3^- reduction (Senn & Hemond, 2002; Oremland et al., 2002). Senn and Hemond (2002) observed that As(V) accumulated in anoxic and NO_3^--bearing waters. In addition, a rapid increase in As(III) which replaced As(V) was observed at NO_3^- depleted depths, indicating Nitrate-Dependent As(III) Oxidation. A similar trend was observed for Fe^{2+}, as it was oxidised in the anoxic and NO_3^--bearing waters, whereas it reduced to Fe^{2+} again in NO_3^--depleted depths.

At Solleveld, frequent cleaning of the system is required due to clogging in the pipes. Fe^{2+} oxidation by NDFO would contribute to the amount of Fe^{2+} oxidation along with the floc formation in the system. Therefore, the presence of NDFO in wells at Solleveld would increase the cleaning frequency as well as the cleaning costs. Therefore, it is of importance to examine the presence of NDFO. It was assumed that NDFO could potentially be present in the upper part of the wells. In order to determine whether Fe^{2+} oxidation by NDFO occurred in the wells, mass balance calculations were performed. Results of MWs X (Figure 21) and MP 3 (Figure 40) were used for these mass balance calculations. Measured Fe^{2+} and NO_3^- were 0.13 mg/L and 2.6 mg/L, respectively (Figure 40). It was assumed that the Fe^{2+} concentrations above the highest MW were 0 mg/L, since the measured Fe^{2+} concentrations in the MWs X were > 0.13 mg/L. In short, Fe^{2+} was present at depths < -2.7 m and NO_3^- was present at depths > -2.7 m.

Iron Oxidation
In order to determine whether NDFO took place, the Fe^{2+} concentrations in MWs X were compared to the measured Fe^{2+} concentration in MP 3 of 0.13 mg/L. At -3, -6 and -9 m, the Fe^{2+} concentrations were measured (Table 11, Supplementary Information 6.13). Between -3 and -6 m, the Fe^{2+} profile was assumed to be linear. Similar Fe^{2+} concentrations were measured at -6 and -9 m. Therefore, the concentrations were assumed to be constant between these depths. The estimated Fe^{2+} concentration in the average well was 0.29 mg/L, which was 0.13 mg/L higher than the measured Fe^{2+} concentration in MP 3. Hence, 0.13 mg/L Fe^{2+} was oxidised.

Nitrate Reduction
In order to prove whether Fe^{2+} was oxidised by NDFO in MWs X, NO_3^- reduction had to be demonstrated. Due to the NO_3^- concentrations under the detection limit, the NO_3^- profile was estimated by the concentration of 2.6 mg/L in MP 3 and the reference profile (Figure 5). In the reference profile, it was observed that the NO_3^- concentration was still close to zero when the As concentration was 15.3 μg/L. However, at an As concentration of approximately 7 μg/L, NO_3^- started to increase. This As concentration corresponded approximately to a depth of -2.5 m (Table 10). It was therefore assumed that the NO_3^- layer started at -2.5 m. The filter started at -1.6 m, giving a NO_3^- layer of 0.9 m. The measured NO_3^- concentration was < 1 mg/L (detection limit), indicating

that the concentration could vary between 0-0.99 mg/L. Using mass balance calculations resulted in an estimated NO_3^- concentration in the average well between 11.3 and 16.7 mg/L (Equation 26, Supplementary Information 6.13). This estimated range of NO_3^- concentration was higher than the input NO_3^- concentration of 2.9 mg/L (Table 2). It was assumed that this elevated concentration was caused by addition of NO_3^- by an external source such as bird excrement. This assumption was confirmed by the observed NO_3^- concentration at MW Z of 5.1 mg/L, which was > 2.9 mg/L. Moreover, in several MPs the measured NO_3^- concentrations were > 2.9 mg/L, indicating addition of NO_3^- (Figure 17). Although the results in MW Z confirmed the hypothesis that NO_3^- was present at depths > 2.5 m, they were conflicting with other assumptions. The measured concentration of 5.1 mg/L in MW Z was much lower than the estimated NO_3^- concentration between 11.3 and 16.7 mg/L. This showed the complexity of the system and the variation in concentrations of the groundwater constituents over the area.

To determine whether NO_3^- was reduced in MWs X, the measured NO_3^- concentrations were compared to the theoretical input NO_3^- concentration of 2.9 mg/L. Ideally, we would have measured NO_3^- concentrations instead of measuring results below the detection limit. However, we could conclude that NO_3^- was reduced as all measured NO_3^- concentrations were < 1 mg/L between -3 and -15 m. The observed NO_3^- reduction in combination with the observed Fe^{2+} oxidation in MWs X, gave an indication of NDFO.

The observed As, Fe^{2+} and NO_3^- profiles in the average well, confirmed the assumptions of water extraction from multiple layers (Figure 40). This explained the measured low dissolved Fe concentrations, the inconsistent DO and NO_3^- measurements and the contradictory As and NO_3^-, and As and SO_4^{2-} results. Strongly fluctuating groundwater tables, in combination with infiltration of oxygenated water, the observed decreased pH and mobilisation of Co, Ni and Zn, indicated that As was most probably mobilised by pyrite oxidation. It was estimated that the As-bearing layer was present between -2.5 and -8.5 m (NAP). With an average filter depth from -1.6 to -7.4 m, water was being extracted from the As-bearing layer. With these findings, the first research question, *What is the contribution of each well section to the elevated As concentrations and where does this As originate from?*, has been answered.

4.2 Performance eAOPs

In this section, the three remaining research questions will be answered by explaining the laboratory results.

4.2.1 Theoretical versus Observed Operation eAOP Cell

Effects of the parameters supplied i and q were examined during the performed experiments. However, other parameters such as cell design, electrolyte, electrode material and mass transport coefficient influenced the eAOP cell performance (Pletcher & Walsh, 1990). Equation 22 describes the cell potential (E_{cell}) [V], with V_0 [V] is a constant which depends on the nature of the electrolyte, ρ [Ωm] is the sensitivity of the electrolyte, d [m] is the distance between the electrodes and i is the current density [A/m^2] (Comninellis & Chen, 2010).

$$E_{cell} = V_0 + \rho * d * i \tag{22}$$

From this Equation could be seen that E_{cell} depended on the cell design, expressed as d and i and the electrolyte, expressed as V_0 and ρ. d must be minimized to minimize the resistivity, while the electrode area must be as large as possible to minimize the i and therefore the E_{cell}. However, the investment costs of an eAOP cell highly increase with increasing electrode area (and thus eAOP cell volume). The used electrolyte and its pH, temperature and concentration (expressed in conductivity) affected the eAOP cell performance (Pletcher & Walsh, 1990). Changing these parameters was unfavourable and was therefore not investigated. Used electrode material determined whether the electrode was 'active' or 'non-active'. At active anodes, such as the one used in this research, strong interactions between electrode surface and $\cdot$OH radicals exist and higher oxidation states are available, whereas this is excluded for non-active electrodes (Martinez-Huitle & Ferro, 2006; Marselli et al., 2003). Active electrodes have a low OER overpotential, whereas this is high for non-active electrodes (Martínez-Huitle & Panizza, 2018; Brillas & Martínez-Huitle, 2015; Marselli et al., 2003). The OER overpotential is the difference between E needed for the OER and E^0 (standard electrode potential for the OER of 1.23 V) (Equation 23).

$$\text{Overpotential} = E - E^0 \tag{23}$$

E values for the OER on different anodes are presented in Figure 60 (Supplementary Information 6.14). The low OER overpotential of the RuO$_2$/IrO$_2$-coated anode, 1.47 V for RuO$_2$ and 1.52 V for IrO$_2$, indicated that this anode was a good catalyst for the OER (Panizza & Cerisola, 2009). The average overpotential value of 1.50 V was used for clarity. In general, the higher the OER overpotential, the weaker the interaction of the MO$_x$($\cdot$OH) with the anode surface and the higher the chemical oxidation reactivity (Martinez-Huitle & Ferro, 2006). As explained, direct As(III) oxidation was possible before the OER (E^0 of 0.56 V). This indicated that for a RuO$_2$/IrO$_2$-coated anode, direct oxidation could have occured at $E < 1.50$ V.

The mass-transport coefficient indicates the diffusion rate. A high coefficient leads to an uniform distribution of pollutants near the electrode and therefore a higher oxidation efficiency (Pletcher & Walsh, 1990). However, the diffusion rate was beyond the scope of this research, so the mass-transport coefficient will not be further discussed.

Anodic As(III) Oxidation

Results containing As(III) speciation according the Clifford method probably consisted of errors up to approximately 20 % (Karori et al., 2006). It was assumed that during the Clifford method for As(III) speciation, the As(V) retaining as well as As(III) passage were not 100 %, leading to measurement errors. In addition, results were inaccurate for As(III) concentrations < 1 µg/L.

Results showed that for a constant HRT, the As(III) oxidation increased with increasing i (Figure 26). Observed As(III) oxidation increased from 25 to 84 % for a i from 3.5 to 5.5 A/m^2. Complete As(III) oxidation was observed at a i of 6 A/m^2 with a q of 41.5 C/L and a HRT of 2.3 min. The constant HRT led to a constant flow rate, while the increase in i led to an increase in q. According to Faraday's law, the increase in q should result in a higher amount of produced or consumed species (Equation 16). Hence, the observed results matched Faraday's law. On the other hand, an increase in As(III) oxidation was shown when increasing i for a constant q (Figure 27). Results of a q of 20 C/L showed an increase in As(III) oxidation from 34 to 96 % for a i between 4.5-9 A/m^2, while a q of 30 C/L showed an increase from 30 to 98 % for a i between 1.5-7.5 A/m^2 (Figure 27). These results contradicted the expectations according to Faraday's law, which stated a constant amount of formed species for a constant q. Moreover, according to Faraday's law a q of 0.21 C/L would be needed to oxidise 80 µg/L As(III) (feed water concentration), which was much lower than the observed needed q. Due to faradaic losses, not all As(III) was directly oxidised at the theoretical q. Although As(III) could be oxidised by intermediates of the OER, oxygen production is known to reduce the oxidation efficiency. High overpotentials are needed in order for the oxidation reaction via intermediates to proceed (Equation 3), making the MO_{x+1} a non-effective oxidant (Chen, 2004). This was observed in study of Lacasa et al. (2011) in which higher oxidation efficiencies were observed for lower i, since the OER was not favoured under these conditions.

Results of As(III) oxidation experiments were combined (Figures 26 and 27) for comparison and are depicted in Figure 41 as percentage As(III) oxidation for i with corresponding HRT. The blue filled bars represent the results for a constant HRT of 2.3 min (Figure 26), indicated as 'Blue', the red dotted bars represent the results of fluctuating HRT (a q of 30 C/L, Figure 27), indicated as 'Red' and the green striped bars represent the other results of the fluctuating HRT (a q of 20 C/L, Figure 27), indicated as 'Green'. For i values 1.5 and 3 A/m^2, HRT (and q) Red > Blue. The results showed a higher As(III) oxidation for Red than for Blue. Furthermore, for a i of 6 A/m^2, HRT (and q) Blue > Red and Green. Here, Blue showed a higher As(III) oxidation than Red and Green. These results were in line with Faraday's law, which stated that a higher HRT (t) results in more oxidation (Equations 14 and 15). However, for a i of 4.5 A/m^2, Blue and Red both had a HRT of 2.3 min and a q of 30 C/L, while the observed As(III) oxidation was not similar. This contradicts the theory of a constant amount of produced or consumed species (Sundén, 2019). An explanation for this could be found in measurement errors during analysis or by the deviation of As(III) speciation by the Clifford method. In general, it was shown that a higher HRT (and q) resulted in higher As(III) oxidation, being in line with Faradays's law. No difference in As(III) oxidation was observed for Blue and Red at i 7.5 A/m^2, since the As(III) oxidation was approximately 100 %. Green showed approximately 90 % As(III) oxidation, indicating that a HRT of 0.9 min and a q of 20 C/L was not sufficient to obtain 100 % As(III) oxidation.
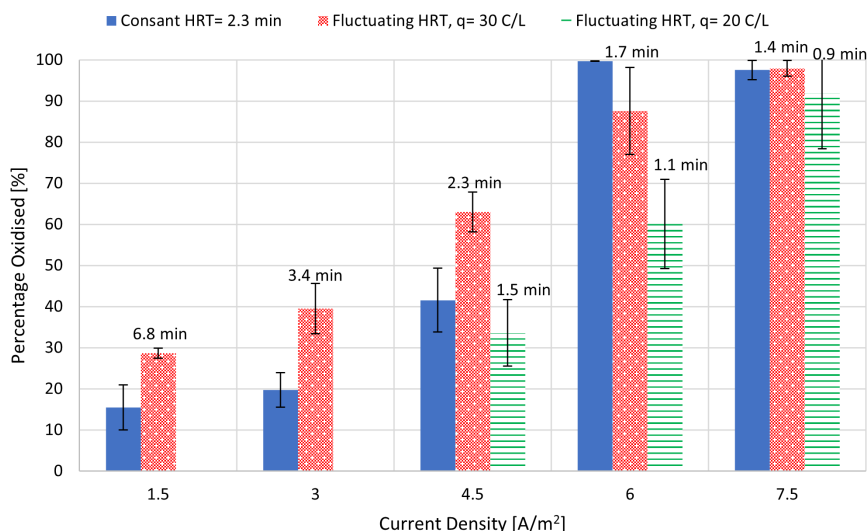
Figure 41: Comparison As(III) Oxidation [%]. The As(III) oxidation is presented per i [A/m^2] with a constant HRT of 2.3 min (blue bars), with a fluctuating HRT [min] and a q of 30 C/L (red dotted bars) and with a fluctuating HRT [min] and a q of 20 C/L (green striped bars). The corresponding HRT [min] and standard deviation are depicted in the graph.

Results showed that the As(III) oxidation was dependent on i, q and HRT. An increase in one of the parameters resulted in more As(III) oxidation, making it difficult to define an optimal configuration. This was emphasised in Figure 41, where a different As(III) oxidation under similar conditions (a i of 4.5 A/m^2) was observed. However, results showed that applying a i of 7.5 A/m^2 with a HRT of at least 1.4 min (flow rate maximum 9 L/h) and a q of at least 30 C/L, will result in complete As(III) oxidation. These results answered the first part of the research question, *What is the eAOP system performance in terms of As oxidation and energy consumption for a RuO_2/IrO_2-coated anode?*

The obtained results were compared to studies that examined As(III) oxidation by eAOPs. Study of Zhao et al. (2010) showed nearly complete As(III) after 30 minutes with a i of 2.4 A/m^2. The initial As(III) concentration was 1 mg/L, which was 12.5 times higher than in this research. Comparing the results was difficult, since As(V) was subsequently removed by electrocoagulation during the HRT of 30 minutes. Therefore, the minimum HRT to reach nearly complete oxidation was not obtained. Without this information, the q could not be determined and the results could not be compared. Study of Lacasa et al. (2011) observed almost complete As(III) oxidation for a mixed ruthenium oxide anode at i 3 A/m^2. However, the corresponding q was approximately 7200 C/L, which was 226 times the applied q in this research.

Anodic pH Observations
Protons (H$^+$) and electrons (e$^-$) were formed during anodic oxidation processes. e$^-$ were transported via the DC power supply to the cathode where they were consumed in the reduction reaction (Equation 6). To obtain electroneutrality, the amount of negatively charged e$^-$ transported to the cathode was compensated by an equal amount of positively charged H$^+$ or other cations (Rozendal et al., 2006). In the performed experiments, the electroneutrality was obtained by transport of H$^+$ and sodium (Na$^+$), through the CEM.

According to Faraday's law (Equation 16), an increase in q should result in an increase in H^+ formation and therefore a decrease in pH. This theory matched the results in which the pH decreased from approximately 8.2 to 7.1 due to an increase in q (and i) (Figure 28). A constant q would theoretically lead to a constant H^+ formation and therefore a constant pH. This was observed in the pH results for experiments with a constant q (Figure 29). However, to keep the q constant in these experiments with increasing i, the flow rate was increased. Study of Dlugolecki et al. (2010) observed a decrease in CEM resistance with increasing flow rate for low NaCl concentrations ($<$ 0.1 M NaCl, which applied to the water matrix in this research). An increase in flow rate reduced the boundary layer thickness of the CEM and therefore the boundary layer resistance. This would promote the H^+ transport over the CEM. Therefore it could be argued that a constant q with an increase in flow rate would result in more H^+ transport to the cathode with a consequent increase in pH at the anode (Kraaijeveld, 2022). Moreover, the increase in i resulted in an increase in OH^-, according to Faraday's law. This would result in more transport of positively charged cations such as Na^+ and H^+ to sustain electroneutrality. Nevertheless, these two processes did not seem to play a role during the performed experiments.

Comparison Energy Consumption
Results showed that the energy consumption increased from approximately 0.002 to 0.13 kWh/m^3 for i in the range of 0.5 to 7.5 A/m^2 with a constant HRT of 2.3 min (Figure 30). Additionally, an increase in energy consumption was observed from approximately 0.035 to 0.075 kWh/m^3 for i in the range of 1.5 to 9 A/m^2 with a constant q of 30 C/L (Figure 31). These results were combined and presented in Figure 42, which shows the difference in energy consumption for similar current densities with a different q. It was observed that the energy consumption increased for increasing i as well as for increasing q. A higher q for a similar i resulted in a higher energy consumption (Equation 12). At a i of 7.5 A/m^2, where 100 % As(III) oxidation was obtained for a q of 30 C/L, the obtained energy consumption was 0.066 kWh/m^3. However, it was shown that applying a higher q of 52 C/L led to an increased energy consumption of 0.13 kWh/m^3. Applying a higher q (and HRT) resulted in less water per kWh, increasing the energy consumption. In terms of costs, the operation of the eAOP cell at a i of 7.5 A/m^2 and a q of 30 C/L (0.066 kWh/m^3), resulted in 0.04 €/m^3 (electricity price of 0.67 €/kWh) (Consumentenbond, 2022). With these results, the research question, *What is the eAOP system performance in terms of As oxidation and energy consumption for a RuO_2/IrO_2-coated anode?*, has been answered.

Comparing the energy consumption and costs of eAOPs to other As(III) oxidation and As removal technologies was based on literature. Study of Criscuoli and Figoli (2019) reported an energy consumption for As removal by nanofiltration and reverse osmosis of 3.21-3.95 and 4.14 kWh/m^3, respectively. This led to operational costs 2.15-2.65 €/m^3 and 2.77 €/m^3 for nanofiltration and reverse osmosis, respectively. Removal of As by electrocoagulation was reported in the study of Demirbas et al. (2019), in which an energy consumption of 0.015 kWh/m^3 for 99 % removal was observed, resulting in operational costs of 0.01 €/m^3. However, other studies such as Alcacio et al. (2014) reported a higher energy consumption of 0.89 kWh/m^3 for 89 % removal, giving operational costs of 0.60 €/m^3. The use of the oxidants O_3 and H_2O_2 for AOPs is known to be a very expensive method for As(III) oxidation (Jiang, 2001). It follows that As(III) oxidation by eAOPs has lower operational costs than nanofiltration and reverse osmosis and comparable costs to electrocoagulation. One could argue that these technologies lead to As removal instead of As(III) oxidation. However, in the DWTP of Dunea, oxidised As(V) is currently being removed during RSF, resulting in no additional operational costs for As(V) removal.
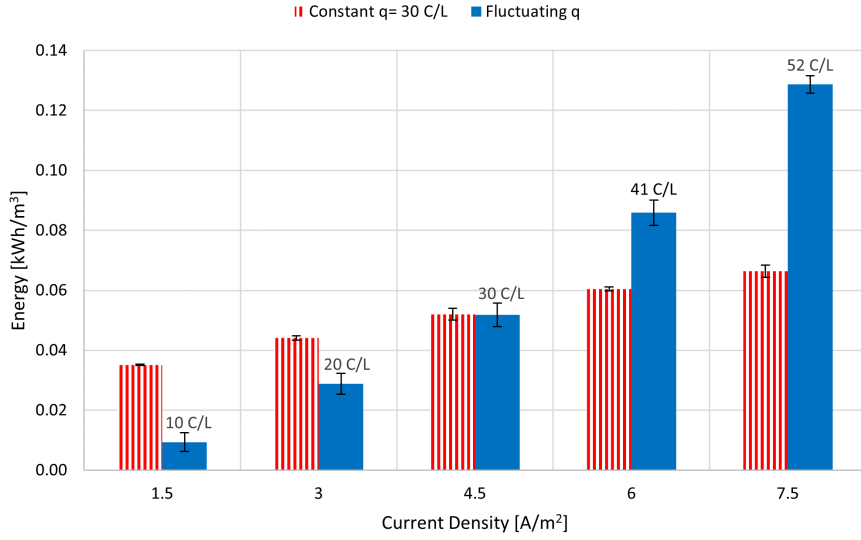
Figure 42: Comparison Energy Consumption Cell [kWh/m³]. The energy consumption is presented per i [A/m²] with a constant q of 30 C/L (red striped bars) and with a fluctuating q (blue bars). The corresponding q [C/L] and standard deviation are depicted in the graph.

Anodic Free Chlorine Formation

Free chlorine could contribute to As(III) oxidation via indirect oxidation, during which free chlorine is consumed as oxidant. Therefore, it was assumed that the observed free chlorine results were an overestimation of the produced free chlorine in As-containing waters (Figure 32). However, it was needed to demonstrate the behaviour of free chlorine formation to understand the effects of q, i and HRT on the free chlorine formation. The observed free chlorine formation was in contrast with the expected formation according to Faraday's law (Equation 16), in which a constant q would result in a constant amount of formed species. Furthermore, a doubled q would theoretically result in a doubled free chlorine concentration. This was not observed in the results, since the concentrations increased by an average factor of 3.2. These two inconsistencies were assumed to be caused by the dependence on E. Although Faraday's law stated that the amount of free chlorine depends on the applied q, species could be oxidised from a specific threshold E (Figure 11). For example, the theoretical amount of Cl_2 produced at a q of 20 C/L is 0.10 mmol/L. However, this amount of Cl_2 will not be formed at a very low E ($E^0 < 1.36$ V). Results showed an increase in E for increasing i (Figure 37). Hence, it was assumed that the increase in i enhanced more reactions to occur, explaining the observed increase in free chlorine concentration for a constant q and increasing i. Moreover, stabilisation in free chlorine formation was observed for a q of 20 and 40 C/L from a i of approximately 16 and 22 A/m², respectively, being in line with Faraday's law. The average stable concentrations were 0.29 (+/- 0.02) and 0.94 (+/- 0.14) mg/L for a q of 20 and 40 C/L, respectively. However, also for stable concentrations, more than a doubling of the free chlorine concentration (factor 3.2) was observed for a doubling of the q. In addition, the assumption of dependence on E would indicate a stabilisation of the free chlorine concentration starting at a similar i, which was not observed.

These contradictory observations could be caused by factors such as pH and turbulence. Experiments with a q of 40 C/L would have a lower pH, according to Faraday's law due to more H^+ formation. However, the decreased pH was assumed to be not beneficial for free chlorine formation, as the reactions do not occur exclusively in acidic media (Figure 11). This rejects the assumption that the increase in free chlorine formation was caused by pH. Moreover, less turbulence was generated at a q of 40 C/L, rejecting the assumption that turbulence caused the more than doubled free chlorine production for a q of 40 C/L. It was hypothesised that the increase in H^+ transport for a higher q could have led to more diffusion, affecting the uniformity of pollutant concentrations. In addition, a higher amount of Cl_2 gas would be produced, affecting the turbulence. However, these hypothesis could not be confirmed or rejected by the observed results. Unfortunately, it was not possible to calculate the theoretical free chlorine formation, as it comprised a combination of the species Cl_2, $HOCl$ and OCl^-, which differed in molar weight.

Figure 43 presents a comparison of the free chlorine formation results for a HRT in the range of 0.8-1.7 [min], for a q of 20 (orange filled bars) and 40 C/L (blue striped bars) (Figure 32). This graph ensured comparison between the free chlorine formation results for a similar HRT and a doubled i (and q). Results showed that doubling the i (and q) for the same HRT resulted in more than a doubled free chlorine formation. Free chlorine concentrations increased by an average factor of 11.6 when the i (and q) were doubled, which was not in line with Faraday's law. When looking at a i of 8 A/m^2, it was observed that doubling the q resulted in more than a doubled free chlorine formation. In short, the observed free chlorine formation increased by a factor 3.2 and 11.6 by doubling the HRT (and q) and i (and q), respectively. The observed stabilised free chlorine formation would indicate that a higher i would eventually not affect the formed free chlorine concentrations after it reached its maximum. Hence, the q should be as low as possible in order to minimize the free chlorine formation. Future research should perform experiments for higher i to confirm the stabilisation in free chlorine concentration and the resulting increase by a factor of 3.2 for a doubled q. These findings answered the research question, *How do anodic operating conditions affect formation of free chlorine?*
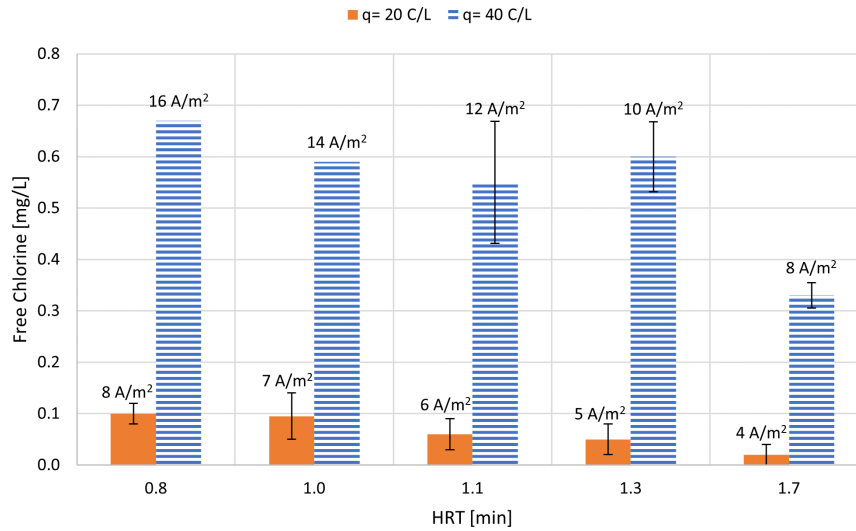

Figure 43: Free Chlorine Formation [mg/L] per HRT [min]. Results are presented for a q of 20 and 40 C/L. The corresponding i [A/m^2] and standard deviation are depicted in the graph.

The E^0 values for possible oxidation reactions in the presence of Cl^- are shown in Figure 44. Here, all possible chlorine species are presented and not exclusively the As(III) oxidising species (Figure 11). It was assumed that only Cl_2, HOCl and OCl^- were measured by the free chlorine test kit. Chlorine measurements during potentiostat operation at E of 0.89 V did not show free chlorine formation. This was in contrast to the presented E^0, which showed that OCl^- should be formed at a E of 0.89 V (Figure 44). However, this oxidation reaction should occur in an alkaline medium (OH^-) at the anode surface (direct oxidation). It was assumed that the pH near the anode surface was very low due to the formed H^+, which presumably prevented the reaction from taking place. Hence, free chlorine was formed at a higher E.

As explained in Chapter 1.3, the presence of Cl_2, HOCl and OCl^- is pH dependent (Ghurye & Clifford, 2001). The observed pH during experiments varied from ≥ 7.5 for low i (0-3.5 A/m^2), during which OCl^- was the predominant form, to < 7.5 for experiments with a higher i (≥ 4 A/m^2), during which HOCl was the predominant form (Luna-Trujillo et al., 2020). As(III) oxidation was observed at a $i \geq 3.5$ A/m^2, indicating that free chlorine was mainly present as HOCl. Hence, it was assumed that HOCl would be the main chlorine form for indirect As(III) oxidation. Moreover, HOCl is a much stronger As(III) oxidant than OCl^-, which strengthens this assumption (Sharma et al., 2007). Besides free chlorine, As(III) could be oxidised by chlorine dioxide (ClO_2) (Ghurye & Clifford, 2001). However, study of Sorlini and Gialdini (2010) observed a very low As(III) oxidation efficiency by ClO_2. Therefore it was assumed that ClO_2 did not play a significant role in As(III) oxidation. Hence, indirect oxidation of As(III) was mainly obtained by HOCl.

The minimum E^0 for HOCl formation, assuming that the reactions in an alkaline medium did not occur, is 1.49 V (Figure 44). This corresponds to a measured i of approximately 25 A/m^2 (Figure 37). This would indicate that produced free chlorine did not contribute to As(III) oxidation via indirect oxidation in the performed As(III) oxidation experiments (Figures 26 and 27). However, the presented E^0 was under standard conditions, which were not obtained during the experiments. As a result, As(III) oxidation by free chlorine at a $E < 1.49$ V was assumed to be possible. Moreover, Cl_2 could be formed at a E^0 of 1.36 V, corresponding to a measured i of approximately 5 A/m^2 (Figure 37). This lower i was obtained during experiments indicating that Cl_2 was probably formed. Cl_2 would be converted to HOCl at pH > 2.5, which was observed in the bulk solution. Therefore, it was assumed that the converted HOCl oxidised As(III) in the bulk solution by indirect oxidation.

As explained in Chapter 1.3, eAOPs can result in direct formation of the inorganic DPBs ClO_2^-, ClO_3^- and ClO_4^-. At low E^0 values of 0.62 and 0.76 V, ClO_3^- and ClO_2^- can be formed, respectively (Figure 44). However, these reactions occur under alkaline conditions, whereas the conditions are probably acidic. At a E^0 of 1.45 V, ClO_3^- can be formed under neutral conditions, which is slightly higher than the ClO_4^- formation E^0 of 1.39 V. In addition, ClO_2^-, ClO_3^- and ClO_4^- can be formed by oxidation of ClO^- (alkaline conditions and a E^0 of 0.66 V), ClO_2^- (alkaline conditions and a E^0 of 0.33 V) and ClO_3^- (a E^0 of 1.19 V), respectively (Vanysek, 2000). The formation of the inorganic DPBs can be obtained for E^0 values that are close to the E^0 values of chlorine species. To quantify the amount of formed inorganic DPBs by direct oxidation, future experiments should monitor the DPBs formation with IC analysis.

Figure 44: E^0 [V] for Chlorine Formation. E^0 is under standard conditions, from (Vanysek, 2000; Kaczur, 1996).

Cathodic e-softening

Results of the cathodic effluent pH, ranging from 8.1 to 10.6 (Figure 33), were in line with the expectations according to Faraday's law. An increase in q led to an increase in produced OH^- and consequently an increase in pH. Similar results were observed in the study of Clauwaert et al. (2020), which showed that for a higher q, more OH^- ions were produced at the cathode side. This resulted in a pH increase, beneficial for water softening. Moreover, the observed linear increase between cathodic produced OH^- (obtained by the PHREEQC model) and applied i (and q) (Figure 36), were in line with Faraday's law (Equation 16). The non-linear behaviour between i and required anodic OH^- (Figure 36) was assumed to be caused by the occurrence of acid forming reactions. An increase in i led to an increase in E (Figure 37). A certain oxidation reaction that produces H^+, occurring at high E values could explain this non-linearity. For example, Cl_2 formation occurs at a E^0 of 1.36 V during which H^+ is generated, affecting the pH.

Figure 45 compares the theoretical OH^- production to the observed estimated OH^- production. The theoretical OH^- production was determined, while assuming 100 % faradaic efficiency. Results had a similar order of magnitude with lower observed than theoretical OH^- production, except for a i of 1.5 and 3 A/m^2. The slightly higher observed than theoretical OH^- production at these points could be explained by pH measurement errors. Lower observed than theoretical OH^- production for a $i \geq 4.5$ A/m^2 was assumed to be caused by transportation of H^+ over the CEM. Moreover, a faradaic efficiency lower than 100 % could have resulted in the lower observed OH^- production. This reduced faradaic efficiency could be caused by the production of H_2O_2 by the reduction of oxygen on the cathode surface (Sirés et al., 2014; Zhou et al., 2012). However, H_2O_2 production was not measured during the performed experiments. Therefore, future research should include measurements of cathodic H_2O_2 production. In general, the observed OH^- production was 4.3 (+/- 5.3) % lower than the theoretical base production, indicating a minor OH^- loss.

55
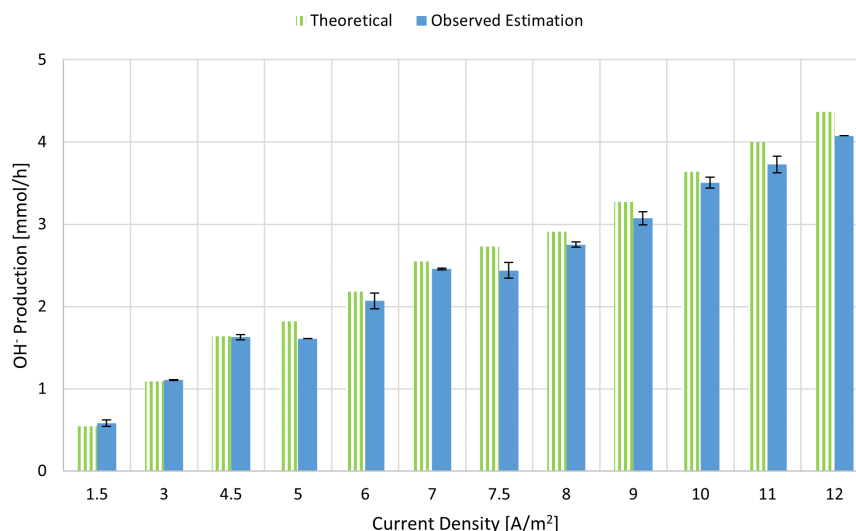
Figure 45: Comparison Theoretical and Observed OH⁻ Production [mmol/h]. Results of theoretical OH⁻ production (green striped bars) and the observed estimated OH⁻ production (blue filled bars) are presented per i [A/m^2] with standard deviation. Estimated by PHREEQC Model, from (Kraaijeveld, 2022).

Results of cathodic produced and anodic required OH⁻ (Figure 36) showed the dependence on i (and q) on usability. Ideally, the produced cathodic OH⁻ would be higher than the required anodic OH⁻ for pH buffering. Hence, a $i \geq 5$ A/m^2 was unfavourable for operation, since more OH⁻ was required than available. However, it was most likely that a $i \geq 5$ would be applied due to the observed high As(III) oxidation results. The rate of increase seemed to decrease towards a i of 8 A/m^2. However, the actual trend for higher i should be investigated by future research.

Important to note is that all discussed results were based on the assumption the the anodic effluent pH had to be returned to the feed water pH (8.04). However, it could be argued that the SI instead of the pH was the relevant parameter in evaluating the performance. For drinking water, the optimal SI value is between -0.2 and 0.3 (Rietveld, n.d.). SI values > 0 may cause scaling by precipitation of calcium (Ca^{2+}) and magnesium (Mg^{2+}), leading to the upper SI limit of 0.3. On the other hand, SI < 0 may cause corrosion, resulting in the lower SI limit of -0.2 (Rietveld, n.d.). It follows that the SI of the anodic effluent after buffering should be between -0.2 and 0.3.

Water is currently softened by PS at Dunea's DWTP to prevent scaling problems. Figure 46 depicts the Ca^{2+}-pH relation in equilibrium (Tillmans curve). The measured Ca^{2+} concentration and pH in the VOW were 1.6 mmol/L and 7.6, respectively. The addition of NaOH to the PS process increased the pH (pink arrow), consequently increased the SI (Equation 18), leading to precipitation of Ca^{2+} on the pellets. This resulted in a decreased Ca^{2+} concentration in the effluent of the PS (orange arrow). After mixture with water from the bypass, the total Ca^{2+} concentration was decreased, making the water less prone to scaling. However, when the eAOP cell would be implemented at Dunea's DWTP, the anodic H$^+$ formation will decrease the pH and lower the SI. Therefore, the water will be less prone to scaling and less Ca^{2+} has to be removed during PS. As a result, less OH⁻ has to be dosed during PS. However, the impact of anodic H$^+$ on the SI was not quantified in this research. Future research on the anodic H$^+$ formation effect on the SI and the resulting required OH⁻ dosage during PS is recommended.
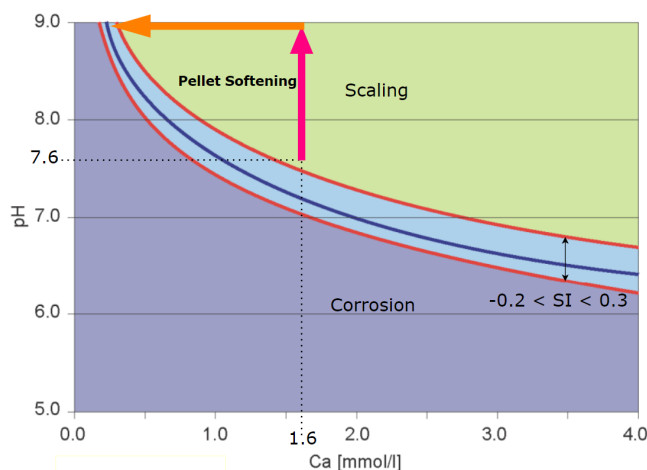
Figure 46: Effect of Pellet Softening on SI. Initial Ca^{2+} concentration and pH are 1.6 mmol/L and 7.6, respectively. Due to pellet softening, the pH increases (pink arrow) and Ca^{2+} will precipitate on the pellets which lowers the Ca^{2+} concentration (orange arrow), adapted from (Rietveld, n.d.).

Leaving the anodic H^+ formation effects aside, the cathodic produced OH^-/h could be compared to the currently dosed OH^-/h during PS. In the current PS process, 8.4 kg OH^-/h was dosed, which equaled 15.5 g OH^-/m^3 (total flow was 900 m^3/h and 60% entered the PS reactor, which equaled 540 m^3/h). During the optimal anodic configuration with a i of 7.5 A/m^2, the observed OH^- production was approximately 2.3 mmol/h, which equaled $3.9*10^{-5}$ kg OH^-/h. The flow rate of 2.2 L/h led to a production of 17.8 g OH^-/m^3, indicating a sufficient amount of produced OH^- to replace NaOH dosage. With these results, the final research question, *What is the optimal cathodic configuration to produce OH^- during the optimal anodic configuration for As(III) oxidation and to what extent can this reduce the chemical use for pellet softening?*, has been answered.

Measured Potentials
Results showed that the E^0 for the OER of 1.50 V was measured at a $i > 27$ A/m^2 (Figure 37). This was higher than the applied i during the experiments. However, the E^0 for the OER depends on the temperature, pH, pressure and solute concentration and the performed experiments deviated from the standard conditions of 25 °C, pH 0, 10^5 Pa and 1 M (Renner, 2007; Armstrong et al., 2013). Hence, a different E for the OER was obtained during the experiments that was < 1.23 V. This was in line with the visual observations where oxygen bubbles were observed on the anode surface during all applied i. Therefore, As(III) could be oxidised by intermediates of the OER at a $E < 1.23$ V. The exact E for the OER was not obtained in this research, since the eAOPs performance in As(III) oxidation was of interest instead of the exact E for the OER.

Improving the System at Laboratory Scale
The focus in the performed experiments was on the minimum required i for As(III) oxidation to minimize the energy consumption as well as the free chlorine formation. However, at larger scale it might be more beneficial to operate at a high i to minimize the eAOP cell area. Supplying a high i leads to a smaller A_{cell} which will save on investment costs. It was observed that a higher i resulted in a higher energy consumption (Figures 30 and 31). However, this higher energy consumption was expected to outweigh the investment costs. Therefore, future experiments should focus on As(III) oxidation with higher applied i in the order of 100 A/m^2.

57

4.2.2 Implementation eAOPs at Dunea

For future pilot experiments in Dunea's DWTP, it was decided to implement the eAOP cell after PS and before aeration followed by RSF (Figure 47). The bypass flow (not softened) will be combined with the PS effluent, together forming the anode influent. This is to ensure for an optimal As(III) oxidation as all water will pass the anode. After eAOP cell passage, the water will continue to aeration and RSF where oxidised As(V) can be removed. It was assumed that a 1 % flow from the PS to the cathode would be sufficient for OH^- production. Before water enters the cathode, it will pass an (cat)ion exchanger (IEX) to remove the remaining Ca^{2+} and Mg^{2+}. Not removing these ions will result in precipitation on the cathode material due to the high pH (and SI), reducing the cathodic operation and hence the OH^- production. Ca^{2+} and Mg^{2+} can be removed by exchange with monovalent ions such as Na^+ (Rangreez & Asiri, 2019). This process increases the salinity, as divalent ions will be replaced by monovalent Na^+ ions with a doubled molar concentration (Clauwaert et al., 2020). However, in the current treatment process NaOH is dosed during PS, so the addition of Na^+ by IEX will compensate for the loss in Na^+ from omitting the NaOH dosage. During the laboratory experiments, no NOM was present in the feed water. Therefore, it was not possible to measure the DBPs formation by the reaction between NOM and free chlorine. It is important that the formed DBPs concentration do not exceed Dutch guidelines as presented in the Drinkwaterbesluit (Overheid, 2021). Hence, DPBs concentrations must be monitored during future pilot experiments.
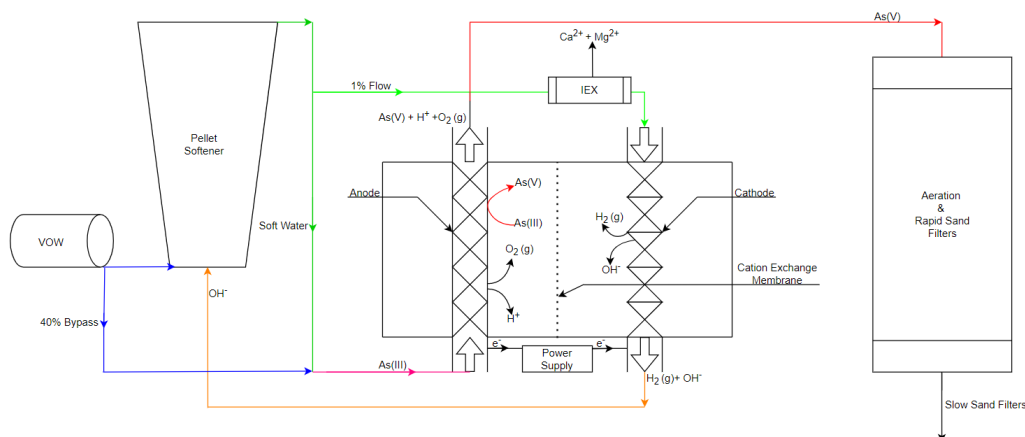
Figure 47: Schematic Overview of Implementation of eAOPs at Dunea. Raw water (VOW), is indicated by the blue arrow. Softened water is indicated by the green arrows and the combination of the softened and bypassed water is indicated by the pink arrow. Anodic and cathodic effluent are indicated by red and orange arrows, respectively.

Another possible location for the eAOP cell is before PS (Figure 61, Supplementary Information 6.15). One major disadvantage is the higher Ca^{2+} concentration in the water before PS, resulting in more required removal during IEX. Hence, more brine consisting of Ca^{2+} and Mg^2 will be generated. This brine could possibly be treated during PS, leading to an additional flow to PS and more required OH^-. Furthermore, a more frequent regeneration of the cation resin will be needed, increasing the operational costs. Hence, the cathode should be implemented after PS. One could argue that it would be possible to implement the cathode after PS, while the anode is before PS. However, installing the anode before PS will affect the SI. As explained in Chapter 4.2.1, the low anodic SI is beneficial when

it comes to required OH^- for PS. However, the SI will be increased during PS by addition of OH^-. The low anodic SI will therefore lead to more required addition of OH^-, making this configuration not beneficial. As a result, it is recommended to implement the eAOP cell after PS.

4.2.3 Water Matrix Dunea

Dunea's water matrix varies from the water matx in the performed experiments. Additional constituents will probably affect the anodic As(III) oxidation. Study of Sharma et al. (2007) observed rapid As(III) oxidation by O_3, ferrate (FeO_4^{2-}) and permanganate (MnO_4^-), which can be generated in the presence of O_2, Fe^{3+} and Mn^{2+} and manganese oxide (MnO_2). In addition, strong electrogenerated oxidants such as peroxydisulfate ($S_2O_8^{2-}$), peroxodiphosphate ($P_2O_8^{4-}$) and peroxydicarbonate ($C_2O_6^{2-}$) can be formed in the presence of SO_4^{2-}, PO_4^{3-} and CO_3^{2-}, respectively (Panizza & Cerisola, 2009; Cañizares et al., 2005; Ruiz et al., 2008). Table 3 shows the E^0 of these (and other) strong oxidants. The generation efficiency of these oxidants depends on the OER overpotential. High OER overpotentials result in high efficiencies, which is the case for non-active anodes (Serrano et al., 2002; Cañizares et al., 2005; Saha et al., 2003). Hence, these oxidants are not expected to play a significant role in As(III) oxidation for the RuO_2/IrO_2-coated anode. However, Mn^{2+} can be oxidised to MnO_2 at a E^0 lower than the OER E^0 (1.23 V), making this reaction thermodynamically favoured (Vanysek, 2000). Study of Gude et al. (2018) showed that As(III) was rapidly oxidised by MnO_2. It was observed that the presence of Fe^{2+} and Mn^{2+} prevented As(III) oxidation by MnO_2. However, Fe^{2+} (with a E^0 of 0.77 V) and Mn^{2+} will be absent when MnO_2 is formed, meaning that the As(III) oxidation by MnO_2 will be enhanced (Vanysek, 2000). The possible indirect As(III) oxidation reactions in Dunea's water are presented in Supplementary Information 6.16.

Table 3: E^0 [V] of the Oxidants at Dunea.

Constituent	E^0 [V]	Reference
Fe^{3+}/FeO_4^{2-}	2.20	(Jiang & Lloyd, 2002)
O_2/O_3	2.07	(Martinez-Huitle & Ferro, 2006)
$PO_4^{3-}/P_2O_8^{4-}$	2.07	(Griffith, Powell, & Skapski, 1988)
$SO_4^{2-}/S_2O_8^{2-}$	2.01	(Chen, 2004; Serrano et al., 2002)
$CO_3^{2-}/C_2O_6^{2-}$	1.80	(Ruiz-Ruiz et al., 2014)
H_2O/H_2O_2	1.77	(Chen, 2004)
MnO_2/MnO_4^-	1.68	(Jiang & Lloyd, 2002; Vanysek, 2000)
Mn^{2+}/MnO_4^-	1.51	(Jiang & Lloyd, 2002; Vanysek, 2000)
Mn^{2+}/MnO_2	1.22	(Vanysek, 2000)

A final constituents that requires attention is bromate (BrO_3^-), which was classified as 'possible human' carcinogen (IARC, 1999; Butler et al., 2005). This shows the importance of monitoring the BrO_3^- production in Dunea's drinking water. BrO_3^- can be formed in the presence of bromide (Br^-), by reacting with O_3 and by direct oxidation of Br^- at 1.42 V (Richardson et al., 2007; Vanysek, 2000). Formed BrO_3^- can be reduced to Br^- with Fe^{2+} converting to Fe^{3+} (Q. Wang et al., 2009; M. Siddiqui et al., 1994). Hence, dosage of Fe^{2+} is recommended when BrO_3^- would be formed.

5 Conclusions and Recommendations

Dunea's drinking water treatment plants (DWTPs) want to reach the new arsenic (As) company target of < 1 μg/L, due to uncertainties on toxicity at the current WHO, European and Dutch guideline of 10 μg/L. During dune infiltration, As enters the water and the concentration increases to 4.9 μg/L. The aim of this research was to lower the As concentration in Dunea's effluent to < 1 μg/L by improving our system understanding and exploring novel techniques for As(III) oxidation.

Fieldwork was performed at the water abstraction field, called Solleveld, to assess whether each well section contributed to the elevated As concentrations. Several groundwater constituents were measured in monitoring points (MPs) and in the DWTP to perform a spatial As analysis. Dissolved trace elements, as well as other groundwater constituents, were measured in monitoring wells (MWs) to create a hydrochemical depth profile. In order to enhance As(III) oxidation at Dunea's DWTP, the use of electrochemical advanced oxidation processes (eAOPs) with a RuO_2/IrO_2-coated anode was examined during laboratory experiments. Parameters of interest included the applied current density (i) [A/m^2] and charge dosage (q) [C/L]. Formation of free chlorine was undesired and the formed concentrations were therefore measured during the experiments. In order to make eAOPs more attractive for implementation, the production of a base (OH^-) at the cathode was examined. This produced OH^- could potentially replace the dosed chemicals (NaOH) during pellet softening (PS).

Fieldwork results showed that the well section connected to MP 3 had the highest contribution to the elevated As concentration with a concentration of 9 μg/L. However, results showed that in each MP the measured As concentration was > 1 μg/L, indicating that each well section contributed to the elevated As concentrations. As a result, it is recommended to lower the As concentration by centralised treatment. The combination of strongly fluctuating groundwater tables, infiltration of oxygenated water, the observed pH decrease and synchronous mobilisation of several TEs, indicated that As was most probably mobilised by pyrite oxidation. Moreover, results showed that water was extracted from multiple layers. It was observed that the As-bearing layer was present between -2.5 and -8.5 m NAP. With an average filter depth from -1.6 to -7.4 m NAP, water was being extracted from the As-bearing layer. It is recommended to extract water from depths > -8.5 m NAP to avoid water extraction from the As-bearing layer. Although it would not be possible to relocate the filters of all the wells to increased depths (> -8.5 m NAP), increased depths should be taken into consideration when constructing future new wells.

Laboratory results showed complete As(III) oxidation by eAOPs at a i of 7.5 A/m^2, with a corresponding q and hydraulic retention time (HRT) of 30 C/L and 1.4 min, respectively. At the aforementioned condition, the energy consumption of the eAOP cell was 0.066 kWh/m^3 with operational costs of 0.04 €/m^3. Free chlorine measurements showed that the free chlorine formation was minimized by lowering the applied i, q and HRT. The observed free chlorine formation increased by a factor 3.2 and 11.6 when doubling the HRT (and q) and i (and q), respectively. Free chlorine could react with natural organic matter to form disinfection by-products (DBPs), which is undesired due to their adverse human health effects. Additionally, some DBPs could be formed by direct oxidation, showing the importance of measuring the formation of DBPs during future research. During the optimal anodic configuration with a i of 7.5 A/m^2, the estimated OH^- production was sufficient to replace the dosed chemicals for PS. However, it was not sufficient to buffer for the anodic pH decrease. Future research should examine the effect of this anodic acidification on the SI and hence the required OH^- for PS. It was proposed to implement the eAOP cell at Dunea's DWTP after PS and before aeration and rapid sand filtration.

References

Alcacio, R., Nava, J., Carreño Aguilera, G., Elorza, E., & Martínez-González, F. (2014, 04). Removal of arsenic from a deep well by electrocoagulation in a continuous filter press reactor. *Water Science & Technology: Water Supply*, *14*, 189. doi: 10.2166/ws.2013.188

Alka, S., Shahir, S., Ibrahim, N., Ndejiko, M. J., Vo, D.-V. N., & Manan, F. A. (2021). Arsenic removal technologies and future trends: A mini review. *Journal of Cleaner Production*, *278*, 123805. Retrieved from https://www.sciencedirect.com/science/article/pii/S0959652620338506 doi: https://doi.org/10.1016/j.jclepro.2020.123805

Andreozzi, R., Caprio, V., Insola, A., & Marotta, R. (1999). Advanced oxidation processes (aop) for water purification and recovery. *Catalysis Today*, *53*(1), 51-59. Retrieved from https://www.sciencedirect.com/science/article/pii/S0920586199001029 doi: https://doi.org/10.1016/S0920-5861(99)00102-9

Antoniou, E., van Breukelen, B., Putters, B., & Stuijfzand, P. (2012). Hydrogeochemical patterns, processes and mass transfers during aquifer storage and recovery (asr) in an anoxic sandy aquifer. *Applied Geochemistry*, *27*(12), 2435–2452. doi: 10.1016/j.apgeochem.2012.09.006

Armstrong, D. A., Huie, R. E., Lymar, S., Koppenol, W. H., Merényi, G., Neta, P., . . . Wardman, P. (2013). Standard electrode potentials involving radicals in aqueous solution: inorganic radicals. *BioInorganic Reaction Mechanisms*, *9*(1-4), 59–61.

Arnau, A. (2004). *Piezoelectric transducers and applications* (Vol. 2004). Springer.

Babu, D. S., Srivastava, V., Nidheesh, P., & Kumar, M. S. (2019). Detoxification of water and wastewater by advanced oxidation processes. *Science of The Total Environment*, *696*, 133961. Retrieved from https://www.sciencedirect.com/science/article/pii/S0048969719339312 doi: https://doi.org/10.1016/j.scitotenv.2019.133961

Berger, B. B. (1987). *Control of organic substances in water and waste water.* Noyes Publications, Park Ridge, NJ.

Bergmann, M. E. H., Koparal, A. S., & Iourtchouk, T. (2014). Electrochemical advanced oxidation processes, formation of halogenate and perhalogenate species: A critical review. *Critical Reviews in Environmental Science and Technology*, *44*(4), 348-390. doi: 10.1080/10643389.2012.718948

Bissen, M., & Frimmel, F. (2003, 09). Arsenic — a review. part ii: Oxidation of arsenic and its removal in water treatment. *Acta hydrochimica et hydrobiologica*, *31*, 97 - 107. doi: 10.1002/aheh.200300485

Bonfatti, F., De Battisti, A., Ferro, S., Lodi, G., & Osti, S. (2000). Anodic mineralization of organic substrates in chloride-containing aqueous media. *Electrochimica Acta*, *46*(2), 305-314. Retrieved from https://www.sciencedirect.com/science/article/pii/S0013468600005867 doi: https://doi.org/10.1016/S0013-4686(00)00586-7

Bonfatti, F., Ferro, S., Lavezzo, F., Malacarne, M., Lodi, G., & Battisti, A. D. (2000). Electrochemical incineration of glucose as a model organic substrate. II. role of active chlorine mediation. *Journal of The Electrochemical Society*, *147*(2), 592. Retrieved from https://doi.org/10.1149/1.1393238 doi: 10.1149/1.1393238

Bonfatti, F., Ferro, S., Lavezzo, F., Malacarne, M., Lodi, G., & De Battisti, A. (1999). Electrochemical incineration of glucose as a model organic substrate. i. role of the electrode material. *Journal of the Electrochemical Society*, *146*(6), 2175.

Brillas, E., & Martínez-Huitle, C. A. (2015). Decontamination of wastewaters containing synthetic organic dyes by electrochemical methods. an updated review. *Applied Catalysis B: Environmental*, *166-167*, 603-643. Retrieved from https://www.sciencedirect.com/science/article/pii/S0926337314007176 doi: https://doi.org/10.1016/j.apcatb.2014.11.016

Brillas, E., Sirés, I., & Oturan, M. A. (2009). Electro-fenton process and related electrochemical technologies based on fenton's reaction chemistry. *Chemical reviews*, *109*(12), 6570–6631.

Broers, H. (2004). Nitrate reduction and pyrite oxidation in the netherlands. *Nitrate in groundwaters, IAH Selected papers on hydrogeology. AA Balkema, Leiden, the Netherlands*, 141–149.

Butler, R., Godley, A., Lytton, L., & Cartmell, E. (2005). Bromate environmental contamination: review of impact and possible treatment. *Critical reviews in environmental science and technology*, *35*(3), 193–217.

Cañizares, P., Larrondo, F., Lobato, J., Rodrigo, M., & Sáez, C. (2005). Electrochemical synthesis of peroxodiphosphate using boron-doped diamond anodes. *Journal of the Electrochemical Society*, *152*(11), D191.

Chaplin, B. P. (2014). Critical review of electrochemical advanced oxidation processes for water treatment applications. *Environmental Science: Processes & Impacts*, *16*(6), 1182–1203.

Chen, G. (2004). Electrochemical technologies in wastewater treatment. *Separation and Purification Technology*, *38*(1), 11-41. Retrieved from https://www.sciencedirect.com/science/article/pii/S1383586603002636 doi: https://doi.org/10.1016/j.seppur.2003.10.006

Clauwaert, P., De Paepe, J., Jiang, F., Alonso-Fariñas, B., Vaiopoulou, E., Verliefde, A., & Rabaey, K. (2020). Electrochemical tap water softening: A zero chemical input approach. *Water research*, *169*, 115263.

Comninellis, C. (1994). Electrocatalysis in the electrochemical conversion/combustion of organic pollutants for waste water treatment. *Electrochimica Acta*, *39*(11), 1857-1862. Retrieved from https://www.sciencedirect.com/science/article/pii/0013468694851751 doi: https://doi.org/10.1016/0013-4686(94)85175-1

Comninellis, C., & Chen, G. (2010). *Electrochemistry for the environment* (Vol. 2015). Springer.

Consumentenbond. (2022). *Wat kost een kilowattuur (kwh) elektriciteit?* Retrieved from https://www.consumentenbond.nl/energie-vergelijken/kwh-prijs

Criscuoli, A., & Figoli, A. (2019). Pressure-driven and thermally-driven membrane operations for the treatment of arsenic-contaminated waters: A comparison. *Journal of Hazardous Materials*, *370*, 147-155. Retrieved from https://www.sciencedirect.com/science/article/pii/S0304389418305776 (II International Caparica Congress on Pollutant Toxic Ions and Molecules) doi: https://doi.org/10.1016/j.jhazmat.2018.07.047

Cullen, W. R., & Reimer, K. J. (1989). Arsenic speciation in the environment. *Chemical reviews*, *89*(4), 713–764.

da Cruz Nizer, W. S., Inkovskiy, V., & Overhage, J. (2020). Surviving reactive chlorine stress: Responses of gram-negative bacteria to hypochlorous acid. *Microorganisms*, *8*(8), 1220.

Das, D., Samanta, G., Mandal, B. K., Roy Chowdhury, T., Chanda, C. R., Chowdhury, P. P., ... Chakraborti, D. (1996). Arsenic in groundwater in six districts of west bengal, india. *Environmental Geochemistry and Health*, *18*(1), 5–15.

Davil, M. F., Mahvi, A. H., Norouzi, M., Mazloomi, S., Amarluie, A., Tardast, A., ... others (2009). Survey of corrosion and scaling potential produced water from ilam water treatment plant. *World Appl Sci J*, *7*(11), 11–24.

Delft, T. (n.d.). *Softening*.

Demirbas, E., Kobya, M., Oncel, M. S., Şık, E., & Goren, A. Y. (2019). Arsenite removal from groundwater in a batch electrocoagulation process: Optimization through response surface methodology. *Separation Science and Technology*, *54*(5), 775–785.

Dillon, P. (2005). Future management of aquifer recharge. *Hydrogeology journal*, *13*(1), 313–316.

Dlugolecki, P., Anet, B., Metz, S. J., Nijmeijer, K., & Wessling, M. (2010). Transport limitations in ion exchange membranes at low salt concentrations. *Journal of Membrane Science*,

346(1), 163-171. Retrieved from `https://www.sciencedirect.com/science/article/pii/S0376738809006905` doi: https://doi.org/10.1016/j.memsci.2009.09.033

Dunea. (n.d.). *Hoe wordt uw drinkwater gemaakt?* Retrieved from `https://www.dunea.nl/drinkwater/hoe-wordt-uw-drinkwater-gemaakt`

Dunea. (2021). *Vwa rapport* (Tech. Rep.). J.W. Lucasweg 2: Het Waterlaboratorium.

European Union. (2020). *Directive (eu) 2020/2184 of the european parliament and of the council of 16 december 2020 on the quality of water intended for human consumption (recast).*

Ghurye, G., & Clifford, D. A. (2001). *Laboratory study on the oxidation of arsenic iii to arsenic v.* National Risk Management Research Laboratory, Office of Research and . . . .

Goebel, H. H., Schmidt, P. F., Bohl, J., Tettenborn, B., Krämer, G., & Gutmann, L. (1990, 03). Polyneuropathy Due to Acute Arsenic Intoxication: Biopsy Studies. *Journal of Neuropathology & Experimental Neurology*, 49(2), 137-149. Retrieved from `https://doi.org/10.1097/00005072-199003000-00006` doi: 10.1097/00005072-199003000-00006

Gomez-Caminero, A., Howe, P. D., Hughes, M., Kenyon, E., Lewis, D., Moore, M., . . . others (2001). *Arsenic and arsenic compounds.* World Health Organization.

Griffith, W. P., Powell, R. D., & Skapski, A. C. (1988). Alkali metal and ammonium peroxodiphosphates: Preparation, vibrational and 31p nmr spectra, and the x-ray crystal structure of ammonium peroxodiphosphate dihydrate (nh4)4[p2o8]·2h2o. *Polyhedron*, 7(14), 1305-1310. Retrieved from `https://www.sciencedirect.com/science/article/pii/S0277538700812280` doi: https://doi.org/10.1016/S0277-5387(00)81228-0

Gude, J., Rietveld, L., & van Halem, D. (2018). *Arsenic removal in rapid sand filters* (Unpublished doctoral dissertation). Delft University of Technology.

Gupta, D. K., & Chatterjee, S. (2017). *Arsenic contamination in the environment: the issues and solutions.* Springer.

Hansen, H. A., Man, I. C., Studt, F., Abild-Pedersen, F., Bligaard, T., & Rossmeisl, J. (2010). Electrochemical chlorine evolution at rutile oxide (110) surfaces. *Physical Chemistry Chemical Physics*, 12(1), 283–290.

Howard, G. (2003). *Arsenic, drinking-water and health risk substitution in arsenic mitigation: a discussion paper* (Vol. 9). World Health Organization.

Hua, G., & Reckhow, D. A. (2007). Comparison of disinfection byproduct formation from chlorine and alternative disinfectants. *Water Research*, 41(8), 1667-1678. Retrieved from `https://www.sciencedirect.com/science/article/pii/S0043135407000619` doi: https://doi.org/10.1016/j.watres.2007.01.032

Huizer, S., Oude Essink, G. H. P., & Bierkens, M. F. P. (2016). Fresh groundwater resources in a large sand replenishment. *Hydrology and Earth System Sciences*, 20(8), 3149–3166. Retrieved from `https://hess.copernicus.org/articles/20/3149/2016/` doi: 10.5194/hess-20-3149-2016

IARC. (1999). Potassium bromate (summary of data reported and evaluation). *International Agency for Research on Cancer, Lyon, France.*

Jain, A., Raven, K. P., & Loeppert, R. H. (1999). Arsenite and arsenate adsorption on ferrihydrite: Surface charge reduction and net oh-release stoichiometry. *Environmental Science & Technology*, 33(8), 1179–1184.

Jiang, J.-Q. (2001). Removing arsenic from groundwater for the developing world-a review. *Water Science and Technology*, 44(6), 89–98.

Jiang, J.-Q., & Lloyd, B. (2002). Progress in the development and use of ferrate(vi) salt as an oxidant and coagulant for water and wastewater treatment. *Water Research*, 36(6), 1397-1408. Retrieved from `https://www.sciencedirect.com/science/article/pii/S004313540100358X` doi: https://doi.org/10.1016/S0043-1354(01)00358-X

Kaczur, J. J. (1996). Oxidation chemistry of chloric acid in nox/sox and air toxic metal removal from gas streams. *Environmental progress*, *15*(4), 245–254.

Kapoor, S., & Gupta, Y. K. (1976). Kinetics and mechanism of oxidations by peroxodiphosphate ions. part i. oxidation of arsenic (iii) in aqueous perchloric acid. *Journal of the Chemical Society, Dalton Transactions*(5), 473–476.

Karori, S., Clifford, D., Ghurye, G., & Samanta, G. (2006, 05). Development of a field speciation method for inorganic arsenic species in groundwater. *Journal American Water Works Association - J AMER WATER WORK ASSN*, *98*, 128-141. doi: 10.1002/j.1551-8833.2006.tb07666 .x

Kraaijeveld, E. (2022). *Quantifying base production as by-product of eaop for arsenic oxidation.*

Lacasa, E., Cañizares, P., Rodrigo, M., & Fernandez Morales, F. (2011, 11). Electro-oxidation of as(iii) with dimensionally-stable and conductive-diamond anodes. *Journal of hazardous materials*, *203-204*, 22-8. doi: 10.1016/j.jhazmat.2011.11.059

Lafferty, B. J., Ginder-Vogel, M., & Sparks, D. L. (2010). Arsenite oxidation by a poorly crystalline manganese-oxide 1. stirred-flow experiments. *Environmental Science & Technology*, *44*(22), 8460–8466.

Lee, G., Song, K., & Bae, J. (2011). Permanganate oxidation of arsenic(iii): Reaction stoichiometry and the characterization of solid product. *Geochimica et Cosmochimica Acta*, *75*(17), 4713-4727. Retrieved from `https://www.sciencedirect.com/science/article/pii/S001670371100353X` doi: https://doi.org/10.1016/j.gca.2011.02.043

Luna-Trujillo, M., Palma-Goyes, R., Vazquez-Arenas, J., & Manzo-Robledo, A. (2020). Formation of active chlorine species involving the higher oxide mox+1 on active ti/ruo2-iro2 anodes: A dems analysis. *Journal of Electroanalytical Chemistry*, *878*, 114661. Retrieved from `https://www.sciencedirect.com/science/article/pii/S1572665720308894` doi: https://doi.org/10.1016/j.jelechem.2020.114661

Marselli, B., Garcia-Gomez, J., Michaud, P.-A., Rodrigo, M., & Comninellis, C. (2003). Electrogeneration of hydroxyl radicals on boron-doped diamond electrodes. *Journal of the Electrochemical Society*, *150*(3), D79.

Martinez-Huitle, C. A., & Ferro, S. (2006). Electrochemical oxidation of organic pollutants for the wastewater treatment: direct and indirect processes. *Chemical Society Reviews*, *35*(12), 1324–1340.

Martínez-Huitle, C. A., & Panizza, M. (2018). Electrochemical oxidation of organic pollutants for wastewater treatment. *Current Opinion in Electrochemistry*, *11*, 62-71. Retrieved from `https://www.sciencedirect.com/science/article/pii/S2451910318301212` (Environmental Electrochemistry Solar Cells) doi: https://doi.org/10.1016/j.coelec.2018.07.010

Masuda, H. (2018). Arsenic cycling in the earth's crust and hydrosphere: interaction between naturally occurring arsenic and human activities. *Progress in Earth and Planetary Science*, *5*. doi: https://doi.org/10.1186/s40645-018-0224-3

McArthur, J., Ravenscroft, P., Safiulla, S., & Thirlwall, M. (2001). Arsenic in groundwater: testing pollution mechanisms for sedimentary aquifers in bangladesh. *Water Resources Research*, *37*(1), 109–117.

McCarty, K. M., Hanh, H. T., & Kim, K.-W. (2011). Arsenic geochemistry and human health in south east asia. *Reviews on environmental health.*

McMahon, P., & Chapelle, F. (2008). Redox processes and water quality of selected principal aquifer systems. *Groundwater*, *46*(2), 259-271. Retrieved from `https://ngwa.onlinelibrary.wiley.com/doi/abs/10.1111/j.1745-6584.2007.00385.x` doi: https://doi.org/10.1111/j.1745-6584.2007.00385.x

Moreira, F. C., Boaventura, R. A., Brillas, E., & Vilar, V. J. (2017). Electrochemical advanced oxida-

tion processes: A review on their application to synthetic and real wastewaters. *Applied Catalysis B: Environmental*, *202*, 217-261. Retrieved from `https://www.sciencedirect.com/science/article/pii/S0926337316306440` doi: https://doi.org/10.1016/j.apcatb.2016.08.037

Nickson, R., McArthur, J., Ravenscroft, P., Burgess, W., & Ahmed, K. (2000). Mechanism of arsenic release to groundwater, bangladesh and west bengal. *Applied Geochemistry*, *15*(4), 403-413. Retrieved from `https://www.sciencedirect.com/science/article/pii/S0883292799000864` doi: https://doi.org/10.1016/S0883-2927(99)00086-4

Nishida, S., & Kimura, M. (1989). Kinetic studies of the oxidation reaction of arsenic (iii) to arsenic (v) by peroxodisulphate ion in aqueous alkaline media. *Journal of the Chemical Society, Dalton Transactions*(2), 357–360.

Nordstrom, D. K. (2000). An overview of arsenic mass poisoning in bangladesh and west bengal, india. *Minor elements*, 21–30.

Oremland, R. S., Hoeft, S. E., Santini, J. M., Bano, N., Hollibaugh, R. A., & Hollibaugh, J. T. (2002). Anaerobic oxidation of arsenite in mono lake water and by a facultative, arsenite-oxidizing chemoautotroph, strain mlhe-1. *Applied and environmental microbiology*, *68*(10), 4795–4802.

Oshiki, M., Ishii, S., Yoshida, K., Fujii, N., Ishiguro, M., Satoh, H., & Okabe, S. (2013). Nitrate-dependent ferrous iron oxidation by anaerobic ammonium oxidation (anammox) bacteria. *Applied and environmental microbiology*, *79*(13), 4087–4093.

Oturan, M. A., & Aaron, J.-J. (2014). Advanced oxidation processes in water/wastewater treatment: principles and applications. a review. *Critical Reviews in Environmental Science and Technology*, *44*(23), 2577–2641.

Overheid. (2021). *Drinkwaterbesluit.*

Pal, P. (2015). *Groundwater arsenic remediation treatment technology and scale up* (P. Pal, Ed.). Butterworth-Heinemann. Retrieved from `https://www.sciencedirect.com/science/article/pii/B9780128012819000011` doi: https://doi.org/10.1016/B978-0-12-801281-9.00001-1

Panizza, M., & Cerisola, G. (2005). Application of diamond electrodes to electrochemical processes. *Electrochimica Acta*, *51*(2), 191–199.

Panizza, M., & Cerisola, G. (2009). Direct and mediated anodic oxidation of organic pollutants. *Chemical reviews*, *109*(12), 6541–6569.

Paulissen, V., Nijboer. (2007). *Grondwater in perspectief.*

Pletcher, D., & Walsh, F. C. (1990). *Industrial electrochemistry.* Springer Science & Business Media.

Podgorski, J., & Berg, M. (2020). Global threat of arsenic in groundwater. *Science*, *368*(6493), 845–850.

Radjenovic, J., Bagastyo, A., Rozendal, R. A., Mu, Y., Keller, J., & Rabaey, K. (2011). Electrochemical oxidation of trace organic contaminants in reverse osmosis concentrate using ruo2/iro2-coated titanium anodes. *Water Research*, *45*(4), 1579-1586. Retrieved from `https://www.sciencedirect.com/science/article/pii/S0043135410008134` doi: https://doi.org/10.1016/j.watres.2010.11.035

Rahman, M. M., Ng, J. C., & Naidu, R. (2009). Chronic exposure of arsenic via drinking water and its adverse health impacts on humans. *Environmental geochemistry and health*, *31*(1), 189–200.

Rangreez, T. A., & Asiri, A. M. (2019). *Applications of ion exchange materials in chemical and food industries.* Springer.

Renner, T. (2007). *Quantities, units and symbols in physical chemistry.* Royal Society of Chemistry.

Richardson, S. D., Plewa, M. J., Wagner, E. D., Schoeny, R., & DeMarini, D. M. (2007). Occurrence, genotoxicity, and carcinogenicity of regulated and emerging disinfection by-products in drinking water: A review and roadmap for research. *Mutation Research/Reviews in Mutation Research*, *636*(1), 178-242. Retrieved from `https://www.sciencedirect.com/science/article/pii/S138357420700035X` (The Sources and Potential Hazards of Mutagens in Complex Environmental Matrices - Part II) doi: https://doi.org/10.1016/j.mrrev.2007.09.001

Rietveld, L. (n.d.). *Softening.*

Rozendal, R. A., Hamelers, H. V., & Buisman, C. J. (2006). Effects of membrane cation transport on ph and microbial fuel cell performance. *Environmental science & technology*, *40*(17), 5206–5211.

Ruiz, E. J., Ortega-Borges, R., Jurado, J. L., Chapman, T., & Meas, Y. (2008). Simultaneous anodic and cathodic production of sodium percarbonate in aqueous solution. *Electrochemical and Solid-State Letters*, *12*(1), E1.

Ruiz-Ruiz, E., Meas, Y., Ortega-Borges, R., & Jurado Baizabal, J. (2014). Electrochemical production of peroxocarbonate at room temperature using conductive diamond anodes. *Surface Engineering and Applied Electrochemistry*, *50*(6), 478–484.

Saha, M. S., Furuta, T., & Nishiki, Y. (2003). Electrochemical synthesis of sodium peroxycarbonate at boron-doped diamond electrodes. *Electrochemical and solid-state letters*, *6*(7), D5.

Saint-Jacques, N., Brown, P., Nauta, L., Boxall, J., Parker, L., & Dummer, T. J. (2018). Estimating the risk of bladder and kidney cancer from exposure to low-levels of arsenic in drinking water, nova scotia, canada. *Environment International*, *110*, 95-104. Retrieved from `https://www.sciencedirect.com/science/article/pii/S0160412017313855` doi: https://doi.org/10.1016/j.envint.2017.10.014

Sancha, A. M. (2006). Review of coagulation technology for removal of arsenic: case of chile. *Journal of health, population, and nutrition*, *24*(3), 267.

Schippers, A., & Jørgensen, B. B. (2002). Biogeochemistry of pyrite and iron sulfide oxidation in marine sediments. *Geochimica et Cosmochimica Acta*, *66*(1), 85-92. Retrieved from `https://www.sciencedirect.com/science/article/pii/S0016703701007451` doi: https://doi.org/10.1016/S0016-7037(01)00745-1

Senn, B., & Hemond, H. (2002, 07). Nitrate controls on iron and arsenic in an urban lake. *Science (New York, N.Y.)*, *296*, 2373-6. doi: 10.1126/science.1072402

Serrano, K., Michaud, P., Comninellis, C., & Savall, A. (2002). Electrochemical preparation of peroxodisulfuric acid using boron doped diamond thin film electrodes. *Electrochimica Acta*, *48*(4), 431-436. Retrieved from `https://www.sciencedirect.com/science/article/pii/S0013468602006886` doi: https://doi.org/10.1016/S0013-4686(02)00688-6

Shams, M., Mohamadi, A., & Sajadi, S. A. (2012). Evaluation of corrosion and scaling potential of water in rural water supply distribution networks of tabas, iran. *World Appl Sci J*, *17*(11), 1484–89.

Sharma, V. K., Dutta, P. K., & Ray, A. K. (2007). Review of kinetics of chemical and photocatalytical oxidation of arsenic (iii) as influenced by ph. *Journal of Environmental Science and Health, Part A*, *42*(7), 997–1004.

Siddiqui, M., Amy, G., Ozekin, K., Zhai, W., & Westerhoff, P. (1994). Alternative strategies for removing bromate. *Journal-American Water Works Association*, *86*(10), 81–96.

Siddiqui, S. I., & Chaudhry, S. A. (2017). Iron oxide and its modified forms as an adsorbent for arsenic removal: A comprehensive recent advancement. *Process Safety and Environmental Protection*, *111*, 592-626. Retrieved from `https://www.sciencedirect.com/science/article/pii/S0957582017302525` doi: https://doi.org/10.1016/j.psep.2017.08.009

Singer, P. C. (1994). Control of disinfection by-products in drinking water. *Journal of environmental engineering*, *120*(4), 727–744.

Sirés, I., Brillas, E., Oturan, M. A., Rodrigo, M. A., & Panizza, M. (2014). Electrochemical advanced oxidation processes: today and tomorrow. a review. *Environmental Science and Pollution Research*, *21*(14), 8336–8367.

Smedley, P., & Kinniburgh, D. (2002). A review of the source, behaviour and distribution of arsenic in natural waters. *Applied Geochemistry*, *17*(5), 517-568. Retrieved from `https://www.sciencedirect.com/science/article/pii/S0883292702000185` doi: https://doi.org/10.1016/S0883-2927(02)00018-5

Sorlini, S., & Gialdini, F. (2010). Conventional oxidation treatments for the removal of arsenic with chlorine dioxide, hypochlorite, potassium permanganate and monochloramine. *Water Research*, *44*(19), 5653-5659. Retrieved from `https://www.sciencedirect.com/science/article/pii/S0043135410004197` (Groundwater Arsenic: From Genesis to Sustainable Remediation) doi: https://doi.org/10.1016/j.watres.2010.06.032

Srivastav, A. L., Patel, N., & Chaudhary, V. K. (2020). Disinfection by-products in drinking water: Occurrence, toxicity and abatement. *Environmental Pollution*, *267*, 115474. Retrieved from `https://www.sciencedirect.com/science/article/pii/S0269749120361625` doi: https://doi.org/10.1016/j.envpol.2020.115474

Straub, K. L., Benz, M., Schink, B., & Widdel, F. (1996). Anaerobic, nitrate-dependent microbial oxidation of ferrous iron. *Applied and environmental microbiology*, *62*(4), 1458–1460.

Stuijfzand, P. (2014). Trace element patterns in dutch coastal dunes after 50 years of artificial recharge with rhine river water. *Environmental Earth Sciences*. doi: 10.1007/s12665-014-3770-z

Stuijfzand, P., van Rossum, P., & Mendizabal, I. (2008). Does arsenic, in groundwaters of the compound rhine-meuse-scheldt-ems delta, menace drinking water supply in the netherlands? In Appelo (Ed.), *Proceedings iah conference. arsenic in groundwater, a world problem* (pp. 102–125). (Seminar Utrecht ; Conference date: 29-11-2006 Through 29-11-2006)

Stuyfzand, P. J. (1998). *Quality changes upon injection into anoxic aquifers in the netherlands: Evaluation of 11 experiments.*

Stuyfzand, P. J., & van der Schans, M. L. (2018). Effects of intake interruptions on dune infiltration systems in the netherlands, their quantification and mitigation. *Science of The Total Environment*, *630*, 757–773.

Sundén, B. (2019). *Hydrogen, batteries and fuel cells.* Academic Press.

Unicef Bangladesh. (2010). *Arsenic mitigation in bangladesh.*

Vanysek, P. (2000). Electrochemical series. *CRC handbook of chemistry and physics*, *8*.

Vasudevan, S., Mohan, S., Sozhan, G., Raghavendran, N. S., & Murugan, C. V. (2006). Studies on the oxidation of as (iii) to as (v) by in-situ-generated hypochlorite. *Industrial & engineering chemistry research*, *45*(22), 7729–7732.

Wang, & Xu. (2012). Advanced oxidation processes for wastewater treatment: formation of hydroxyl radical and application. *Critical reviews in environmental science and technology*, *42*(3), 251–325.

Wang, D., Bolton, J. R., Andrews, S. A., & Hofmann, R. (2015). Formation of disinfection by-products in the ultraviolet/chlorine advanced oxidation process. *Science of The Total Environment*, *518-519*, 49-57. Retrieved from `https://www.sciencedirect.com/science/article/pii/S0048969715002478` doi: https://doi.org/10.1016/j.scitotenv.2015.02.094

Wang, Q., Snyder, S., Kim, J., & Choi, H. (2009). Aqueous ethanol modified nanoscale zerovalent iron in bromate reduction: synthesis, characterization, and reactivity. *Environmental science & technology*, *43*(9), 3292–3299.

WHO. (2011a). *Arsenic in drinking-water. background document for preparation of who guidelines for drinking-water quality.* (Tech. Rep. No. WHO/SDE/WSH/03.04/75/Rev/1). Geneva: World Health Organization.

WHO. (2011b). *Evaluation of certain contaminants in food: seventy-second [72nd] report of the joint fao/who expert committee on food additives.* World Health Organization.

WHO. (2017). *Guidelines for drinking-water quality: fourth edition incorporating first addendum* (4th ed + 1st add ed.) [Publications]. World Health Organization.

Wiel, P., Janssen, L., & Hoogland, J. (1971). Electrolysis of a carbonate-borate solution with a platinum anode—i. current efficiency at perborate concentration of zero. *Electrochimica Acta*, *16*(8), 1217-1226. Retrieved from `https://www.sciencedirect.com/science/article/pii/0013468671851101` doi: https://doi.org/10.1016/0013-4686(71)85110-1

Zhang, P., Tong, M., Yuan, S., & Liao, P. (2014). Transformation and removal of arsenic in groundwater by sequential anodic oxidation and electrocoagulation. *Journal of Contaminant Hydrology*, *164*, 299-307. Retrieved from `https://www.sciencedirect.com/science/article/pii/S0169772214000928` doi: https://doi.org/10.1016/j.jconhyd.2014.06.009

Zhao, X., Zhang, B., Liu, H., & Qu, J. (2010). Removal of arsenite by simultaneous electro-oxidation and electro-coagulation process. *Journal of Hazardous materials*, *184*(1-3), 472–476.

Zhou, M., Tan, Q., Wang, Q., Jiao, Y., Oturan, N., & Oturan, M. A. (2012). Degradation of organics in reverse osmosis concentrate by electro-fenton process. *Journal of Hazardous Materials*, *215-216*, 287-293. Retrieved from `https://www.sciencedirect.com/science/article/pii/S0304389412002609` doi: https://doi.org/10.1016/j.jhazmat.2012.02.070

6 Supplementary Information

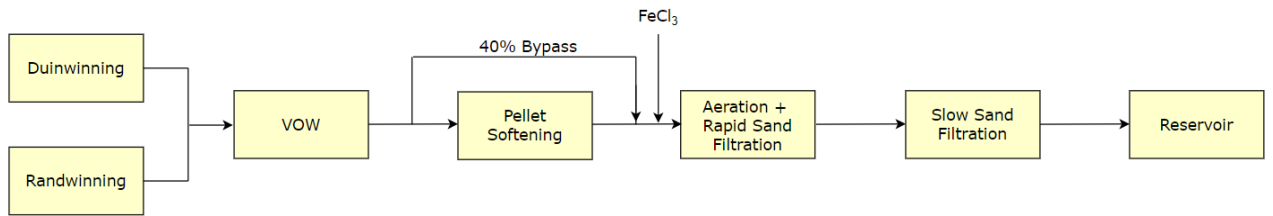## 6.1 Post-Treatment Scheme

Figure 48: Post-Treatment Scheme.
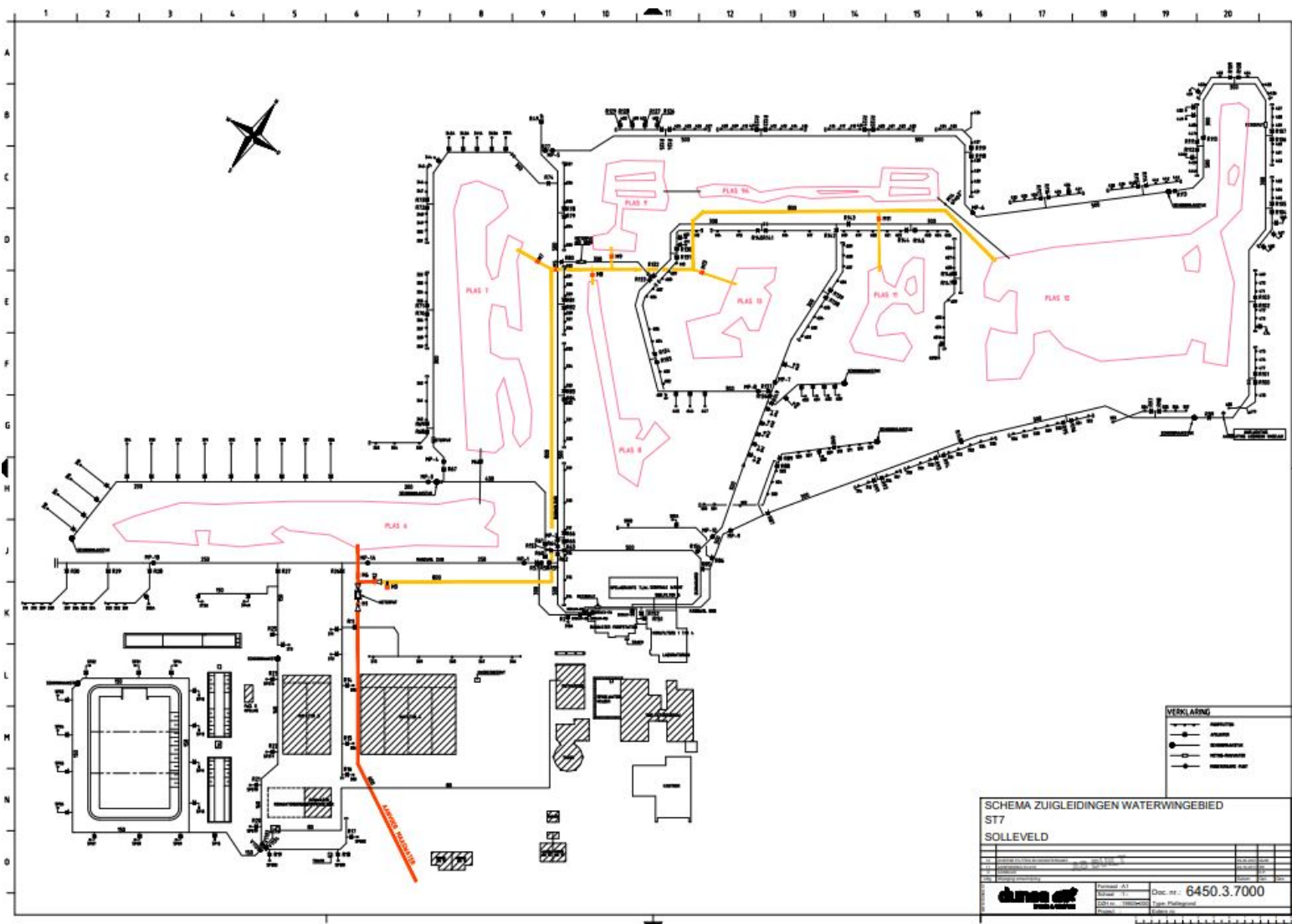
6.2   Overview of Solleveld

Figure 49: Map of Solleveld.
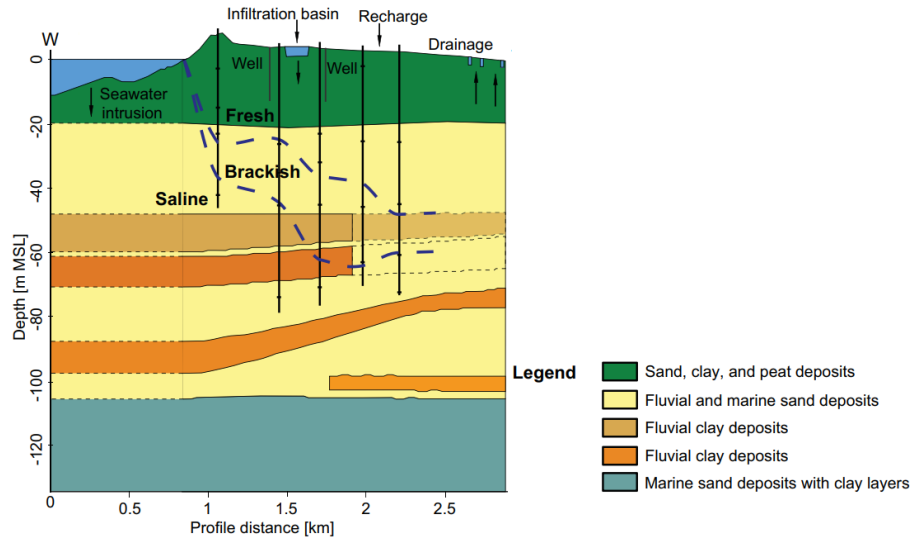
Figure 50: Geological Profile of Solleveld, modified from (Huizer et al., 2016).

Table 4: **Overview Monitoring Points at Solleveld.**

Monitoring Point	Transport Pipe	Previous Monitoring Points
MP1	Randwinning	MP1A, MP1B
MP1A	Randwinning	MP1B
MP1B	Randwinning	-
MP2	Duinwinning	MP5, MP6
MP3	Duinwinning	-
MP4	Duinwinning	-
MP5	Duinwinning	MP6
MP6	Duinwinning	-
MP7	Duinwinning	-
MP8	Duinwinning	-
MP9	Randwinning	-
MP10	Duinwinning	MP7, MP8

6.3 Water Matrix Infiltration Water, Dune Filtrate and Drinking Water

Table 5: Water Matrix Infiltration Water, Dune Filtrate and Drinking Water. Data from 2021 and received from (Dunea, 2021).

Constituent	Infiltration Water	Dune Filtrate	Drinking Water
As [µg/L]	0.99	4.88	3.41
Ca [mg/L]	66.89	63.46	44.70
Fe [mg/L]	0.03	0.18	0.003
Mg [mg/L]	8.95	9.11	8.79
Mn [µg/L]	0.72	58.06	0.03
NH4 [mg/L]	0.01	0.17	0.01
NO3 [mg/L]	2.89	0.86	1.04
PO4 [mg/L]	0.06	0.09	0.04
pH	7.92	7.67	8.68
DO [mg/L]	10.37	2.16	10.36

6.4 Monitoring Wells

Figure 51: Depths of Monitoring Wells Y [m]. Monitoring wells Y1-Y5 with a description of their depths. The ground level was at +2.8 m and the groundwater table was at -0.1 m, from (Dunea, 2022).
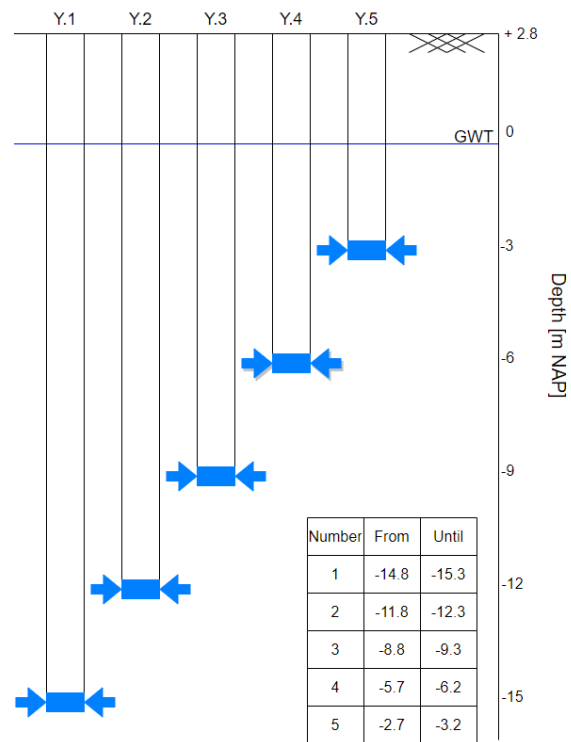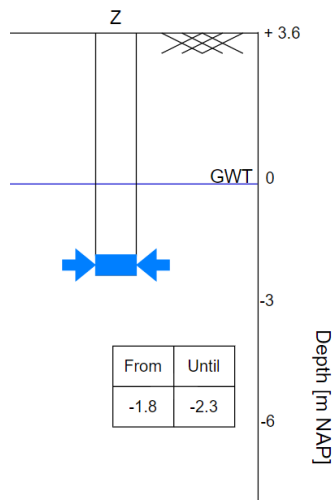
Figure 52: Depth of Monitoring Well Z [m]. Monitoring well Z with a description of its depth. The ground level was at +3.6 m and the groundwater table was at 0 m, from (Dunea, 2022).
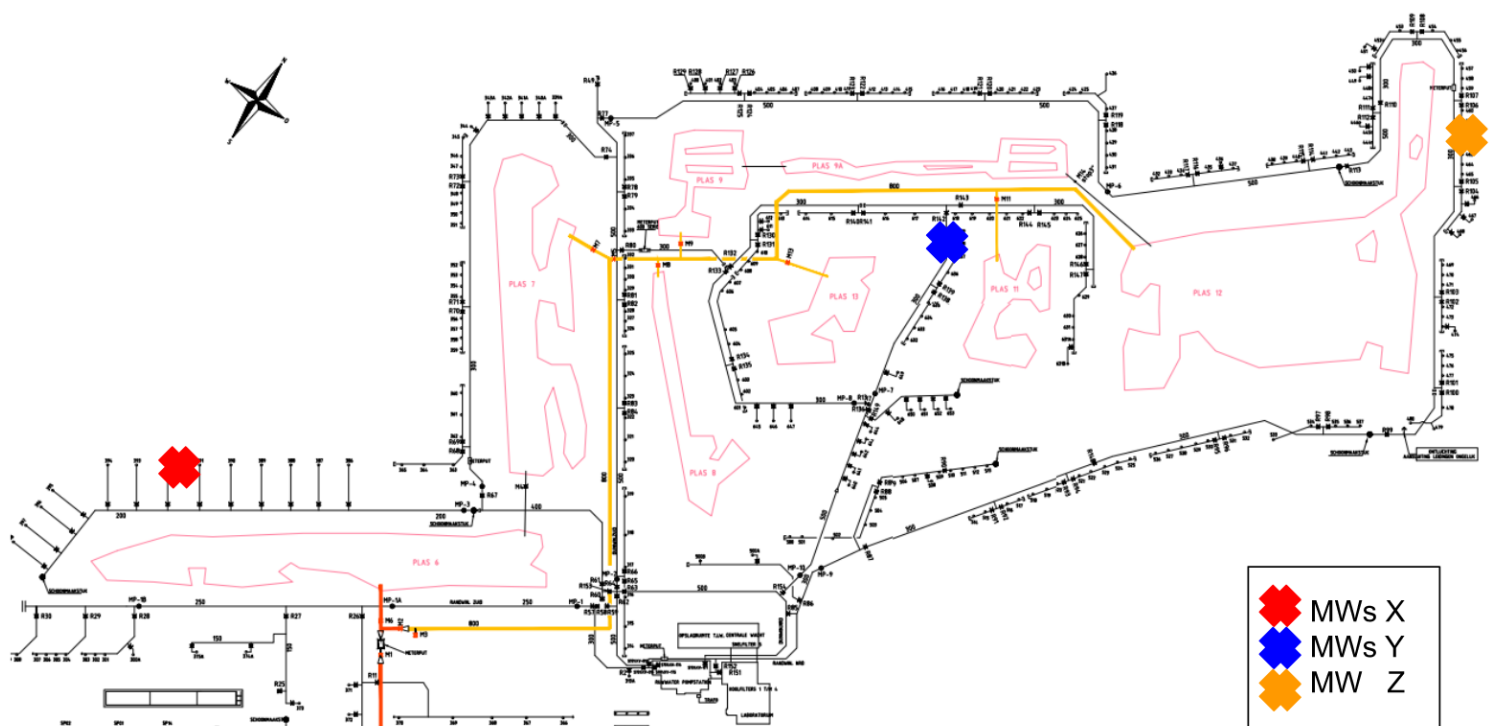
Figure 53: Locations Monitoring Wells. Locations of MWs X (red), MWs Y (blue) and MW Z (orange) in Solleveld.

6.5   Experimental Setup in the Laboratory
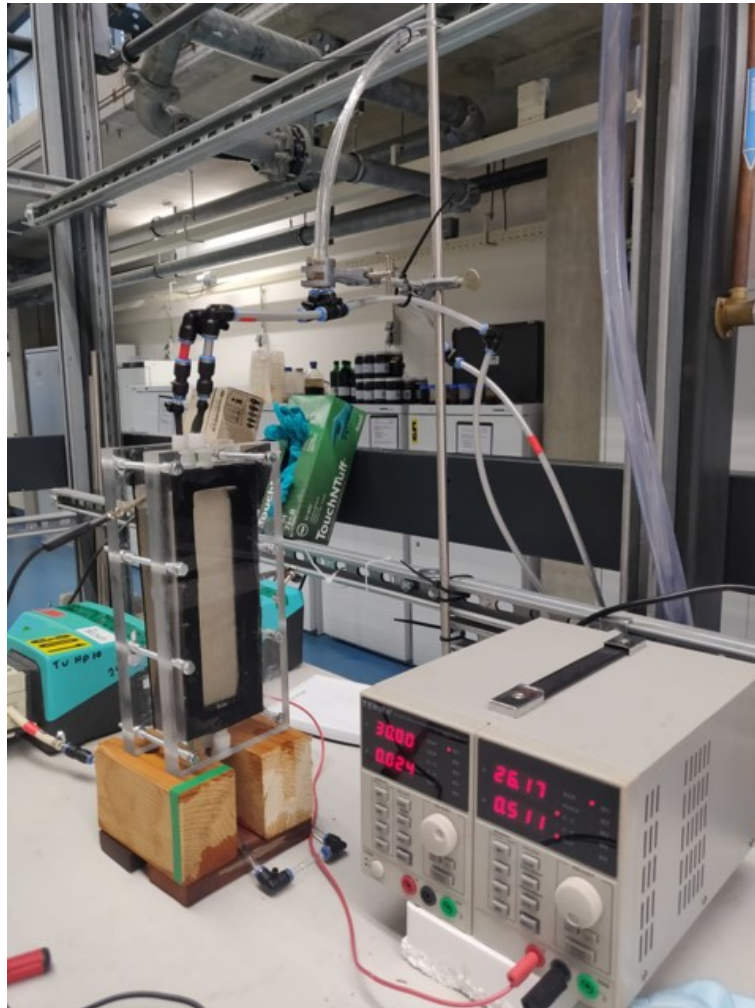
Figure 54: Experimental Setup in the Laboratory. The cathodic side with stainless steel mesh and DC power supply are presented.

Figure 55: RuO$_2$/IrO$_2$-Coated Anode of the eAOP Cell.

6.6 Water Matrix Feed Water

Table 6: Water Matrix of Anodic and Cathodic Feed Water.

Constituent	Anode [mg/L]	Cathode [mg/L]
Na^+	121	121
Cl^-	50	50
HCO_3^-	170	170
As^{3+}	0.08	-

6.7 PHREEQC Model

Model 1: Quantification of Base Formation
SOLUTION 1 Input reactor

-units mg/l

-temp 8

pH 8.237 #Set initial pH

Alkalinity 180 as HCO3

Na 97

Cl 45

END PHASES # Trick used to fix the pH at a specified value.

Fix_H+

H+ = H+

$log_k 0.0$

END

USE solution 1

EQUILIBRIUM_PHASES

Fix_H+ -9.899 NaOH 1.0 #Here you set the pH measured at the effluent of the reactor #NaOH is used as representative base

END

Model 2: Quantification of Required Base Dosing
 SOLUTION 1 Input reactor

-units mg/l

-temp 8

pH 8.041 #Original pH of the influent

Alkalinity 180 as HCO3

Na 97

Cl 45

END PHASES # Trick used to fix the pH at a specified value.

Fix$_H$+

H+ = H+

log$_k$0.0

END USE solution 1

EQUILIBRIUM_PHASES

Fix$_H$+ -7.059 HCl 1.0 #Here you set the pH measured at the effluent of the reactor #HCl is used as representative acid to be converted to a base value

END

6.8 Produced Base Flow
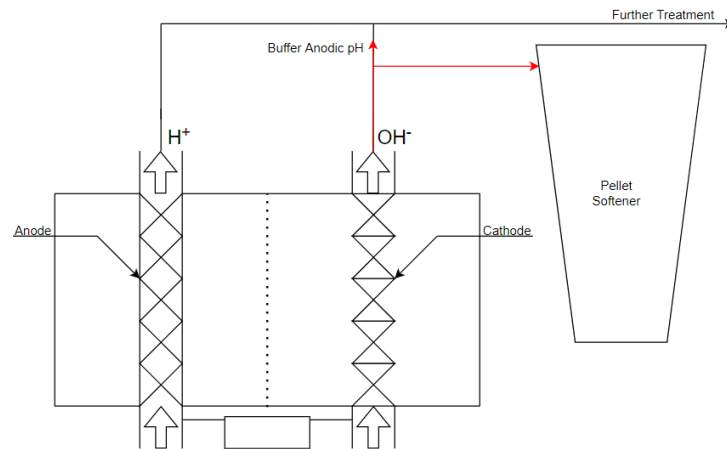
Figure 56: Produced Base Flow. The produced base flow (red) is split into a flow to the pellet softener and a flow to the anodic effluent to buffer the pH.

6.9 Rainfall Contribution at Solleveld

Table 7: Rainfall Contribution at Solleveld.

Rainfall	800	mm/year
Estimated area of Solleveld	600	m^2
Total yearly flux	480,000	m^3/year
Water abstraction	900	m^3/h
Yearly water abstraction	7884000	m^3/year
Rainfall contribution	6	%

6.10   Cell Voltage
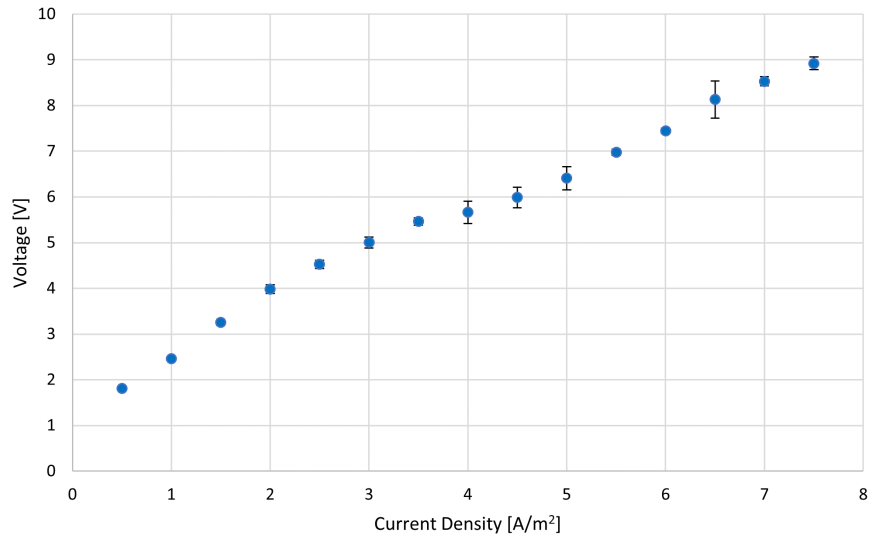
Figure 57: Measured Cell Voltage [V] with a constant HRT [min]. The operational voltage is presented per i [A/m^2] with a constant HRT of 2.3 min and standard deviation.
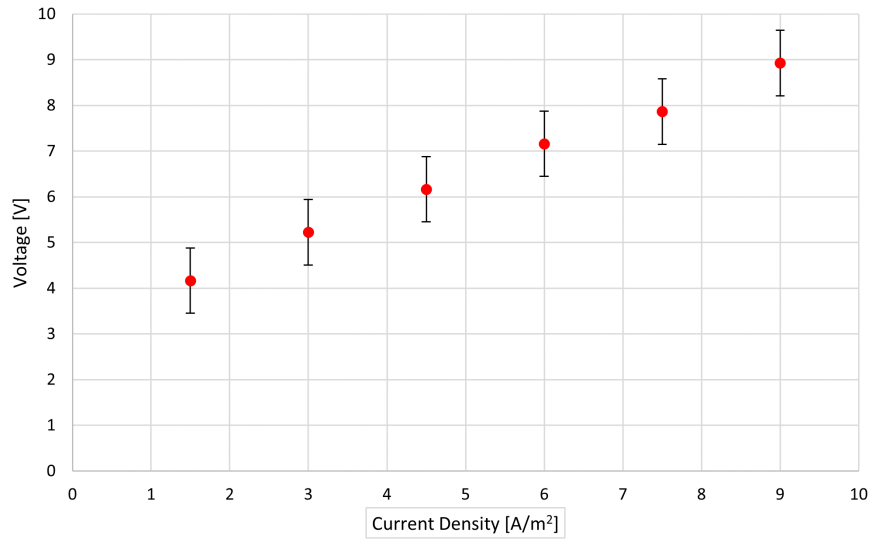
Figure 58: Measured Cell Voltage [V] with a constant q [C/L]. The operational voltage is presented per i [A/m^2] with a constant q of 30.4 C/L and standard deviation.

6.11 Interconnected Monitoring Points

Table 8: Interconnected Monitoring Points.

Monitoring Point	Previous Monitoring Point
MP1	MP1A
MP2	MP5, MP6
MP5	MP6
MP10	MP7, MP8
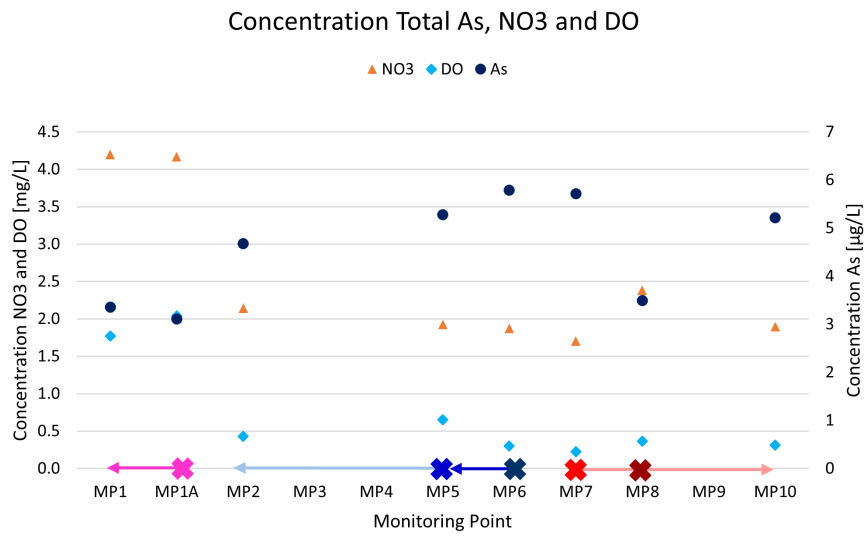
Figure 59: **Concentrations NO$_3^-$ and DO [mg/L] and Total As [µg/L] at Interconnected MPs.** A cross indicates the previous MP and the arrow indicates the connected MP.

6.12 Pyrite Oxidation at MWs Y

Table 9: Pyrite Oxidation at MWs Y.

Depth [m]	$\Delta SO4_{PYRITE}$	Result
-3 m	25.9	Oxidation
-6 m	29.8	Oxidation
-9 m	20.2	Oxidation
-12 m	20.1	Oxidation
-15 m	-19.0	Reduction

6.13   Estimated Arsenic, Iron and Nitrate Concentrations

The estimated As concentration in the average well was calculated by multiplying every As concentration [µg/L], with its height [m] and dividing this by the total filter height of 5.78 m (Equation 24).

$$\text{As}_{\text{estimated}} = \frac{\sum \text{As} * \text{Depth}}{5.8 \text{ m}} \tag{24}$$

Table 10: Estimated Total Dissolved As Concentrations [µg/L]. Values in bold represent the measured concentrations in MWs X.

Depth [m]	As [µg/L]	From [m]	Until [m]	Height [m]
-7.4	1.2	-7.25	-7.4	0.12
-7	1.5	-6.75	-7.25	0.5
-6.5	1.8	-6.25	-6.75	0.5
-6	**2.1**	-5.75	-6.25	0.5
-5.5	8.5	-5.25	-5.75	0.5
-5	14.9	-4.75	-5.25	0.5
-4.5	16.6	-4.25	-4.75	0.5
-4	18.2	-3.75	-4.25	0.5
-3.5	16.6	-3.25	-3.75	0.5
-3	**14.9**	-2.75	-3.25	0.5
-2.5	7.7	-2.25	-2.75	0.5
-2	0.5	-1.75	-2.25	0.5
-1.6	0.5	-1.6	-1.75	0.16

The estimated Fe^{2+} concentration in the average well was calculated by multiplying every Fe^{2+} concentration by the height and dividing this by the total filter height of 5.8 m (Equation 25).

$$\text{Fe}^{2+}_{\text{estimated}} = \frac{\sum \text{Fe}^{2+} * \text{Depth}}{5.8 \text{ m}} \tag{25}$$

Table 11: Estimated Fe^{2+} Concentrations [mg/L]. Values in bold represent the measured concentrations in MWs X.

Depth [m]	Fe^{2+} [mg/L]	From [m]	Until [m]	Height [m]
-6	**0.26**	-5.7	-7.37	1.64
	0.39	-3.24	-5.73	2.49
-3	**0.52**	-2.74	-3.24	0.5

The estimated NO_3^- concentration in the average well was calculated by multiplying the measured NO_3^- concentration of 2.6 mg/L (MP 3) by the filter height of 5.8 m. The measured NO_3^- concentration, indicated as X, that varied between 0-0.99 mg/L, was multiplied by the height of 4.9 m (total height - height NO_3^- layer) and subtracted. This was divided by the assumed NO_3^- layer height of 0.9 m (Equation 26).

$$\text{NO}_3^- {}_{\text{estimated}} = \frac{2.6 \text{ mg/L} * 5.8 \text{ m} - X * 4.9 \text{ m}}{0.9 \text{ m}} \tag{26}$$

6.14 Potential for Oxygen Evolution Reaction on Different Anodes

anode	value vs SHE	conditions
RuO_2	1.47	0.5 M H_2SO_4
IrO_2	1.52	0.5 M H_2SO_4
Pt	1.6	0.5 M H_2SO_4
oriented pyrolytic graphite	1.7	0.5 M H_2SO_4
SnO_2	1.9	0.05 M H_2SO_4
PbO_2	1.9	1 M H_2SO_4
BDD	2.3	0.5 M H_2SO_4

Figure 60: E [V] for the OER on Different Anodes. Standard E^0 for oxygen evolution is 1.23 V, from (Panizza & Cerisola, 2009)

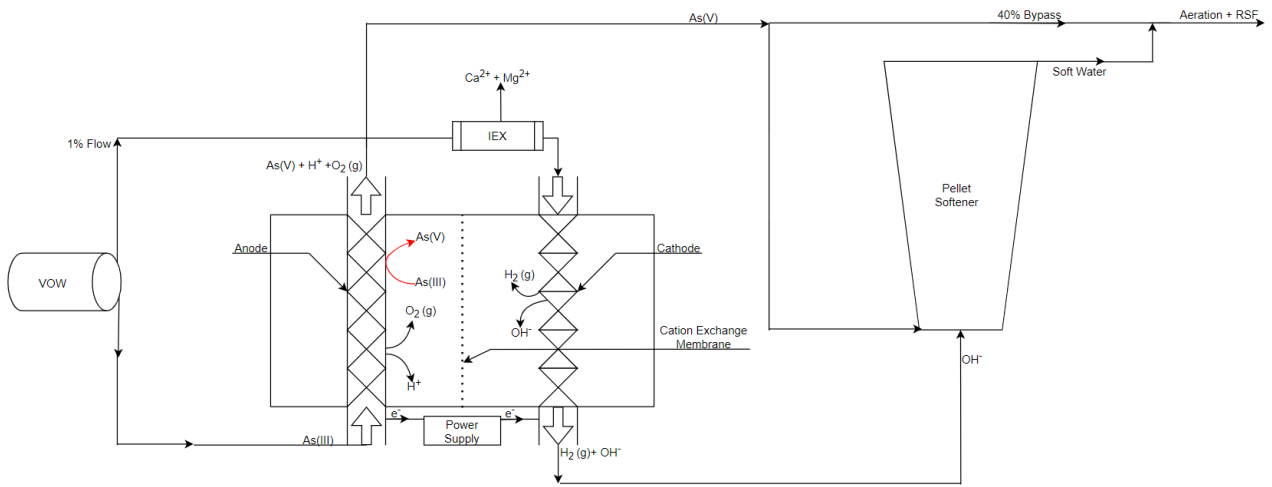## 6.15   Configuration of eAOPs before Pellet Softening

Figure 61: Configuration of eAOPs before Pellet Softening.

6.16   Oxidation Reactions Dunea Water

The As(III) oxidation reactions by FeO_4^{2-}, O_3, $P_2O_8^{4-}$, $S_2O_8^{2-}$, $C_2O_6^{2-}$, H_2O_2, MnO_4^- and MnO_2 are presented by the following reactions (Sharma et al., 2007; Kapoor & Gupta, 1976; Nishida & Kimura, 1989; Wiel et al., 1971; Lee et al., 2011; Lafferty et al., 2010).

$$3H_3AsO_3 + 2FeO_4^{2-} + 7H^+ \rightarrow 3H_2AsO_4^- + 2Fe^{3+} + 5H_2O \tag{27}$$

$$H_3AsO_3 + O_3 \rightarrow H_2AsO_4^- + O_2 + H^+ \tag{28}$$

$$H_3AsO_3 + P_2O_8^{4-} + H_2O \rightarrow H_2AsO_4^- + 2PO_4^{3-} \tag{29}$$

$$H_3AsO_3 + S_2O_8^{2-} \rightarrow H_2AsO_4^- + 2SO_4^{2-} + 3H^+ \tag{30}$$

$$H_3AsO_3 + C_2O_6^{2-} \rightarrow H_2AsO_4^- + 2CO_3^{2-} + 3H^+ \tag{31}$$

$$H_3AsO_3 + H_2O_2 \rightarrow H_2AsO_4^- + H_2O + H^+ \tag{32}$$

$$1.5H_3AsO_3 + MnO_4^- \rightarrow 1.5H_2AsO_4^- + MnO_2 + 0.5H_2O + 0.5H^+ \tag{33}$$

$$H_3AsO_3 + MnO_2 + H^+ \rightarrow H_2AsO_4^- + Mn^{2+} + H_2O \tag{34}$$